

**A Water-Soluble Phosphate-Footed Cavitand: Synthesis and Binding  
Properties with Small Neutral Organic Molecules**

by

**XUAN GUI**

B.Sc., Nankai University, P.R.China, 1995

A THESIS SUBMITTED IN PARTIAL FULFILLMENT OF  
THE REQUIREMENTS FOR THE DEGREE OF  
MASTER OF SCIENCE

in

THE FACULTY OF GRADUATE STUDIES  
(Department of Chemistry)

We accept this thesis as conforming to the required standard

THE UNIVERSITY OF BRITISH COLUMBIA

August, 2000

© Xuan Gui, 2000

In presenting this thesis in partial fulfilment of the requirements for an advanced degree at the University of British Columbia, I agree that the Library shall make it freely available for reference and study. I further agree that permission for extensive copying of this thesis for scholarly purposes may be granted by the head of my department or by his or her representatives. It is understood that copying or publication of this thesis for financial gain shall not be allowed without my written permission.

Department of Chemistry

The University of British Columbia  
Vancouver, Canada

Date Sept. 24, 2000

## Abstract

This thesis presents a study of apolar host-guest complexations between a bowl-shaped cavitand host and small neutral organic guest molecules in aqueous solutions. The water-soluble host molecule-cavitand **1**, with methyl groups on the rim positions and hydrophilic phosphate groups at the pendent positions, was synthesized. It forms 1:1 host-guest complexes in aqueous solutions exclusively with most investigated guest molecules. Binding constants of these complexes were determined from  $^1\text{H}$  NMR titration experiments. The strongest bindings were found between host **1** and small ester guest molecules. Variable temperature  $^1\text{H}$  NMR titration experiment uncovered that binding processes were driven by favorable enthalpy changes accompanied with unfavorable entropy changes. These results were discussed in terms of the attractive van der Waals interactions between host and guest as well as the hydrophobic effect. The geometry of the complexes in aqueous solution was elucidated by  $^1\text{H}$  NMR spectroscopy and molecular mechanics calculations. For guests containing two potential binding sites, they form isomeric complexes with host **1**.

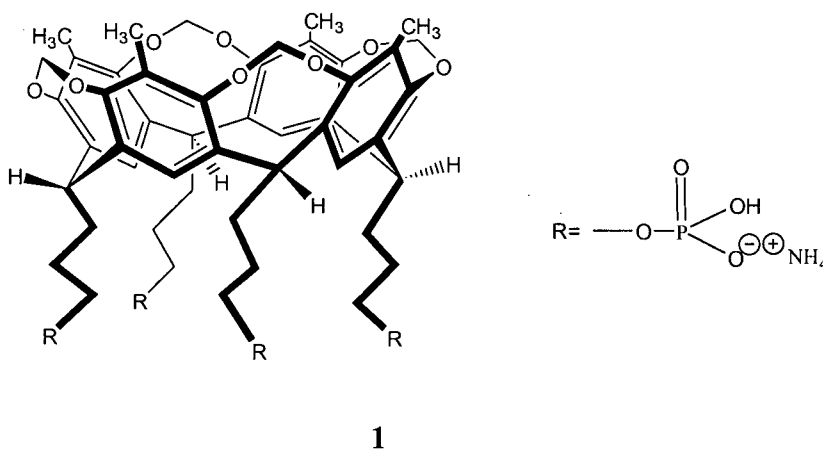


# Table of Contents

Abstract.....	ii
List of Tables.....	v
List of Figures.....	vii
List of Equations.....	ix
List of Schemes.....	ix
List of Abbreviations.....	x
Acknowledgements.....	xi

## **CHAPTER 1. INTRODUCTION ..... 1**

1.1 General Introduction.....	1
1.2 Water-Soluble Hosts and Their Complexing Properties .....	4
A Water-Soluble Cyclophanes and Their Complexation Properties.....	5
B Water-soluble Calixarenes .....	11
C Water-soluble Resorcin[4]arenes .....	18
D Water-Soluble Cavitands .....	24
i Introducing Hydrophilic Functionalities into the Cavitand Rims.....	24
ii Introduction of Hydrophilic Functionalities into the Cavitand's Pendent Groups ...	27
iii Water-Soluble Carceplexes .....	30
1.3 Summary and Thesis Goal.....	32
1.4 References and Notes .....	33

## **CHAPTER 2. SYNTHESIS AND BINDING STUDIES OF WATER-SOLUBLE PHOSPHATE-FOOTED CAVITAND..... 39**

2.1. Introduction.....	39
2.2. Synthesis and Characterization of phosphate-footed cavitands.....	40
2.3. Binding studies .....	46
A. Theory and Procedure .....	46
i. Determination of Stoichiometry of the Complexes .....	47

ii. Determination of the Binding Constant.....	49
iii. Determination of Thermodynamic Data.....	51
B. Result and Discussion .....	51
i. Solubility of Cavitand 1 in Aqueous Solutions .....	51
ii. Aggregation Behavior of the Host 1 .....	52
iii. Binding Studies .....	53
1. Guest Screening.....	53
a). Unsuccessful Guests .....	54
b). Successful Guests That Were Not Included in Binding Studies.....	55
2. Determination of Stoichiometry of the Complex 1•Guest.....	56
3. Determination of the Binding Constants $K_a$ .....	57
a). Selection of the Optimal Concentration Range .....	60
b). Conformations of Complexation .....	61
c). Stability of the complexation.....	65
iv. Determination of Thermodynamic Data of Binding with Esters.....	70
v. Computer Assisted Molecular Modeling.....	77
2.4. Conclusion and Future.....	82
2.5. Experimental.....	84
A. Synthesis .....	84
i. General.....	84
ii. Synthetic Procedures .....	85
B. Binding Study.....	87
i. General.....	87
ii. Determination of Binding Stoichiometry .....	88
iii. General Procedure for Determination of Binding Constants .....	90
iv. Variable Temperature (VT) $^1\text{H}$ NMR Experiments .....	95
1. Calibration of the Temperature.....	97
2. Calibration of the Chemical Shift of the $\text{D}_2\text{O}$ Solvent Residue Peak.....	99
v. Molecular Mechanics Calculations.....	100
2.6. References and Notes .....	100

## List of Tables

Table 2.1	Reaction conditions and the yields of the phosphorylating reaction.....	43
Table 2.2	Successful guest molecules .....	54
Table 2.3	Unsuccessful guest molecules.....	54
Table 2.4	The calculated CIS on 100% binding of <b>1</b> with various guests .....	62
Table 2.5	The binding constants of <b>1</b> •guests and hydrophobicities of the guests at 298K.....	66
Table 2.6	Binding constants calculated from fitting of different proton data of the guests.....	67
Table 2.7	Binding constants ( $K_a$ ) of complex <b>1</b> •methyl acetate at different temperatures ...	72
Table 2.8	The binding constants of complex <b>1</b> •ethyl acetate at different temperatures.....	72
Table 2.9	The binding constants of complex <b>1</b> •methyl propionate at different temperatures	73
Table 2.10	Thermodynamic data (at 298K) for the investigated <b>1</b> •guest systems.....	74
Table 2.11	Observed chemical shift change of methyl acetate protons in solutions with 5 times excess of various hosts at 298K in organic solvents. ....	75
Table 2.12	Relevant distances (in Å) for host <b>1</b> and its complexes with investigated guests obtained by MM+ optimization. ....	82
Table 2.13	Calculated energy difference between two binding modes of “unsymmetrical” guest. ....	82
Table 2.14	<sup>1</sup> H NMR assignments of guest chemical shifts for Job’s plot of methyl acetate at ambient room temperature. ....	88
Table 2.15	<sup>1</sup> H NMR assignment of guest signals for Job’s plot of ethyl acetate at ambient room temperature. ....	89
Table 2.16	<sup>1</sup> H NMR assignment of guest signals for Job’s plot of methyl propionate at ambient room temperature. ....	89
Table 2.17	<sup>1</sup> H NMR assignment of guest signals for Job’s plot of dimethyl carbonate .....	90
Table 2.18	Guest signal assignment for acetone binding in pD 9.4 carbonate buffer at 298K. ....	91

Table 2.19	$^1\text{H}$ NMR assignment of guest signal for $\text{CH}_3\text{CN}$ binding in pD 9.4 carbonate buffer at 298K. ....	91
Table 2.20	$^1\text{H}$ NMR assignment of guest signal for benzene binding in pD 9.4 carbonate buffer at 298K. ....	92
Table 2.21	$^1\text{H}$ NMR assignment of guest signals for toluene binding in pD 9.4 carbonate buffer at 298K. ....	92
Table 2.22	$^1\text{H}$ NMR assignment of guest signal for chloroform binding in pD 9.4 carbonate buffer at 298K. ....	93
Table 2.23	$^1\text{H}$ NMR chemical shift of guest protons for methyl acetate binding in pD 9.4 carbonate buffer at 298K. ....	93
Table 2.24	$^1\text{H}$ NMR assignment of guest protons for ethyl acetate binding in pD 9.4 carbonate buffer at 298K. ....	94
Table 2.25	$^1\text{H}$ NMR assignment of the guest protons for the methyl propionate binding in pD 9.4 carbonate buffer at 298K. ....	94
Table 2.26	$^1\text{H}$ NMR assignment of guest protons for methyl acetate VT experiments .....	95
Table 2.27	$^1\text{H}$ NMR assignment of guest protons for of ethyl acetate VT experiments .....	96
Table 2.28	$^1\text{H}$ NMR assignment of guest protons for methyl propionate VT experiments ....	96

## List of Figures

Figure 1.1	Selective complexation (molecular recognition) of a convex molecular guest by a spatially complementary (concave) organic host molecule. ....	1
Figure 1.2	Structure of cavitand.....	4
Figure 1.3	Schematic representation of $\alpha$ -, $\beta$ -, and $\gamma$ -cyclodextrin.....	5
Figure 1.4	Cram and Steinberg's [2,2]paracyclophane 2.....	5
Figure 1.5	Koga's type cyclophane.....	6
Figure 1.6	Diederich's cyclophane 4 and guest perylene .....	8
Figure 1.7	Structure of cyclophane <b>5</b> .....	9
Figure 1.8	Structure of glycophane <b>6</b> .....	9
Figure 1.9	Structures of cyclophane <b>7-10</b> .....	11
Figure 1.10	Conformations of calix[4]arene.....	12
Figure 1.11	Calixarenes <b>11a-d</b> .....	12
Figure 1.12	Calixarenes <b>12</b> .....	13
Figure 1.13	Ferrocene derivatives <b>15-17</b> .....	15
Figure 1.14	Calixarenes <b>18a-c</b> .....	16
Figure 1.15	Calixarenes <b>19-21</b> .....	17
Figure 1.16	Ionic guests <b>22</b> and <b>23</b> .....	17
Figure 1.17	Structures of the aromatic guests.....	20
Figure 1.18	Structures of resorcinarenes <b>26-28</b> .....	21
Figure 1.19	Structures of resorcinarenes <b>29-31</b> .....	23
Figure 1.20	Structures of cavitands <b>32-35</b> .....	25
Figure 1.21	Structures of cavitands <b>36-38</b> .....	26
Figure 1.22	Structures of cavitands <b>42a-b</b> .....	28
Figure 1.23	Proposed schematic representation of the C <sub>4v</sub> -C <sub>2v</sub> -D <sub>2d</sub> conformation equilibrium for water-soluble cavitand <b>39b</b> . ....	29
Figure 1.24	Hemicarcerands <b>43, 44</b> and their building blocks <b>45, 46</b> .....	30
Figure 1.25	Hosts <b>47, 48</b> and their building blocks <b>49, 50</b> .....	31



Figure 2.1	400 MHz $^1\text{H}$ NMR spectra of the ammonium salt <b>1</b> (a) and its sodium salt analogue (b) in $\text{D}_2\text{O}$ at ambient temperature .....	44
Figure 2.2	Job's plots .....	56
Figure 2.3	Stack plot of $^1\text{H}$ NMR (500 MHz) spectra of $\text{CHCl}_3$ with increased amount of compound <b>1</b> in 50 mM $(\text{NH}_4)_2\text{CO}_3$ buffered $\text{D}_2\text{O}$ solutions.....	58
Figure 2.4	Binding isotherm of <b>1</b> • $\text{CHCl}_3$ binding system.....	59
Figure 2.5	Three linear forms of the binding isotherm .....	59
Figure 2.6	Scatchard plot of <b>1</b> •methyl propionate binding system. ....	61
Figure 2.7	Observed CIS as a function of host concentration.....	64
Figure 2.8	Schematic presentation of dual modes inclusion of the guest. ....	65
Figure 2.9	van't Hoff plots of investigated <b>1</b> •guest binding systems .....	73
Figure 2.10	Computed top and side view of cavitand <b>1</b> .....	79
Figure 2.11	Schematic presentation of cavity size of host <b>1</b> (side view).....	79
Figure 2.12	Stable conformations of <b>1</b> •guests obtained by MM+ optimization .....	81
Figure 2.13	VT calibration curves for Bruker AMX 500 spectrometer.....	98
Figure 2.14	$\text{D}_2\text{O}$ residue peak chemical shift as a function of temperature.....	99

## List of Equations

Equation 2.1 .....	47
Equation 2.2 .....	47
Equation 2.3 .....	48
Equation 2.4 .....	49
Equation 2.5 .....	49
Equation 2.6 .....	49
Equation 2.7 .....	50
Equation 2.8 .....	50
Equation 2.9 .....	51
Equation 2.10 .....	55
Equation 2.11 .....	65
Equation 2.12 .....	65
Equation 2.13 .....	76

## List of Schemes

Scheme 1.1 Deprotonation of <b>24</b> under basic condition .....	19
Scheme 1.2 Synthetic route of cavitand <b>41</b> .....	27
Scheme 2.1 Synthesis of cavitand <b>52</b> via methylene bridging. ....	40
Scheme 2.2 Synthetic route of phosphate-footed cavitand. ....	41
Scheme 2.3 Schematic representation of different deprotonation states of the phosphate feet in the cavitand under varying conditions .....	45

## List of Abbreviations

Å	-	angstroms
δ	-	chemical shift
Δ	-	change in chemical shift
CPK	-	Corey-Pauling-Koltun (models)
DMA	-	<i>N,N</i> -dimethylacetamide
<i>J</i>	-	coupling constant
m	-	meta
M	-	parent mass (mass spectra); or molarity
m/z	-	mass to charge ratio
MALDI	-	matrix assisted laser desorption ionization
3-NBA	-	3-nitrobenzyl alcohol
NMR	-	nuclear magnetic resonance (spectroscopy)
ppm	-	parts per million
Ph	-	phenyl (-C <sub>6</sub> H <sub>5</sub> )
TFA	-	trifluoroacetic acid
THF	-	tetrahydrofuran

## Acknowledgements

First of all, I would like to thank my research supervisor, Dr. John Sherman for giving me the chance to study in UBC. His guidance, encouragement and wise advice throughout the last two years are essential to my education and research in department of chemistry and will benefit my future life.

I would also like to thank all the past and present members of Sherman group. Special thanks go to Adam Mezo for his enthusiastic help at the beginning of this project. I would like to thank Ayub Jasat who is the nicest person I have ever met. He devoted his time and patience to teaching me research skills, offering me suggestions and helping me to gain computer expertise. His friendship and help made this project much easier. I am grateful to Ayub Jasat, Darren Makeiff, Diana Wallhorn, Ashley Causton and Rajesh Mangroo for proof-reading this thesis. I won't forget Sam Place and Christoph Naumann for their encouragement during the preparation of this thesis.

This work would not have been possible without the help of other members of the UBC chemistry department. I would particularly like to thank Dr. Nick Burlinson for his advice on NMR experiments. I would also like to thank the staff of NMR laboratory, Mass Spectrometry, biological services laboratory and Mr. Peter Borda of the Elemental Analysis laboratory as well as departmental staff.

I am grateful to everyone in my family, especially to my husband. Without his support and encouragement on my research and my life, I would never finish my degree. I would also like to thank my parents. They devote their every penny to support me on my education.

Finally, I would like to thank all my friends. They shared my happiness and difficulties here in Vancouver. They will be in my memory forever.

**Dedicated to My Parents and My Late Brother**  
**with the Deepest Love**

# Chapter 1. Introduction

## 1.1. General Introduction

Molecular recognition is the process by which molecules selectively recognize other molecules in a structurally well-defined pattern through weak intermolecular forces.<sup>1</sup> This process, i.e., the formation of host-guest complexes, plays a fundamental role in many biological processes. Enzymes, receptors, antibodies, membranes, carriers and channels are all examples of natural systems that take part in molecular recognition events. Figure 1 depicts a schematic representation of host-guest complexation.<sup>2</sup> These biological processes are typically highly efficient and selective towards a given substrate. Despite extensive research efforts, the forces that control molecular recognition processes in nature are not yet fully understood.

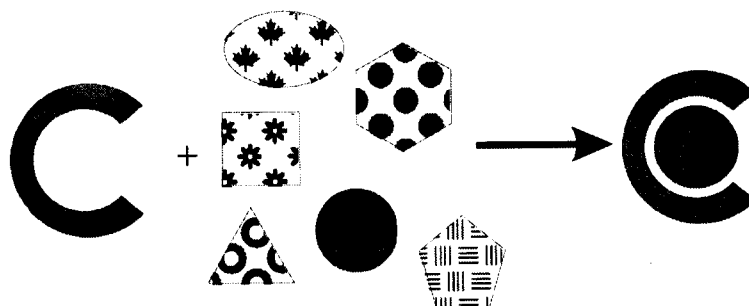


**Figure 1.1** Selective complexation (molecular recognition) of a convex molecular guest by a spatially complementary (concave) organic host molecule.<sup>2</sup>

Pederson's discovery of stable crown ether metal ion complexes in 1967 was the first published example of complexation with synthetic receptors.<sup>3</sup> Since then, others have put much effort into mimicking and understanding biological molecular recognition processes by using structurally much simpler synthetic receptors.<sup>4</sup> This has led to the development of the field of *supramolecular chemistry*. Supramolecular chemistry is the discipline of chemistry which involves all intermolecular interactions where covalent bonds are not established between the interacting species.<sup>5</sup> One aspect of the supramolecular chemistry, *host-guest chemistry*, is mimicking nature to develop substrate specific receptor molecules. Many of these non-natural systems studied are characterized by the formation of inclusion complexes between a larger, well-defined, structurally rigid host possessing a relatively apolar cavity and the specific smaller organic guests.

Many of these systems have been studied in organic media,<sup>6</sup> in which weak noncovalent interactions can be readily observed and utilized. The studies in aqueous media are of particular interest as they closely resemble the natural systems and as such may provide better insight into them. The intermolecular forces that occur in aqueous solutions, which include van der Waals, hydrophobic interactions, hydrogen bonding, and electrostatic interactions, are identical to those partaking in fundamental biological processes. Among these *noncovalent* forces, hydrophobic interactions play a predominant role in biological processes. Hydrophobic interaction denotes the tendency of nonpolar molecules to form aggregates in aqueous solutions. In 1959, Kauzmann introduced the concept of hydrophobic interactions as the solvent-induced attractive forces between apolar molecules or moieties in aqueous solution.<sup>7</sup> These interactions are related to the nature of water which is a liquid characterized by an extended network of hydrogen bonds and an



extremely high cohesive energy density.<sup>8</sup> One point of view to account for hydrophobic interaction is when the nonpolar molecules intrude into water, the strong intermolecular hydrogen bonding of water must be modified at the surface of the nonpolar solute molecule to accommodate them. The resulting orientations are more restricted in the presence of nonpolar solute molecules, which lead to a large loss of entropy. The tendency for water molecules to avoid entropically unfavorable interactions with apolar solutes provides the large driving force for the aggregation of the apolar solutes.<sup>8</sup> This demonstrates the “classical” view of interactions between apolar species in water, which is believed to be entropy driven. But this view is still quite controversial since many workers have found that the hydrophobic association may be either driven entropically or enthalpically.<sup>9</sup> This encouraged scientists to explore new water-soluble synthetic host molecules that facilitate the study of hydrophobic association in water.

This thesis studies the hydrophobic association between cavitand host **1** (Figure 1.2) and various small, neutral organic guest molecules in aqueous solutions. By measuring the binding constants and thermodynamic data involved in the complexation processes, we gain valuable insight into the non-covalent forces that control the molecular recognition in water. The next sections of this chapter will give an overview on several well-known examples of water-soluble hosts and their complexation properties in aqueous solutions.

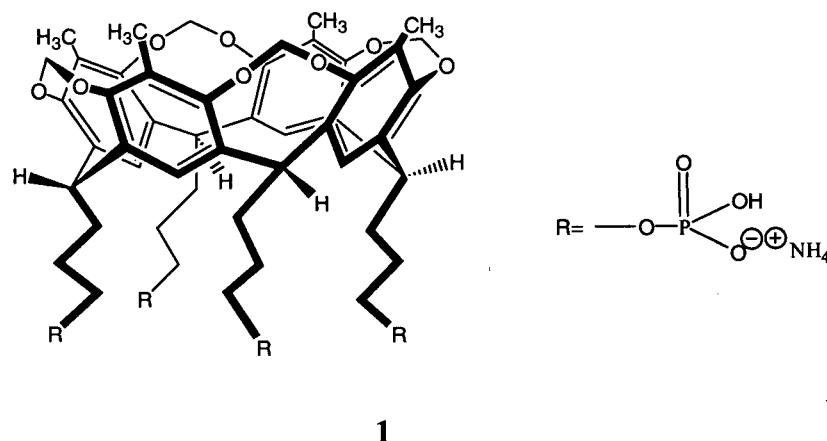


**Figure 1.2** Structure of cavitand

## 1.2. Water-Soluble Hosts and Their Complexing Properties

Of all known water-soluble hosts, cyclodextrins (CDs) provided the first, and probably the most important, examples of relatively simple organic compounds that exhibited complex formation with other organic molecules in water.<sup>10-14</sup> CDs are  $\alpha$ -1,4-linked cyclic oligomers of D-glucopyranose (six, seven or eight sugar moieties for  $\alpha$ -,  $\beta$ -,  $\gamma$ -CD's, respectively), (Figure 1.3). Since they are nontoxic, and commercially available natural products, they have found wide applications in pharmaceutical science,<sup>10</sup> food chemistry, and separation and sensor technologies.<sup>11,12</sup> The host-guest chemistry of cyclodextrins has been the subject of numerous books and recent review articles.<sup>11,13-14</sup> In context of the present work, an in depth discussion of CD's host guest chemistry is beyond the scope of this thesis. Thus, the following sections will primarily focus on artificial hosts.

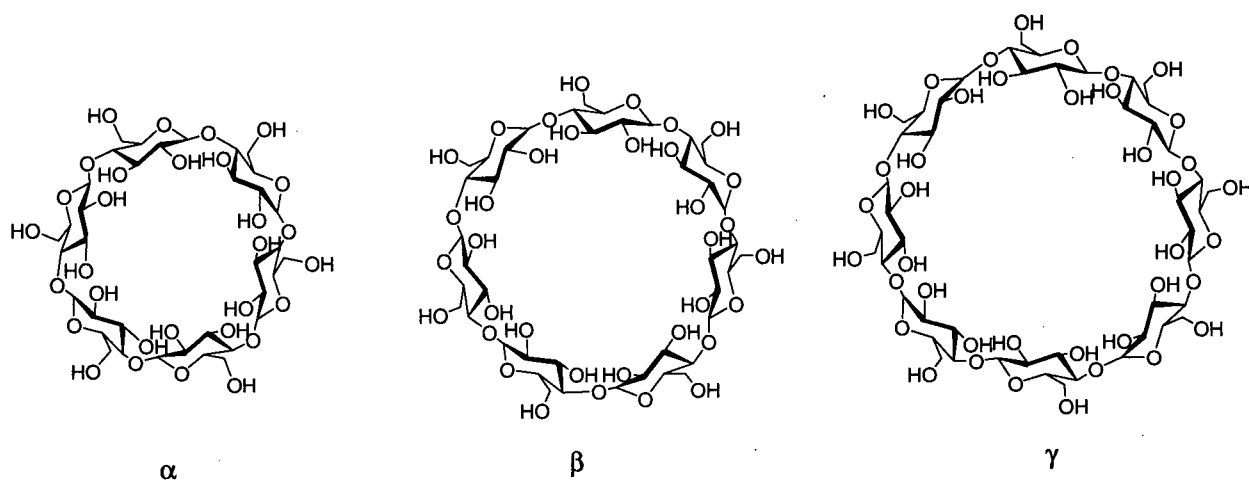
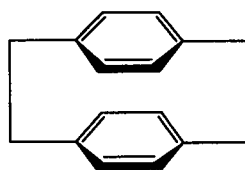


**Figure 1.3** Schematic representation of  $\alpha$ -,  $\beta$ -, and  $\gamma$ -cyclodextrin

#### **A. Water-Soluble Cyclophanes and Their Complexation Properties**

Cyclophanes, which are bridged aromatic macrocycles, play a central role in supramolecular chemistry.<sup>15</sup> The term “cyclophane” (derived from Cram and Steinberg’s [2,2]paracyclophane **2**)<sup>16</sup> encompass all molecular receptors with at least one aromatic ring bridged by at least one aliphatic n-membered chain.<sup>15a</sup>



**2**

**Figure 1.4** Cram and Steinberg’s [2,2]paracyclophane **2**

Cyclophanes have become the major class of synthetic organic hosts that substitute cyclodextrins to study host-guest chemistry in aqueous solutions.<sup>15</sup> Other macrocycles such as calixarenes, resorcinarenes and cavitands, which will be discussed in more detail in later sections, are all in fact special types of cyclophanes.

In the early 1970's, Tabushi, Murakami and co-workers first examined host-guest interactions of cyclophanes in aqueous solution.<sup>17</sup> Since then, a large variety of water-soluble cyclophanes with diverse hydrophobic cavities have been synthesized and their complexation properties with a variety of guest molecules have been studied extensively.<sup>15</sup> However, it was not until 1980, that Koga reported the first conclusive evidence for the inclusion of an apolar guest within the cavity of cyclophane **3** in aqueous media.<sup>18</sup> Cyclophane **3** is water soluble only at pH < 2 due to protonation of the nitrogen. X-ray crystallography showed the product that was crystallized from an aqueous solution doped with durene contained the durene guest in the central cavity of cyclophane **3**. This data provided the first unambiguous proof that it was indeed possible to design and build a water-soluble organic molecule with a hydrophobic cavity into which lipophilic guests would bind.<sup>18</sup>

This subsequently led to the synthesis of numerous analogues of Koga's initial design, differing only in the aliphatic linker.<sup>19</sup> These Koga-type host's selectively bind aromatic guests over aliphatic guests on the basis of steric complementary between host and guest.<sup>20</sup>

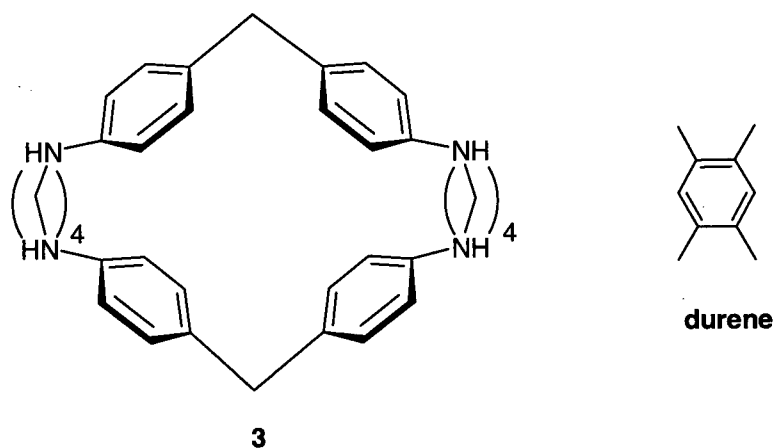


**Figure 1.5** Koga's type cyclophane

Diederich introduced an important class of hosts, e.g., macrocycle **4**, which has a spiro-fused ring containing a quaternary ammonium moiety to induce water solubility.<sup>21</sup> In these systems, the water solubilizing nitrogens were located away from the cavity. These structures and their derivatives contain a purely hydrophobic binding site and have been extensively studied by Diederich and co-workers.<sup>21</sup> For example, host **4** binds perylene very strongly (with  $\Delta G^0 = -40.2 \text{ kJ mol}^{-1}$  ( $K_a > 10^7$ )).<sup>21c</sup> Diederich studied binding with a number of lipophilic aromatic hydrocarbons. The  $K_a$  (binding constants) values obtained extensively follow the aqueous solubility sequence for these guests. At the mean time, a large reduction in binding stability was observed when the complexation was studied in methanol. These binding studies showed a favorable enthalpic contribution and a large unfavorable entropic contribution to the free energy of complexation in water. It is found that this large favorable enthalpic driving force is present only in aqueous solution, which indicate a special driving force for complexation exists only in water. Since water molecules are much less polarizable than organic substrates, the dispersion interactions between water molecules and the organic surfaces of both the binding site and the guest are less favorable than the interactions between the organic surfaces in the complex. Therefore, it is believed that hydrophobic and van der Waals interactions were the main forces for complexation of neutral aromatic guests in water for this host.<sup>21</sup>

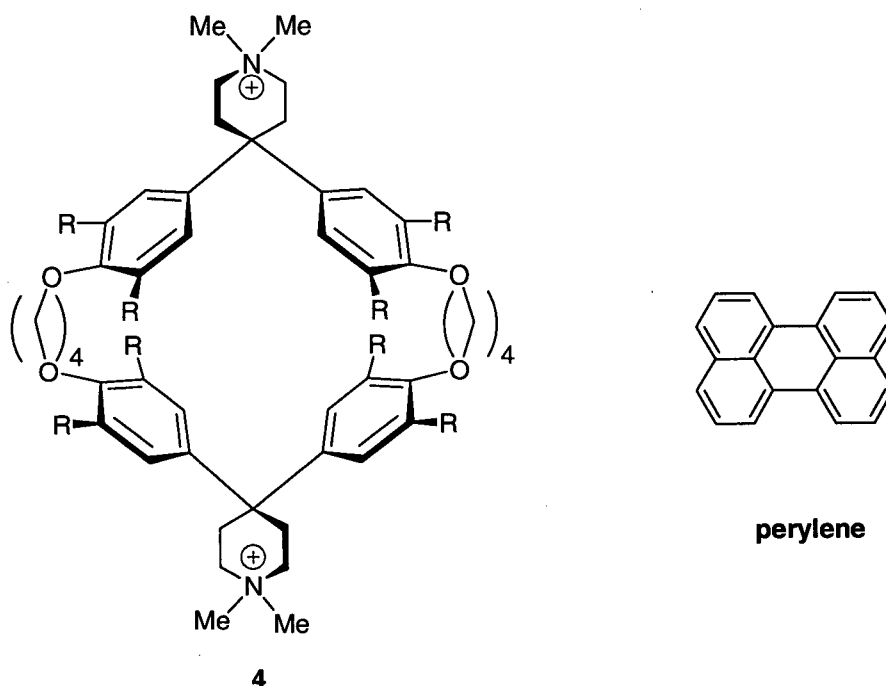


**Figure 1.6** Diederich's cyclophane **4** and guest perylene

Dougherty introduced a series of anthracene-bridged cyclophanes with the prototypical structure **5**.<sup>22</sup> The bicyclic bridge greatly preorganized the structure, locking the diphenyl methane unit into a rigid, face-to-face arrangement that would appear to be optimal for binding. Also, it allowed the introduction of carboxylate groups, held rigidly in a position remote from the hydrophobic cavity, to impart water-solubility. Interestingly, Dougherty found that these hosts (e.g. **5**) preferentially bound electron-deficient aromatic guests, which provided evidence that electron donor-acceptor  $\pi$ -stacking interactions were more important than hydrophobic effects for complexations between these electron rich hosts and neutral guest molecules in aqueous media.<sup>22</sup> Thermodynamic data revealed that large negative enthalpic values were accompanied with binding of electron-deficient guests (e.g. **G1** and **G2**), while a more positive entropy was found when binding with a more hydrophobic guest (e.g. **G4**).

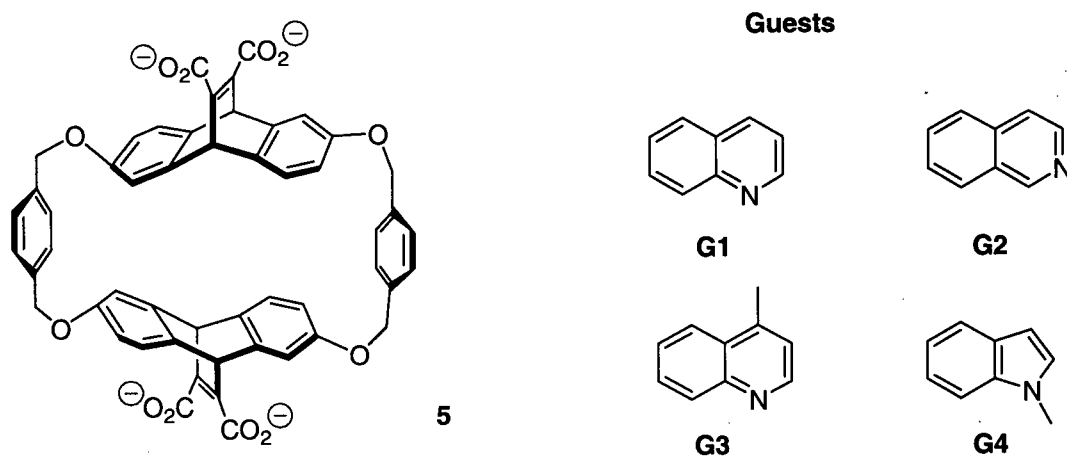


**Figure 1.7** Structure of cyclophane 5

Penadés made a number of “glycophanes” (e.g. 6) which can be considered as hybrids of cyclodextrins and cyclophanes.<sup>23</sup> These are particularly useful for studying carbohydrate recognition processes; such recognition is considered to be more complicated than recognition of other biological molecules such as amino acids (for example) due to the molecular complexity of the carbohydrates.

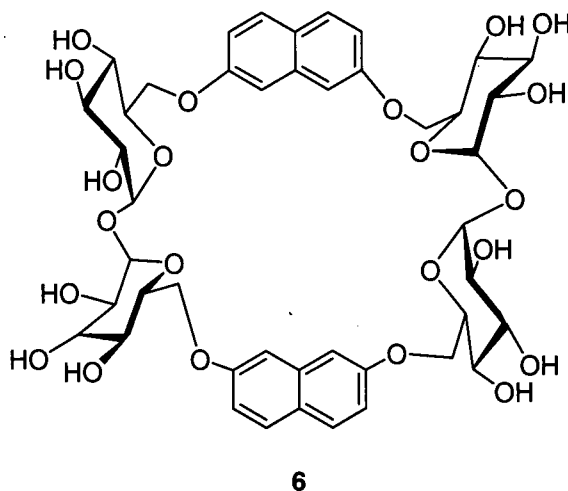


**Figure 1.8** Structure of glycophane 6

Vogtle,<sup>24</sup> Diederich<sup>25</sup> and Collet<sup>26</sup> have developed a number of elegant “macrobicyclic” systems, for example, **7**,<sup>24</sup> **8**,<sup>24</sup> **9**,<sup>25</sup> and **10**.<sup>26</sup> (Figure 1.9) These macrobicyclics provide a preorganized three-dimensional enforced hydrophobic cavity which is far superior for hydrophobic binding since noncovalent host-guest interactions are more effective in a well-desolvated and hydrophobic microenvironment.<sup>6</sup>

For example, compound **10a** can incorporate dichloromethane and chloroform into the spherical cavity in D<sub>2</sub>O at 300 K.<sup>26</sup> The driving force for stoichiometric CH<sub>2</sub>Cl<sub>2</sub> inclusion was measured as  $\Delta G^0 = -5.3 \pm 0.5 \text{ kcal mol}^{-1}$ . These complexes are approximately 1.4-2.0 kcal mol<sup>-1</sup> more stable than those formed by the same guests and the analogous host **10b** (R=Me) in organic solvents.<sup>26</sup> This reflects the stronger driving forces for neutral molecular complexation in aqueous solutions compared to organic solvents.

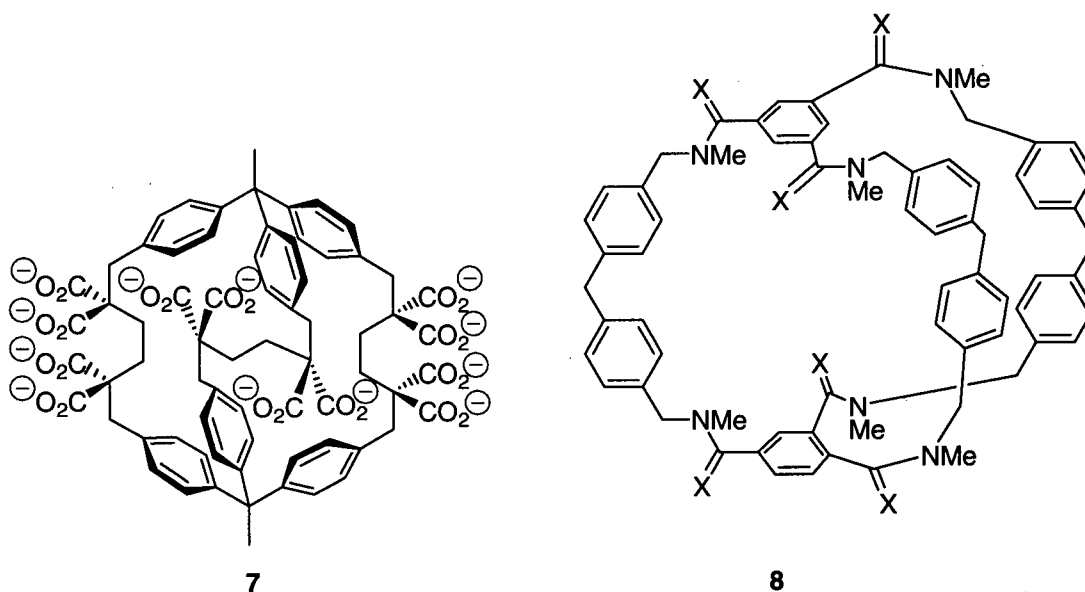


**Figure 1.9** Structures of cyclophane **7-10** (to be continued)



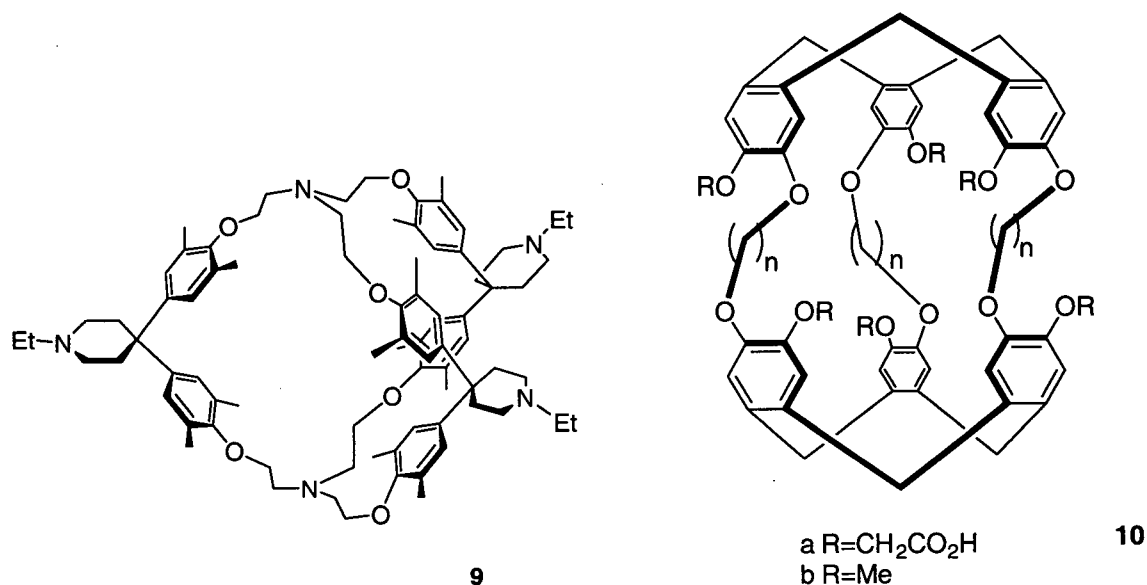


**Figure 1.9** Structures of cyclophane 7-10

## B. Water-Soluble Calixarenes

Calix[n]arenes are [1<sub>n</sub>] metacyclophanes, which are synthesized by condensation of formaldehyde with phenol under basic conditions.<sup>27</sup> The bracketed number “n” between “calix” and “arene” specifies the size (or the number of benzene rings) of the macrocycle (mainly 4, 6 and 8). Calixarenes are a type of receptor that are structurally related to the cavitand host **1** (see Figure 1.2) which is the research focus of this thesis.

The calix[4]arene skeleton has four different possible conformations in which the cone conformation (Figure 1.10) with all phenolic oxygen atoms on the same side of the molecule is most widely used. Calixarenes contain two distinct regions: (i) the “upper rim”

defined by the substituents para to the phenolic hydroxyl groups, and (ii) the “lower rim” defined by the phenolic groups adjacent to the methylene bridges. Derivatization of the upper and lower rims with appropriate polar groups can result in substantial solubility in aqueous media.

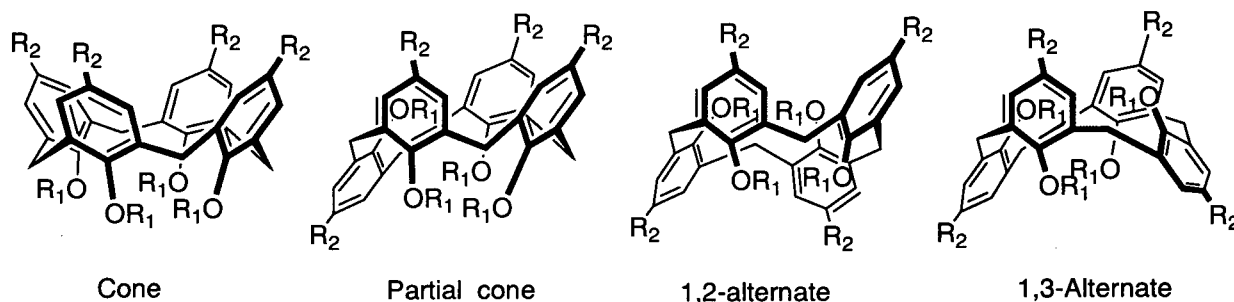


**Figure 1.10** Conformations of calix[4]arene

Ungaro reported the first example of a water-soluble calix[4]arene in the fixed cone conformation,<sup>28</sup> i.e., compound **11b**, which was obtained by introducing four carboxylate groups at the lower rim of the parent compound **11a**. Further reaction of tetracarboxylic acid **11b** with amino acids gave the chiral water-soluble compound **11c**.<sup>29</sup>

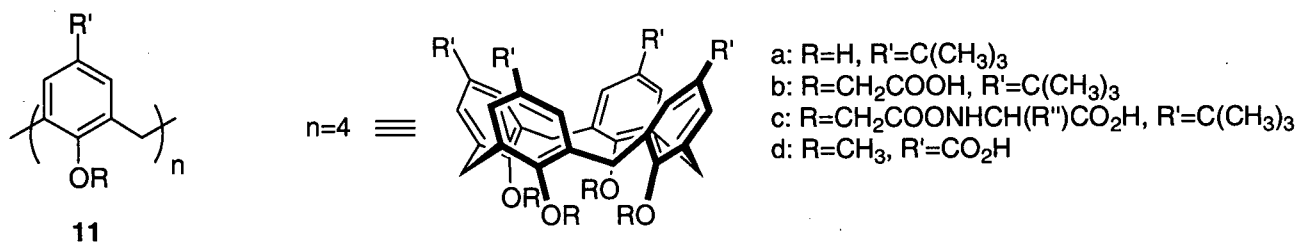


**Figure 1.11** Calixarenes **11a-d**

Introduction of carboxylic acid moieties at the upper rim, giving calixarene such as **11d**, for example, has been reported by Gutsche et al.<sup>30</sup>

Calix[4]arene **11a** forms inclusion complexes with aromatic guests such as benzene, toluene, and *p*-xylene in the solid-state, but complexation of these guests in water by the analogous calix[4]arene tetracarboxylic acid **11b** could not be observed.<sup>28</sup> The same behavior was also observed by Gutsche with tetracarboxylic acid derivatives **11d**.<sup>30</sup> Due to their larger dimensions, the higher calixarenes **11d** (*n*=6, 8) were able to bind polyaromatic guests such as naphthalene and perylene in water with association constants varying from less than 100 up to  $4.4 \times 10^4 \text{ M}^{-1}$ .<sup>30b</sup> Recently, the chiral tetracarboxylic acid **11c** was used as a mobile phase additive in capillary electrophoresis allowing the enantiomeric resolution of racemic ( $\pm$ )-1,1'-binaphthyl-2,2'-diyl hydrogen phosphate (BNHP).<sup>29</sup>

Shinkai and co-workers have reported several highly water-soluble sulfonated calix[*n*]arenes such as **12b**.<sup>31</sup> By applying similar methodology, Ungaro synthesized many lower rim functionalized, upper rim sulfonatocalix[4]arenes **12c<sub>4</sub>-12h<sub>4</sub>** (The subscript has the same meaning with the bracketed number "*n*").<sup>32</sup> Synthetically, these compounds were readily obtained by treating the appropriate protio calixarene precursor (e.g. **12a<sub>4</sub>**) with concentrated sulfuric acid.<sup>31</sup> Calixarene **12b<sub>4</sub>** is conformationally mobile, while sulfonated calix[4]arenes **12c<sub>4</sub>-12h<sub>4</sub>** are all locked in the cone conformation, differing only in cavity shape and rigidity due to the substituents at the lower rims.

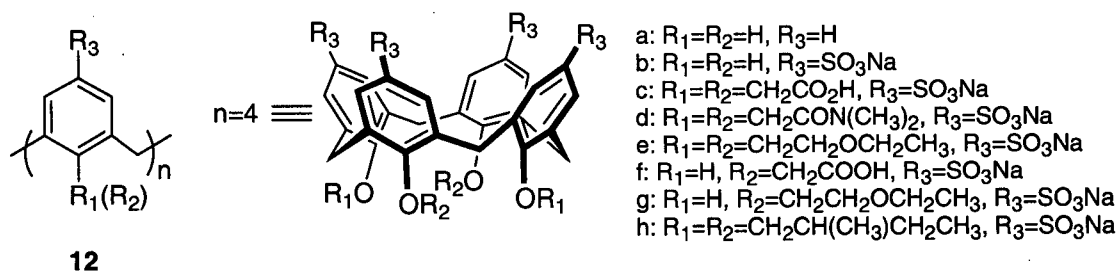
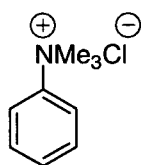
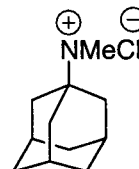


Figure 1.12 Calixarenes 12

At pD=7.3, calix[4]arene **12b<sub>4</sub>** formed complexes with trimethylanilinium cation **13** (TMA,  $K_a=5600\text{ M}^{-1}$ ) and adamantyltrimethylammonium cation **14** ( $K_a=21000\text{ M}^{-1}$ ).<sup>31</sup>



**13**



**14**

The hexasulfonated calix[6]arene **12b<sub>6</sub>** and octasulfonated calix[8]arene **12b<sub>8</sub>** have greater conformational flexibility compared to the homologous calix[4]arene **12b<sub>4</sub>**. However both these hosts can bind ions and neutral molecules through an “induced fit” mechanism.<sup>31</sup> Organic cations such as TMA form 1:1 host-guest complexes with calix[6]arene **12b<sub>6</sub>**, and both 1:1 and 1:2 complexes with the calix[8]arene **12b<sub>8</sub>**. The stability constants are, however, lower than those found for calix[4]arene **12b**. Examination of the thermodynamic parameters for the complexation process reveals that binding is due to both electrostatic and apolar forces, with the latter contributing more significantly in the case of hexa- and octa- sulfonated compounds (A large negative enthalpy was found in binding of **12b<sub>4</sub>**, while a positive entropy change was accompanied with the complexation of **12b<sub>6</sub>** and **12b<sub>8</sub>**).<sup>31</sup> A similar conclusion was reached in 1993 by Lokel and Kaifer who studied the inclusion complexation of ferrocene derivatives **15-17** in calix[6]arene hexasulfonate **12b<sub>6</sub>** in aqueous solution.<sup>33</sup>  $K_a$ 's of  $10930\pm960\text{ M}^{-1}$ ,  $7610\pm680\text{ M}^{-1}$ ,  $3650\pm360\text{ M}^{-1}$  were calculated respectively for the ferrocene derivatives **15-17**. <sup>1</sup>H NMR

data showed that the ferrocene moiety of the guests were included into the flexible calixarene cavity.

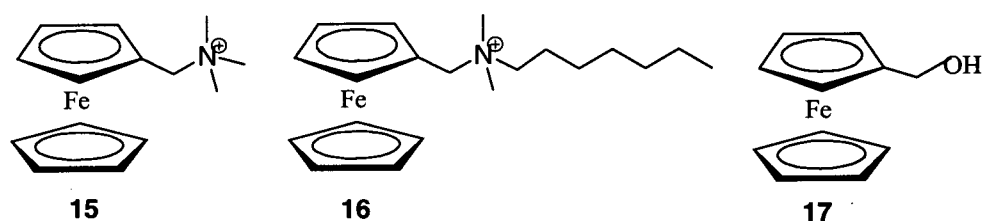


**Figure 1.13** Ferrocene derivatives 15-17

The complexation behavior of calix[4]arene **12c<sub>4</sub>-12h<sub>4</sub>** with TMA, tetramethyl ammonium cation (TEMA), and  $\alpha$ -amino acids were also investigated.<sup>32</sup> Although the observed inclusion of the apolar groups of TMA and  $\alpha$ -amino acids suggest that hydrophobic effects may account for their complexation, all the studies thus far, indicated that these inclusion processes are in fact charge assisted. For example, using an analogue of **12c<sub>4</sub>** which lacks of the sulfonate groups on the upper rim of the calixarene as host leads to a much smaller binding affinity with the guests that mentioned above. Usually the electrostatic interactions between the ammonium ion and the charged aromatic cavity are the major driving forces for this inclusion.<sup>32</sup>

Interestingly, derivatizing the lower versus the upper rim of calix[n]arenes with sulfonate groups results in hosts with different binding properties.

A comparison of the binding properties of water-soluble calixarenes of type **12** ( $R_1=R_2=Me, Bu, Hex$ ) and of type **18** using pyrene as the guest led to the conclusion that compounds **12** have a strong but non-selectively apolar binding site, whereas calixarenes **18** have a relative weak but more selective binding site.<sup>34</sup> For example, pyrene was

selectively bound by the calix[6]arene **18c**, but not by the tetra- or octa- derivatives of **18c**. In contrast, the binding strengths of pyrene with calix[n]arenes **12** ( $R_1=R_2=Bu$ ) increased with the number of n ( $n=4-8$ ). This may be accounted for as follows: that alkyl groups on the different positions of the calixarenes act differently in the binding, viz.: alkyl groups at lower rims act as a cooperative binding site, while alkyl groups at upper rims control the cavity size.

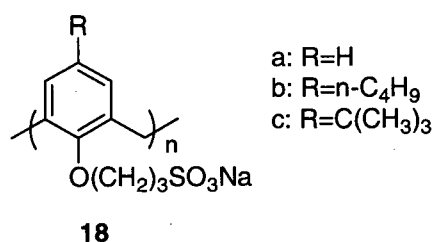
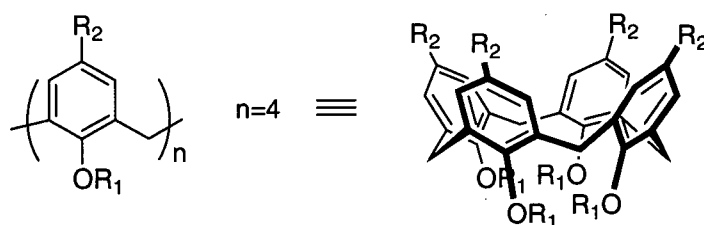


**Figure 1.14** Calixarenes **18a-c**

Other methods for imparting water-solubility include introduction of phosphonate,<sup>35</sup> trialkyl ammonium,<sup>36</sup> and amino acid<sup>37</sup> groups at the upper rim of the calixarene.

Besides the charged calixarenes that were mentioned above, some neutral water-soluble calix[n]arenes have also been synthesized.<sup>38-41</sup> The first such example was reported in 1990 by Shinkai and Reinhoudt,<sup>38</sup> who synthesized calix[4]arene sulfonamide **19<sub>4</sub>** by conversion of sulfonatocalix[4]arene **12b<sub>4</sub>** to its acid chloride using thionyl chloride and subsequent reaction with diethanolamine.



- 19:**  $R_1=H$ ,  $R_2=SO_2N(CH_2CH_2OH)_2$   
**20:**  $R_1=CH_3$ ,  $R_2=CH_2C[C(O)NHC(CH_2OH)_3]_3$   
**21a:**  $R_1=CH_2CO_2CH_2CH_3$ ,  $R_2=SO_2NHC(CH_2OH)_3$   
**21b:**  $R_1=CH_2CO_2CH_2CH_3$ ,  $R_2=SO_2N(CH_2CH_2OH)_2$

**Figure 1.15** Calixarenes **19-21**

Neutral water-soluble calixarenes **19** ( $n=6,8$ ) bind strongly with naphthalene sulfonate compounds **22** and **23**.<sup>39</sup> It was discovered that **23** is bound to calix[6]arene **19<sub>6</sub>** and calix[8]arene **19<sub>8</sub>** more strongly than **22**, which was attributed to the fact that the more linear molecule **23** could be bound deeper into the calixarene cavity than the wider and bulkier shaped **22**. Calix[8]arene **19<sub>8</sub>** has a  $K_a$  value 4.2 times greater than that of hexa-derivative.<sup>39</sup> Since calix[8]arene **19<sub>8</sub>** is advantageous in an induced-fit-type complexation; it is easier for calix[8]arene **19<sub>8</sub>** to adopt a face-to-face orientation, which is required for hydrophobic interactions. Hydrophobic forces are explained as the main driving forces behind complexation in this system.

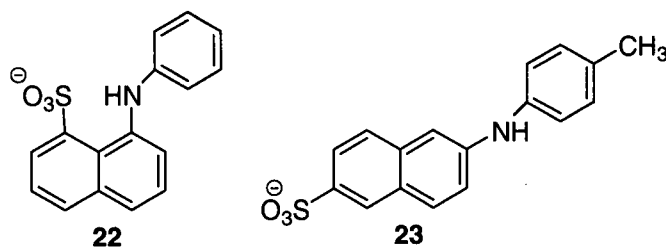


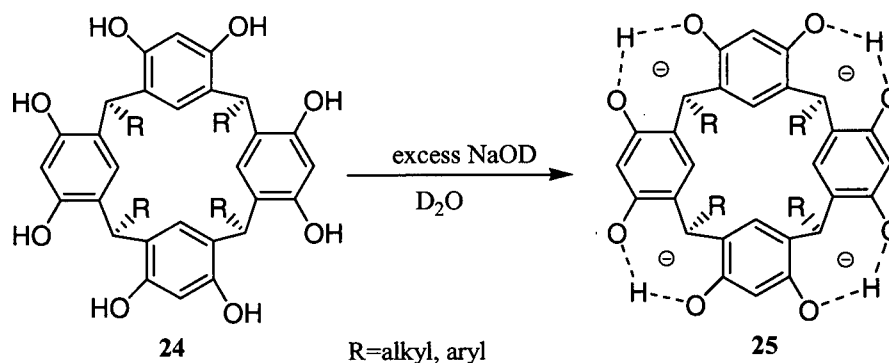
**Figure 1.16** Ionic guests **22** and **23**

Newkome et. al. developed the *silvanols* (e.g. **20**) with hydroxyl group-containing amides at the upper rim,<sup>40</sup> of which the calix[4]arene derivative contains 36 hydroxyl groups. Reinhoudt found that water-solubility of calixarenes can be dramatically improved by increasing the number of hydroxyl groups in calix[4]arene sulfonamides. Each additional hydroxyl group per aromatic unit of the calix[4]arene leads roughly to a hundred-fold increase in water-solubility.<sup>41</sup> For example, compound **21a** can dissolve in water up to 0.3 M, while calix[4]arene **21b** is only water soluble up to  $9 \times 10^{-4}$  M.<sup>41</sup>

### C. Water-Soluble Resorcin[4]arenes

Resorcin[n]arenes are calixarenes that are made using resorcinol. The acid-catalyzed condensation of resorcinol and aldehydes (formaldehyde, aliphatic and substituted benzaldehydes) lead to the selective formation of resorcin[4]arenes **24**.<sup>42</sup> Just like calix[4]arenes, resorcin[4]arenes consist of a number of distinct conformers of which the crown conformer (comparable to the cone conformer of the calix[4]arenes) is predominantly formed. Although resorcinarenes have been known for decades,<sup>42</sup> very little complexation studies in aqueous media have been conducted with these systems.





**Scheme 1.1** Deprotonation of **24** under basic condition

It is well known that in alkaline solution, each of the resorcinol units in resorcin[4]arene **24** is only singly deprotonated, resulting in the tetra-anion **25**, which exhibits high stability (even in sodium methoxide solution) due to the formation of four charged hydrogen bonds and the delocalization of the negative charges.<sup>43a</sup>

Schneider et al. first studied the host-guest complexation of resorcin[4]arene **25** in alkaline solution with a series of trimethyl ammonium derivatives.<sup>43</sup> They concluded that the observed strong binding ( $K_a = 3 \times 10^4 \text{ M}^{-1}$  in 0.5N NaOD) with this host is due to electrostatic attraction between  $\text{R}_3\text{N}^+\text{Me}$  and the anionic macrocycle. The binding strength is only moderately affected by changing the solvent polarity,<sup>43b</sup> which indicates that the hydrophobic effect is not the main driving force for this inclusion. It was found that the decrease in binding energy  $\Delta G^\circ$  has a linear relationship with the increase in distance ( $r$ ) between the charge centers  $\text{O}^-$  (on the host) and  $\text{N}^+$  (on the guest) (estimated from CPK models), and it satisfied the simple Coulombic relationship. Also, neutral molecules, e.g. tert-butylphenol ( $K_a = 7 \text{ M}^{-1}$  in 0.5N NaOD) are hardly complexed with the resorcin[4]arene **25**.<sup>44</sup> This indicates that the interaction is based almost exclusively on electrostatic interactions between the positively charged  $\text{R}_3\text{N}^+\text{Me}$  and the negative charges in **25**.<sup>45</sup> More recently, the complexation of alkylammonium cations with resorcin[4]arenes

**25** has also been confirmed by X-ray crystallographic analysis.<sup>46</sup> This strong binding of methylammonium cations by resorcinarene **25** also suggests potential application as a molecular sensor.<sup>47</sup> For example, the orange fluorescence of the pyrene modified pyridinium dyes can be strongly quenched by complexation with **25**. On addition of the neurotransmitter acetylcholine to the nonfluorescent solution of pyridinium dyes and **25**, the fluorescence regeneration can be observed. But the fluorescent spectra can not be affected by the addition of any other low molecular weight neurotransmitters.

In 1990, Manabe and Shinkai made a new water-soluble resorcin[4]arene (**26**) by introducing hydrophilic sulfonate groups into resorcinarene **24** through a diazo-coupling reaction with *p*-sulfonato benzene diazonium.<sup>48</sup> Such extension of the upper cavity of resorcin[4]arenes enables complexation of even larger guest molecules, for example, adamantane ( $K_a = 2.0 \times 10^4 \text{ M}^{-1}$ ), pyrene ( $K_a = 3.7 \times 10^4 \text{ M}^{-1}$ ) and coronene ( $K_a = 4.6 \times 10^4 \text{ M}^{-1}$ ).<sup>48</sup>

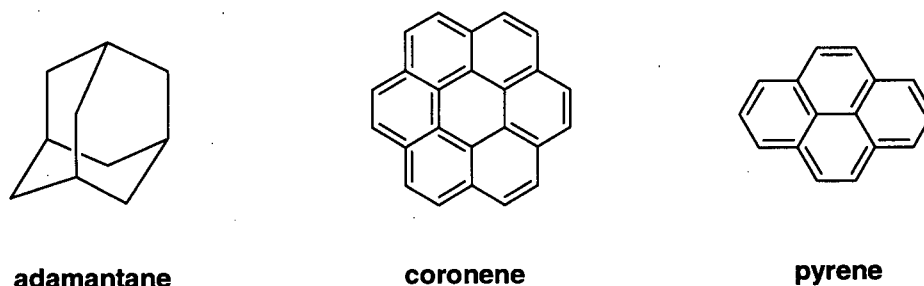


**Figure 1.17** Structures of the aromatic guests

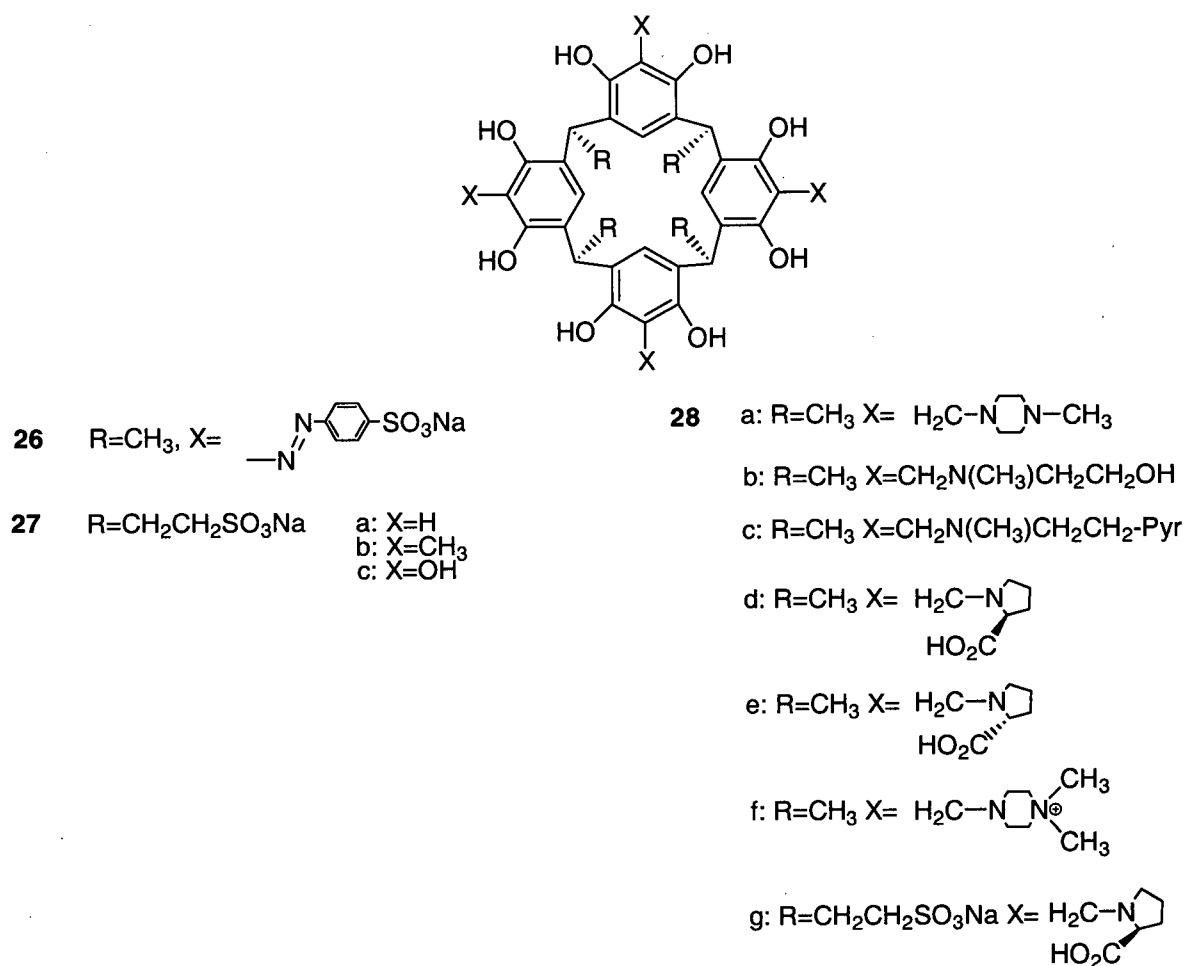


**Figure 1.18** Structures of resorcinarenes **26-28**

Acid-catalyzed condensation of sodium 2-formyl ethane-1-sulfonate with resorcinol afforded tetra-sulfonate derivatives of resorcinarenes **27a-c**.<sup>49</sup> These molecules are readily soluble in water with solubilities up to 0.4 M at room temperature.

Resorcin[4]arene tetrasulfonates **27a-c** bind a series of relatively hydrophobic mono saccharide derivatives (some aldopentases and deoxy and methylated sugars), aliphatic alcohols (ethanol-hexanol)<sup>49</sup> and (hydrophobic) amino acids<sup>50</sup> in water with association constants in the order of 1 to  $10^2$   $M^{-1}$ .  $^1H$  NMR complexation induced shift data indicate that the hydrophobic moiety of the guest is incorporated in the aromatic cavity of the host.

Higher binding affinities were obtained in the cases of **27b** ( $X=CH_3$ ) and **27c** ( $X=OH$ ) than with **27a** ( $X=H$ ), due to the electron-donating capacity of the  $CH_3$  and  $OH$  groups. Both **27b** and **27c** favor hydrophobic over hydrophilic guests, viz., saccharides bearing three or more hydroxyl groups are hardly complexed by either of the hosts ( $K_a < 10\text{ M}^{-1}$ ). However, hydrophilic guest molecules form stronger complexes with **27b**, which has a more hydrophobic cavity. These results lead to the conclusion that for these calixarene derivatives, binding in water is not simply due to the hydrophobic effect but the  $CH-\pi$  interactions involving the electron-rich benzene rings of the host as  $\pi$ -bases play an important role.<sup>51</sup>

Matsushita and Matsui utilized the Mannich reaction to functionalize resorcin[4]arenes.<sup>52</sup> Reaction of **24** ( $R=CH_3$ ) with formaldehyde and a secondary amine gave compounds **28a-c** in 59-69% yield all of which are water-soluble under neutral conditions.

Schneider and Schneider permethylated aminoresorcin[4]arene **28a** to afford the quaternary ammonium salt **28f**.<sup>53</sup> More recently, Aoyama et. al. synthesized the chiral derivative **28g** by introducing the L-prolinylmethyl moieties on the upper rim of the sulfonated resocinarene **27a** using the Mannich reaction.<sup>54</sup> Resorcin[4]arene **28g** was used as a non-lanthanide chiral NMR shift reagent for aromatic guests in water. Thus, upon complexation of a pair of enantiomers, readily distinguishable NMR shifts for the aromatic hydrogen atoms of the guest appear.<sup>54</sup>

Kijima et al obtained water-soluble dicationic resorcin[4]arene **29** by condensation of *p*-amino benzaldehyde and resorcinol under acidic conditions, but no binding studies were reported.<sup>55</sup>

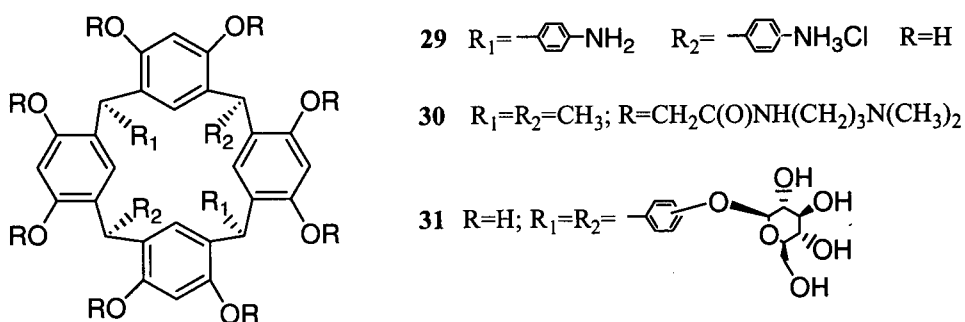


**Figure 1.19** Structures of resorcinarenes 29-31

Williams et al. made the first neutral, water-soluble octaamino resorcin[4]arene **30** by alkylation of the hydroxyl group of the precursor resorcin[4]arene **24** with ethyl bromoacetate, followed by conversion of the ester groups with 3-(N, N-dimethylamino) propylamine to octaamide **30**.<sup>56</sup> These authors have used **30** as an artificial esterase for 4-nitrophenyl esters of a variety of carboxylic acids. The overall mechanism is believed to involve complexation of the substrate with the resorcin[4]arene **30** in the first step, followed by an intracomplex nucleophilic reaction of the dimethylamino moiety with the ester. The reactive N-acyl-ammonium species that is then formed breaks down rapidly via reaction with water to form an acid and regenerates the amines. At pH 9.6, resorcin[4]arene **30** has a catalytic efficiency towards 4-nitro phenyl acetate 180 times higher than a dimethyl amino group of similar  $pK_a$ .<sup>56</sup>

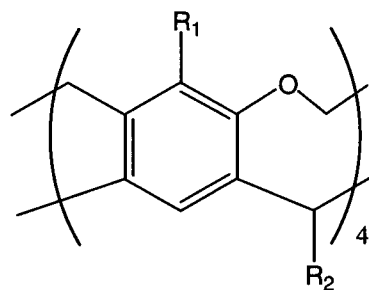
Curtis developed the glycoside resorcin[4]arenes **31** by condensation of resorcinol with glycosidic aldehydes followed by deacylation of the hydroxyl group.<sup>57</sup> It was suggested that **31** can be used as a potential chiral receptor.

#### D. Water-Soluble Cavitands

By bridging the hydroxyl groups of the resorcinarene, one can make a new type of macrocycle with an extremely rigid cavity. The name cavitands was given by Cram to this class of synthetic compounds, which contain an enforced concave cavity sufficiently large to accommodate other molecules or ions.<sup>58</sup> Cavitands are excellent receptors for specific binding of cations and neutral molecules due to their rigidity and enforced cavity. Most of the complexation studies to date of the cavitands have been performed in organic media.<sup>58</sup> Water-soluble cavitand hosts are not as readily available as the other synthetic water-soluble hosts discussed this far. As a result, little research has been published on the host-guest complexation in aqueous media for these systems.

##### i. Introducing Hydrophilic Functionalities into the Cavitand Rims

Our group first synthesized the water-soluble cavitands **32a** and **32b**.<sup>59</sup> Both have similar solubilities (up to 0.4 M) in aqueous solutions, but they behave differently in water. The <sup>1</sup>HNMR spectrum of **32b** in D<sub>2</sub>O is sharp, well resolved and concentration independent. In contrast, the spectrum of **32a** is broad, suggesting the pendent phenethyl groups promote aggregation in water.<sup>59</sup> The thiol derivative **33a** has been used to create de novo protein in aqueous solutions, by coupling **33a** with peptide chains to give the so-called "caviteins" **33b** (i.e., cavitand protein hybrid).<sup>60</sup> However, no complexation studies were reported.

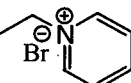


32 a:  $R_1 = ^-\text{ONa}^+$   $R_2 = \text{CH}_2\text{CH}_2\text{Ph}$

b:  $R_1 = ^-\text{ONa}^+$   $R_2 = \text{CH}_3$

33 a:  $R_1 = \text{SH}$   $R_2 = \text{CH}_3$

b:  $R_1 = \text{S-Peptide}$   $R_2 = \text{CH}_3$

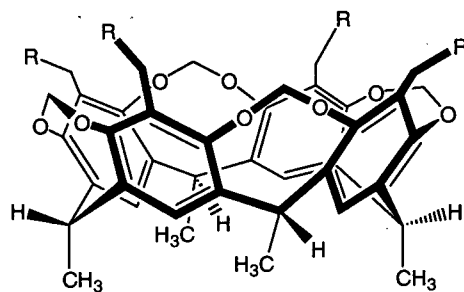
34  $R_1 =$   a.  $R_2 = \text{CH}_3$   
 b.  $R_2 = \text{C}_5\text{H}_{11}$   
 c.  $R_2 = \text{C}_{11}\text{H}_{23}$

35  $R_1 = \text{CH}_2\text{Br}$  a.  $R_2 = \text{CH}_3$   
 b.  $R_2 = \text{C}_5\text{H}_{11}$   
 c.  $R_2 = \text{C}_{11}\text{H}_{23}$

**Figure 1.20** Structures of cavitands **32-35**

More recently, Reinhoudt's group synthesized cationic cavitands **34a-c** by reaction of bromomethyl cavitands **35** with pyridine in ethanol.<sup>61</sup> These new cavitands show different behavior in water. Interestingly, it was found that the most hydrophobic cavitand **34c** exhibits the highest water-solubility. This is attributed to the formation of aggregates as is evidenced from the considerable peak broadening observed in the  $^1\text{H}$  NMR spectra of **34b** and **34c** in water.

Synthesis of another water-soluble cavitand by incorporating water-solubilizing groups at the rim position has been reported by Lemaire.<sup>62</sup> Reaction between cavitand **35a** and KCN in dry DMSO gave the tetrakis(cyanomethyl) cavitand which was hydrolyzed in an EtOH/H<sub>2</sub>O mixture with KOH to give the carboxymethylene analogue **36** in 74% yield. Reaction between **35a** and diethanol amine in dry DMSO gave **37** in 88% yield.<sup>62</sup> Water-solubility studies showed that tetracarboxylic acid **36** was only soluble at pH 11,<sup>62</sup> while cavitand **37** was soluble both in neutral and basic aqueous media.<sup>62</sup>



**36** R=COOH

**37** R=N(CH<sub>2</sub>CH<sub>2</sub>OH)<sub>2</sub>

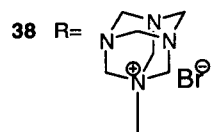


**Figure 1.21** Structures of cavitands **36-38**

Lamaire studied the complexing behavior of cavitands **32b**, **36**, and **37** with Cs<sup>+</sup> by UV-visible analysis.<sup>62</sup> By measuring the absorption changes in the UV wavelength range for the ligand in the presence of increasing amounts of CsCl, they found only **32b** showed a significant hypsochromic shift, which led to a stability constant value of  $35 \times 10^3 \text{ M}^{-1}$  for a 1:1 stoichiometry of Cs<sup>+</sup> and **32b**.<sup>62</sup>

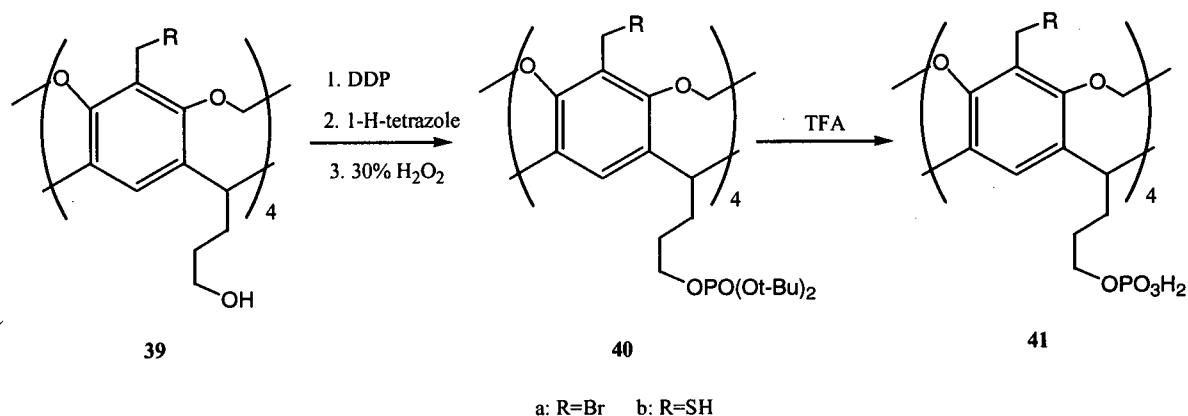
Hong and coworkers synthesized another water-soluble cavitand **38** by reaction of bromomethylcavitand **35a** with hexamethylenetetramine in CHCl<sub>3</sub>.<sup>63</sup> This cationic host binds anionic, aromatic guests strongly ( $K_a$  varied from  $10^2$  to  $10^4 \text{ M}^{-1}$ ).<sup>63</sup> In this instance, electrostatic interactions as well as hydrophobic interactions are the major binding forces for the strong complexation in water.



## ii. Introduction of Hydrophilic Functionalities into the Cavitand's Pendent Groups

Incorporating the water-solubilizing functionalities into the pendent group of the cavitand can lead to a more "clear-cut" separation between the hydrophobic cavity and the polar groups that are necessary for water solubility. This could increase the lipophilicity of the binding site and aid in the analysis of binding phenomena by delocalization of the hydrophilic end from hydrophobic cavity.

Recently, our group has synthesized novel water-soluble cavitand **41** from the hydroxyl-footed methylene-bridged cavitand **39**.<sup>65a</sup> Phosphate footed benzyl bromide **41a** and benzyl thiol **41b** were synthesized by phosphorylation of the propanolic feet with di-tert-butyl N, N-diethylphosphoramidite (DDP). Oxidation with hydrogen peroxide at  $-78^{\circ}\text{C}$  followed to afford tetra tert-butyl-protected phosphate **40**. Subsequent removal of the tert-butyl groups with TFA afforded phosphate-footed benzyl bromide **41a**. **41b** was obtained via similar route accompanied by the protection and deprotection of the thiol group.



**Scheme 1.2** Synthetic route of cavitand **41**

Unfortunately, the phosphorylation did not proceed to completion and resulted in residual amounts of the corresponding tris-phosphate impurity. Attempts to further purify

the compound before and after removal of the tert-butyl groups were unsuccessful, but further derivatization led to isolable products. Thus, these new types of water-soluble cavitands open the door to a variety of new areas of cavitand chemistry for molecular recognition studies. They have also been used as templates for the organization of peptide structures.<sup>65b</sup>

Rebek made the water-soluble cavitand **42b** with an extended deep cavity.<sup>64b</sup> Octaamido cavitand **42a** shows moderate affinity for adamantane and cyclohexane derivatives in nonpolar solvents.<sup>64a</sup> The resulting complexes exhibit high kinetic stability. Desilylation of **42a** with aqueous HCl yields a dodecahydroxy cavitand, which quickly rearranged to the corresponding octahydroxyl tetraammonium salt **42b**.<sup>64b</sup> **42b** exhibits excellent water solubility and shows gross conformational changes by adding appropriate guests. The resulting complexes show slow exchange on the NMR time scale and high kinetic stability in water.<sup>64b</sup>

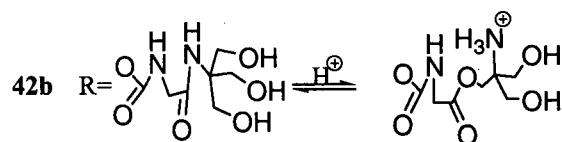
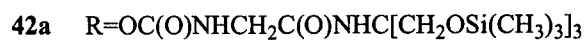
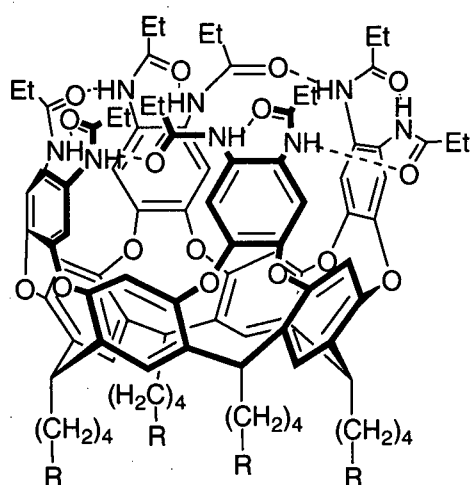
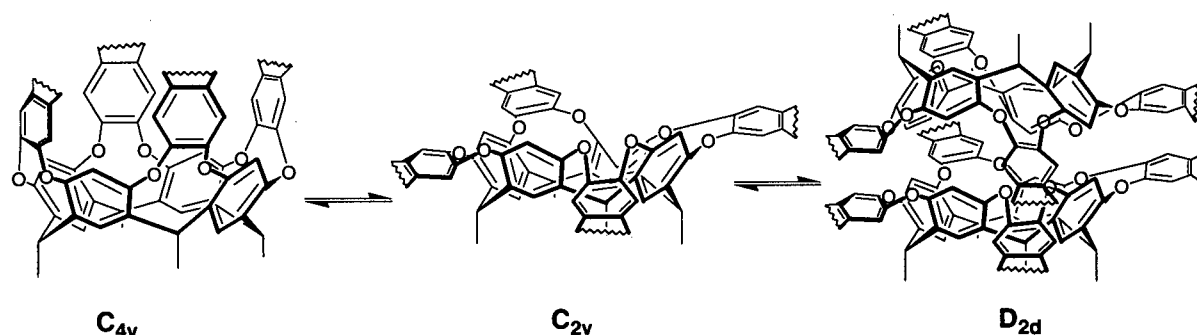


Figure 1.22 Structures of cavitands **42a-b**

Compound **42b** forms dimer in water in its kite form ( $C_{2v}$  symmetry, Figure 1.23) which equilibrates with the velcrand form ( $D_{2d}$  symmetry), as is evident from  $^1\text{H}$  NMR and mass spectroscopies. By addition of appropriate guests, such as aminomethyladamantane and aminomethylcyclohexane hydrochlorides and N-methyl quinuclidinium trifluoroacetate, the host symmetry returns to  $C_{4v}$  with guest signals showing slow exchange on  $^1\text{H}$  NMR time scale in which both the bound and the free guest signals are observed.<sup>64b</sup>



**Figure 1.23** Proposed schematic representation of the  $C_{4v}$ - $C_{2v}$ - $D_{2d}$  conformation equilibrium for water-soluble cavitand **39b**

Hydrophobic interactions are believed to be the main driving forces here. Additionally, the convex hydrocarbon surfaces of the guests are complementary to the concave  $\pi$ -bonded inner surface of host **42b**. However, cation- $\pi$  interactions are not strong, since the smaller guest *isobutylammonium* hydrochloride also fixes the vase cavity of **39b** but doesn't result in a kinetically stable complex (indication of a weaker binding). There is certainly not enough hydrophobic contact within the host-guest complex to slow the exchange.<sup>64b</sup>

### iii. Water-Soluble Carceplexes

Hemicarceplexes are well-known candidates for drug delivery systems.<sup>66</sup> Yoon and Cram synthesized the first water-soluble hemicarcerand **44** in 15% yield by reaction of tetrol **45** with dibromide **46** in N-methylpyrrolidinone (NMP) in the presence of  $\text{Cs}_2\text{CO}_3$ .<sup>67</sup> The resulting ester **44** was then hydrolyzed to give octaacid **43** in 90% yield.<sup>67</sup>

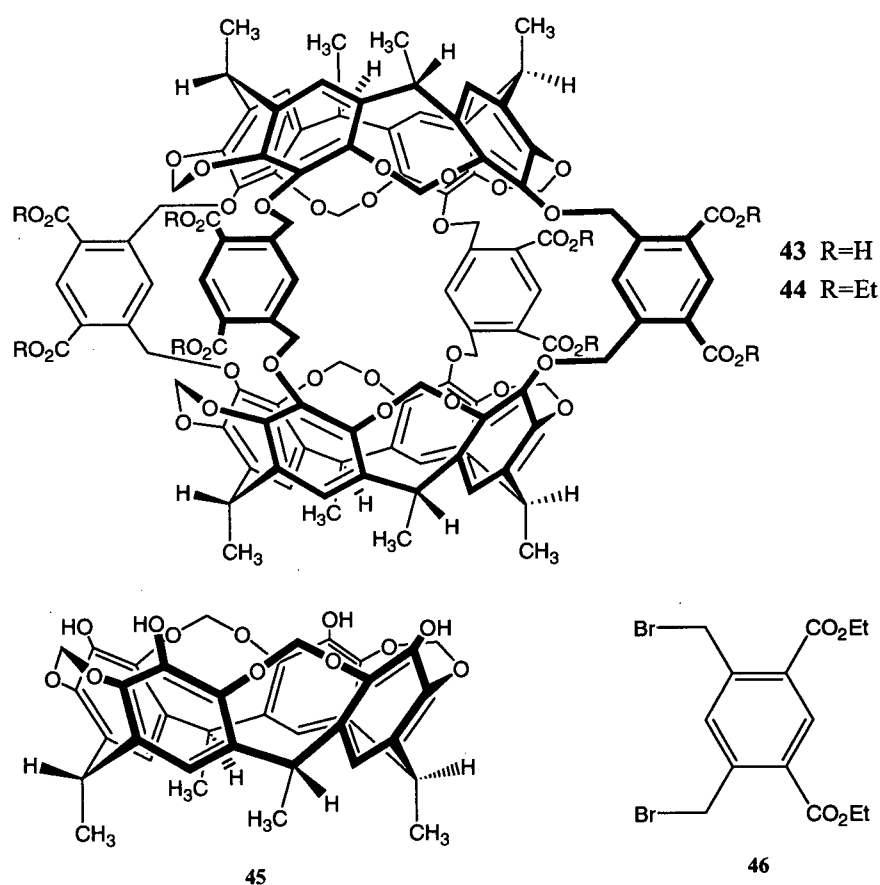
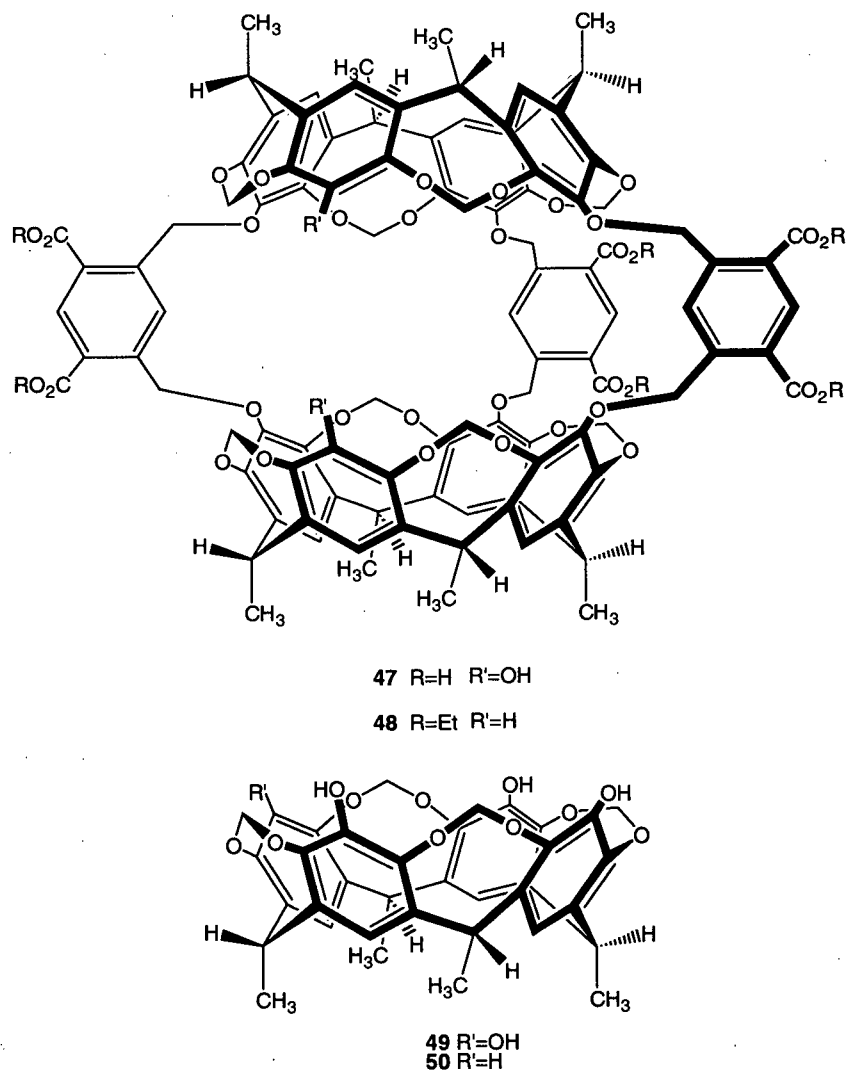


Figure 1.24 Hemicarcerands **43**, **44** and their building blocks **45**, **46**

Hemicarcerand **43** can include various neutral aromatic and aliphatic compounds with different size, polarity and water-solubility within its enforced spherical cavity.  $^1\text{H}$  NMR spectroscopy shows the guest's chemical shifts moved upfield by as much as 4 ppm.

indicating that the guest is deeply held within the shielding interior of host **43**. Unfortunately, no thermodynamic data was reported.<sup>66</sup>

Based on Cram's structure, two novel closed-shell hemicarcerands with enlarged portals have also been synthesized by Deshayes group.<sup>68</sup> Host **47** was prepared from tetrol **49**, and **48** was obtained from triol **50**, which is a by-product of **49**.



**Figure 1.25** Hosts **47**, **48** and their building blocks **49**, **50**

Deshayes determined the thermodynamic values for hosts **47** and **48** for binding of neutral organic molecules. <sup>1</sup>H NMR and microcalorimetry studies show this class of hosts

can tightly bind organic guests in water with binding constants in some cases greater than  $10^8 \text{ M}^{-1}$ , and that the binding depends upon guest hydrophobicity and shape.<sup>68</sup> In all cases, the binding is enthalpy controlled, which indicates the association between host and guest is driven by guest desolvation as well as specific CH- $\pi$  interactions. Also, a general preference for binding aromatic guests over saturated ones was observed. An increase in van der Waals interactions between aromatic components could be responsible.

### 1.3. Summary and Thesis Goal

From the overview that was discussed so far, we can see that the study of host-guest chemistry in water with simple synthetic organic host molecules is quite promising to understand the fundamental aspect of molecular recognition involving organic guests. Many classes of water-soluble macrocycles like cyclophanes, calixarenes and resorcinarenes have been investigated extensively. Hydrophobic forces are definitely the main driving forces for binding of neutral, lipophilic organic molecules in water, but it is still unclear as to the nature of hydrophobic binding in these systems. Since many studies concluded that hydrophobic binding in these non-natural systems are controlled by the favorable change in enthalpy, which is contrary to that observed in many bio-systems where binding is driven by a favorable entropy change. Other attractive intermolecular forces, such as van der Waals forces, must also be considered.

As we have seen, little research has been done on the hydrophobic association with cavitand type hosts. Will the cavitand, which is advantageous from its highly-preorganized structure, show stronger binding affinity toward neutral hydrophobic guests? If so, to what

extent will the hydrophobicity contribute to the binding in these systems? These questions compelled us to study the binding properties of water-soluble cavitand **1** (described in section 1.1) in aqueous solutions. The results are discussed in the following chapter.

## 1.4. References and Notes

1. Lehn, J. M. *Angew. Chem. Int. Ed. Engl.* **1988**, *27*, 89.
2. In *Comprehensive Supramolecular Chemistry*; Vögtle, F., Ed.; Pergamon: Tarrytown, NY, 1996; Vol.2, pp. 212.
3. (a) Pederson, C. J. *J. Am. Chem. Soc.* **1967**, *89*, 2495. (b) Pederson, C. J. *J. Am. Chem. Soc.* **1967**, *89*, 7017.
4. Cram, D. J.; Cram, J. M. *Science*, **1974**, *183*, 803.
5. Szejtli, J. *Chem. Rev.* **1998**, *98*, 1743.
6. *Comprehensive Supramolecular Chemistry* Vögtle, F., Ed.; Pergamon: Tarrytown, NY, 1996.
7. Kauzmann, W. *Adv. Protein Chem.* **1959**, *14*, 1.
8. Blokzijl, W.; Engberts, J. *Angew. Chem. Int. Ed. Engl.* **1993**, *32*, 1545.
9. *For support of the hydrophobic effect being entropy driven, see:* Stauffer, D. A.; Barrans, R. E.; Dougherty, D. E. *J. Org. Chem.* **1990**, *55*, 2762. *For enthalpy driven support, see:* a. Ferguson, S. B.; Seward, E. M.; Diederich, F.; Sanford, E. M.; Chou, A.; Inocencio-Szweda, P.; Knobler, C. B., *J. Org. Chem.* **1988**, *53*, 5593. b. Harata, K.; Tsuda, K.; Uekama, K.; Otagiri, M.; Hirayama, F. *J. Inclusion Phenom.* **1988**, *6*, 135.
10. Uekama, K.; Hirayama, F.; Irie, T. *Chem. Rev.* **1998**, *98*, 2045.
11. Szejtli, J. *Cyclodextrin Technology*; Kluwer Academic Publishers, 1988.
12. Bugler, J.; Sommerdijk, N.; Visser, A.; Hoek, A.; Notre, R.; Engbersen, J.; Reinhoudt, D. *J. Am. Chem. Soc.* **1999**, *121*, 28.

13. Bender, M. L.; Komiyama, M. *Cyclodextrin Chemistry*; Springer: Berlin, 1978.
14. (a) *Comprehensive Supramolecular Chemistry*; Szejtli, J.; Osa, T. Ed.; Pergamon Elsevier: Oxford, 1996, Vol. 3. (b) review articles in *Chem Rev.* D'Sonza, V. T.; Lipkowitz, K. B.(ed.) **1998**, 1741-2076. (c) Szejtli, *Cyclodextrin and their Inclusion Complexes*; Akademiai Kiado; Buolopest, 1982.
15. (a) Diederich, F. *Cyclophanes*; The Royal Society of Chemistry, Cambridge, 1991. (b) Vogtle, F. *Cyclophanes Chemistry: Synthesis, Structures, and Reactions*; Wiley, New York, 1993.
16. Cram, D. J.; Steinberg, H. *J. Am. Chem. Soc.* **1951**, 73, 5691.
17. (a) Tabushi, I.; Yamamura, K. *Top. Curr. Chem.* **1983**, 113, 145. (b) Murakami, Y. *Top. Curr. Chem.*, **1983**, 115, 107.
18. Odashima, K.; Itai, A.; Iitaka, Y.; Koga, K. *J. Am. Chem. Soc.* **1980**, 102, 2504.
19. (a) Takahashi, I.; Hirano, Y.; Arakawa, H.; Kitajima, H.; Katanaka, M.; Isa, K.; Odashima, K.; Koga, K. *Heterocycles* **1997**, 46, 589. (b) Schneider, H.-J.; Blatter, T.; Simova, S.; Theis, I. *J. Chem. Soc., Chem. Commun.* **1989**, 580; (c) Lai, C. F.; Odashima, K.; Koga, K. *Chem. Pharm. Bull.* **1989**, 37, 2351. (d) Vogtle, F.; Merz, T.; Wirtz, H. *Angew. Chem. Int. Ed. Engl.* **1985**, 24, 221; (e) Schwabacher, A.; Zhang, S.; Davy, W. *J. Am. Chem. Soc.*, **1993**, 115, 6995; (f) Schwabacher, A.; Lee, J.; Lei, H. *J. Am. Chem. Soc.*, **1992**, 114, 7597.
20. (a) Kikuchi, J.-I.; Egami, K.; Suehiro, K.; Murakami, Y. *Chem. Lett.* **1992**, 1685. (b) Miyake, M.; Kirisawa, M.; Koga, K. *Chem. Pharm. Bull.* **1992**, 40, 3124. (c) Manabe, K.; Odashima, K.; Koga, K. *Chem. Pharm. Bull.* **1992**, 40, 580. (d) Miyake, M.; Kirisawa, M.; Koga, K. *Tetrahedron Lett.* **1991**, 32, 7295. (f) Murakami, Y.; Kikuchi, J.-I.; Ohno, T.; Hayashida, O.; Kojima, M. *J. Am. Chem. Soc.* **1990**, 112, 7672.
21. (a) Diederich, F.; Dick, K.; *J. Am. Chem. Soc.* **1984**, 106, 8024. (b) Ferguson, S.; Sanford, E.; Seward, E.; Diederich, F. *J. Am. Chem. Soc.* **1991**, 113, 5410. (c) Diederich, F. *Angew. Chem. Int. Ed. Engl.* **1988**, 27, 362. (d) Ferguson, S.; Seward, E.; Diederich, F.; Sanford, E.; Chou, A.; Onocencio-Szweda, P.; Knobler, C. B. *J. Org. Chem.* **1988**, 53, 5595.
22. (a) Stauffer, D.; Barrans, R.; Dougherty, D. *J. Org. Chem.* **1990**, 55, 2762. (b) Kearney, P.; Mizoue, L.; Kumpf, R.; Forman, J.; McCurdy, A.; Dougherty, D. A. *J. Am. Chem. Soc.* **1993**, 115, 9907. (c) Ngola, S.; Kearney, P.; Mecozzi, S.; Russell, K.; Dougherty, D. *J. Am. Chem. Soc.* **1999**, 121, 1192.
23. (a) Morales, J. C.; Zurita, D.; Penadés, S. *J. Org. Chem.* **1998**, 63, 9212. (b) Jiménez-Barbero, J.; Junquera, E.; Martín-Pastor, M.; Sharma, S.; Vicent, C.; Penadés, S. *J. Am. Chem. Soc.* **1995**, 117, 11198.



24. (a) Vögtle, F.; Muller, W.; Werner, U.; Losensky, H.-W. *Angew. Chem. Int. Ed. Engl.* **1987**, 26, 901. (b) Franke, J.; Vogtle, F.; *Angew. Chem. Int. Ed. Engl.* **1985**, 24, 219.
25. (a) Smithrud, D.; Wyman, T.; Diederich, F. *J. Am. Chem. Soc.* **1991**, 113, 5420. (b) Denti, T.; Gunsteren, W.; Diederich, F. *J. Am. Chem. Soc.* **1996**, 118, 6044.
26. Canceill, J.; Lacombe, L.; Collet, A.; *J. Chem. Soc., Chem. Commun.* **1987**, 219.
27. Gutsche, C. D. *Calixarenes* Stoddart, J. F. Ed.; Royal Society of Chemistry, Cambridge, **1989**, Vol.1.
28. (a) Arduini, A.; Pochini, A.; Reverberi, S.; Ungaro, R.; *J. Chem. Soc., Chem. Commun.* **1984**, 981. (b) Ungaro, R.; Pochini, A. *J. Incl. Phenom.* **1984**, 2, 199.
29. Sanchez Peña, M.; Zhang, Y.; Thibideaux, S.; McLaughlin, M. L.; Munoz de La Peña, A.; Warner, I. M. *Tetrahedron Lett.* **1996**, 37, 5841.
30. (a) Gutsche, C. D.; Pagoria, P. F. *J. Org. Chem.* **1985**, 50, 5795. (b) Gutsche, C. D.; Alam, I. *Tetrahedron* **1988**, 44, 4689.
31. Induced fit mechanism denotes the phenomena of conformational changes of host and guest molecules upon binding. (a) Shinkai, S.; Mori, S.; Tsubaki, T.; Sone, T.; Manabe, O. *Tetrahedron Lett.* **1984**, 25, 5315. (b) Shinkai, S.; Araki, K.; Korishi, H.; Tsubaki, T.; Manabe, O. *Chem. Lett.* **1986**, 1351. (c) Morozumi, T.; Shinkai, S. *Chem. Lett.* **1994**, 1515. (d) Morozumi, T.; Shinkai, S. *J. Chem. Soc., Chem. Commun.* **1994**, 1219. (e) Shinkai, S.; Araki, K.; Manabe, O. *J. Am. Chem. Soc.* **1988**, 110, 7214.
32. (a) Arena, G.; Casnati, A.; Contino, A.; Lombardo, G. G.; Sciotto, D.; Ungaro, R.; *Chem. Eur. J.* **1999**, 5, 738. (b) Arena, G.; Casnati, A.; Mirone, L.; Sciotto, D.; Ungaro, R. *Tetrahedron Lett.* **1997**, 38, 1999. (c) Arena, G.; Casnati, A.; Contino, A.; Gulino, F. G.; Sciotto, D.; Ungaro, R. *J. Chem. Soc., Perkin Trans.* **2000**, 2, 419. (d) Casnati, A.; Ting, Y.; Berti, D.; Fabbi, M.; Pochini, A.; Ungaro, R.; Sciotto, D.; Lombardo, G. G. *Tetrahedron* **1993**, 49, 9815.
33. (a) Zhang, L.; Macias, A.; Isnin, R.; Lu, T.; Gokel, G. W.; Kaifer, A. E. *J. Inclusion Phenom. Mol. Recognit. Chem.* **1994**, 19, 361. (b) Zhang, L.; Macias, A.; Lu, T.; Gordon, J. I.; Gokel, G. W.; Kaifer, A. E. *J. Chem. Soc., Chem. Commun.* **1993**, 1017.
34. (a) Shinkai, S.; Kawabata, H.; Arimura, T.; Matsuda, T.; Satoh, H.; Manabe, O. *J. Chem. Soc., Perkin Trans. 1* **1989**, 1073. (b) Shinkai, S.; Arimura, T.; Araki, K.; Kawabata, H.; Satoh, H.; Tsubaki, T.; Manabe, O.; Sunamoto, J. *J. Chem. Soc., Perkin Trans. 1* **1989**, 2039.

35. (a) Almi, M.; Arduini, A.; Casnati, A.; Pochini, A.; Ungaro, R. *Tetrahedron* **1989**, *45*, 2177. (b) Arimura, T.; Nagasaki, T.; Shinkai, S.; Matsuda, T. *J. Org. Chem.* **1989**, *54*, 3766.
36. (a) Nagasaki, T.; Sisido, K.; Arimura, T.; Shinkai, S. *Tetrahedron* **1992**, *48*, 797. (b) Shinkai, S.; shirahama, Y.; Tsubaki, T.; Mamabe, O. *J. Chem. Soc., Perkin Trans.1* **1989**, 1859.
37. Sansone, F.; Barbosa, S.; Casnati, A.; Sciotto, D.; Ungaro, R. *Tetrahedron Lett.* **1999**, *40*, 4741.
38. Shinkai, S.; Araki, K.; Grootenhuis, P. D. J.; Reinhoudt, D. N. *J. Chem. Soc., Perkin Tras. 2* **1991**, 1883.
39. Shinkai, S.; Kawabata, H.; Matsuda, T.; Kawaguchi, H.; Manabe, O. *Bull. Chem. Soc. Jpn.* **1990**, *63*, 1272.
40. Newkome, G. R.; Hu, Y.; Saunders, M. J. *Tetrahedron Lett.* **1991**, *32*, 1133.
41. (a) Gansey, M. G.; Steemers, F. J.; Verboom, W.; Reinhoudt, D. N. *Synthesis* **1997**, 643. (b) Gansey, M. G.; Verboom, W.; Reinhoudt, D. N. *Tetrahedron Lett.* **1994**, *35*, 7127.
42. (a) Niederl, J. B.; Vogel, H. J. *J. Am. Chem. Soc.* **1940**, *62*, 2512. (b) For a review article see: Timmerman, P.; Verboom, W.; Reinhoudt, D. N. *Tetrahedron* **1996**, *52*, 2663.
43. (a) Schneider, H.-J.; Güttres, D.; Schneider, U. *Angew. Chem. Int. Ed. Engl.* **1986**, *25*, 647. (b) Scheider, H.-J.; Kramer, R.; Simova, S.; Schneider, U. *J. Am. Chem. Soc.* **1988**, *110*, 6442.
44. Schneider, H.-J.; Güttres, D.; Scheider, U. *J. Am. Chem. Soc.* **1988**, *110*, 6449.
45. Schneider, H.-J.; Theis, I. *Angew. Chem. Int. Ed. Engl.* **1989**, *28*, 753.
46. Lippmann, T.; Wilde, H.; Pink, M.; Schäfer, A.; Hesse, M.; Mann, G. *Angew, Chem. Int, Ed, Engl.* **1993**, *32*, 1195.
47. Inouye, M.; Hashimoto, K.; Isagawa, K. *J. Am. Chem. Soc.* **1994**, *116*, 5517.
48. Manabe, O.; Asakura, K.; Nishi, T. *Chem. Lett.* **1990**, 1219.
49. Kobayashi, K.; Asakawa, Y.; Kato, Y.; Aoyama, Y. *J. Am. Chem. Soc.* **1992**, *114*, 10307.

50. Kobayashi, K.; Tominga, M.; Asakawa, Y. Aoyama, Y. *Tetrahedron Lett.* **1993**, 34, 5121.
51. Fujimoto, T.; Yanagihara, R.; Kobayashi, K.; Aoyama, Y. *Bull. Chem. Soc. Jpn.* **1995**, 68, 2113.
52. Matsushita, y.; Matsui, T. *Tetrahedron Lett.* **1993**, 34, 7433.
53. Schneider, U.; Schneider, H.-J. *Chem. Ber.* **1994**, 127, 2455.
54. Yanagihara, R.; Tominaga, M.; Aoyama, Y. *J. Org. Chem.* **1994**, 59, 6865.
55. Kijima, T.; Kato, Y.; Ohe, K.; Machida, M.; Matsushita, Y.; Matsui, T. *Bull. Chem. Soc. Jpn.* **1994**, 67, 2125.
56. Pirrincioglu, N.; Zaman, F.; Williams, A. *J. Chem. Soc., Perkin Trans. 2* **1996**, 2561.
57. Curtis, A. D. M. *Tetrahedron Lett.* **1997**, 38, 4295.
58. (a) Moran, J. R.; Karbach, S.; Cram, D. J. *J. Am. Chem. Soc.* **1982**, 104, 5826. (b) Cram, D. J.; Cram, J. M. *Container Molecules and their Guests*, Monographs in Supramolecular Chemistry Vol.4; Stoddart, J. F., Ed.; Royal Society of Chemistry: Cambridge; **1994**.
59. Fraser, J.R.; Borecka, B.; Trotter, J.; Sherman, J. C. *J. Org. Chem.* **1995**, 60, 1207.
60. (a) Gibb, B. C.; Mezo, A. S.; Sherman, J. C. *Tetrahedron Lett.* **1995**, 36, 7587. (b) Gibb, B. C.; Mezo, A. R.; Causton, A. S.; Fraser, J. R.; Tsai, F. C. S.; Sherman, J. C. *Tetrahedron* **1995**, 51, 8719.
61. Gansey, M. H. B. G.; Bakker, F. K.; Feiters, M. C.; Geurts, H. P. M.; Verboom, W.; Reinhoudt, D. N. *Tetrahedron Lett.* **1998**, 39, 5447.
62. Pellet-Rostaining, S.; Nicod, L.; Chitry, F.; Lamaire, M. *Tetrahedron Lett.* **1999**, 40, 8793.
63. Ahn, D.-R.; Kim, T. W.; Hong, J.-I. *Tetrahedron Lett.* **1999**, 40, 6045.
64. (a) Renslo, A. R.; Rudkevich, D. M.; Rebek, J., Jr. *J. Am. Chem. Soc.* **1997**, 119, 9911. (b) Haino, T.; Rudkevich, D. M.; Rebek, J., Jr. *J. Am. Chem. Soc.* **1999**, 121, 11253.
65. (a) Mezo, A. R.; Sherman, J. C. *J. Org. Chem.* **1998**, 63, 6824. (b) Mezo, A. R.; Sherman, J. C. *J. Am. Chem. Soc.* **1999**, 121, 8983.
66. Cram and coworkers synthesized the *carcerands*, the molecules consisting of two cavitands connected by four spacers, which can contain small molecules in their inner

spaces without the possibility of leaving the cavity. Such complexes are called carceplexes. The prefix *hemi* is used for those host molecules that the guests can escape from or enter their cavities.

67. Yoon, J.; Cram, D. J. *Chem. Commun.* **1997**, 497.

68. Piatnitski, E. L.; Flowers II, R. A.; Deshayes, K. *Chem. Eur. J.* **2000**, 6, 999.

## **Chapter 2.        Synthesis and Binding Studies of Water-Soluble Phosphate-Footed Cavitand**

### **2.1. Introduction**

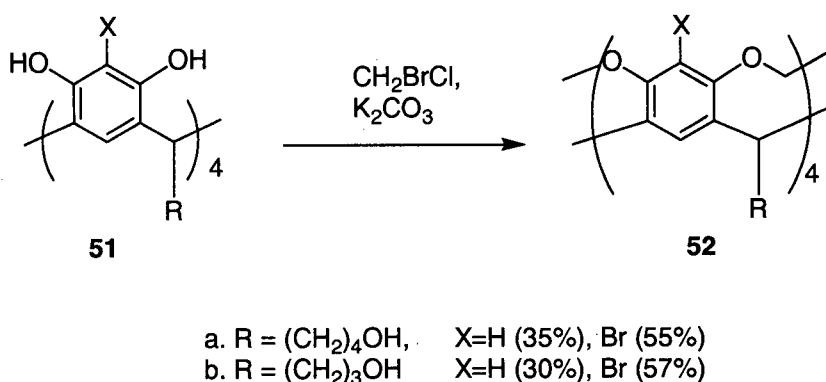
In chapter one, several types of water-soluble receptor host molecules were introduced. Many examples of diverse hydrophobic cavities suitable for selective inclusion of specific guest molecules were discussed. Besides the extensively studied water-soluble cyclophanes, calixarenes and resorcinarenes, there are only a few examples of water-soluble cavitands. The complexation behavior of cavitand-based receptors has been far less investigated (see chapter one). Cavitands are ideal for the study of host-guest complexation, since, unlike the above, they possess rigid concave cavities.<sup>1,2</sup> The rigidity of cavitands has been extensively exploited to explore binding with neutral molecules in organic solvent,<sup>3</sup> while little work has been done in water.<sup>4</sup>

Our group first introduced a method of incorporating water-solubilizing phosphate groups into the pendent groups of the cavitand.<sup>5</sup> This design is essential for study of host-guest chemistry in aqueous solution, since the “charge-free” rim position is suitable for further derivatization to generate cavities with diverse size and shape. This facilitates us to study the host-guest chemistry of cavitand in water. Complexation of neutral molecules with cavitands may be much stronger in aqueous solutions due to the hydrophobic effect.

In this thesis, we describe the synthesis of a new water-soluble phosphate-footed cavitand **1** with methyl groups on the upper-rim positions of the hydrophobic cavity and the complexation behavior of cavitand **1** toward small neutral organic molecules in water. The importance of possible driving forces, i.e., hydrophobic interactions, van der Waals interactions, that control the observed associations were investigated by studying the binding thermodynamics. Our results suggests that the hydrophobic binding in water is controlled by both van der Waals and hydrophobic interactions.

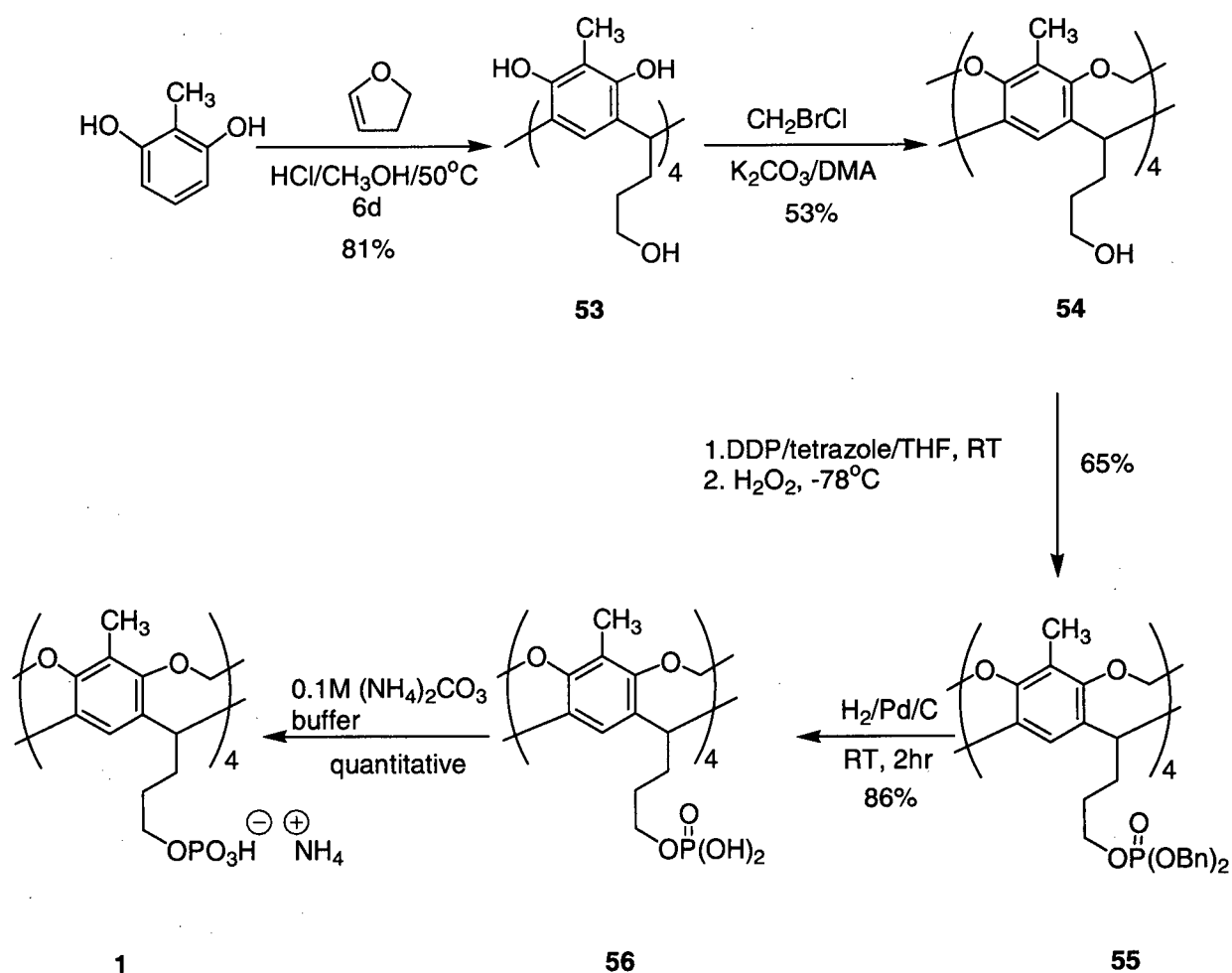
## 2.2. Synthesis and Characterization of Phosphate-Footed Cavitands

Our group has previously reported the selective bridging of hydroxyl footed resorcinarenes **51a** and **51b** to afford cavitands **52a** and **52b** in yields up to 60%.<sup>6</sup> The selective intramolecular bridging of adjacent phenols leaves the hydroxyl feet untouched. Subsequent derivatization led to functionalization of the upper rim and the incorporation of phosphate feet to give benzylthiol and benzylbromo cavitands **41a-41b** as described earlier in chapter one.<sup>5</sup>



**Scheme 2.1** Synthesis of cavitand **52** via methylene bridging.

Hydroxyl-footed 2-methyl cavitand **54** was synthesized according to a previously reported procedure.<sup>5</sup> Reaction of 2-methyl resorcinol with 2,3-dihydrofuran under acidic conditions gave compound **53** after one week in 81% yield. Subsequently, selective bridging of the phenolic hydroxyl groups with BrCH<sub>2</sub>Cl afforded rigid 2-methyl cavitand **54** in 53% yield.



**Scheme 2.2** Synthetic route of phosphate-footed cavitand.

Introduction of phosphate functionalities to the pendent groups of propanol footed **54** was accomplished by a tetrazole catalyzed phosphorylating reaction<sup>7</sup> to give **55**. This reaction is often used for phosphorylation of many biomolecules such as phospholipids, carbohydrates and oligonucleotides.<sup>8</sup> In our lab, di-tert-butyl-*N,N*-diethylphosphoramidite was previously used to phosphorylate the hydroxyl feet of cavitand **41a** and **41b**. This reagent works quite well for the benzylthiol cavitand **41b**, but doesn't react completely with the benzyl-bromo cavitand **41a** giving around 15% of the tris-phosphorylated by-product, which is inseparable from **41a**.<sup>5</sup> Di-tert-butyl-*N,N*-diethylphosphoramidite was first chosen to phosphorylate the 2-methyl cavitand **54**. This phosphorylation reaction gave **55** in very low yield; presumably tetrazole facilitated the decomposition of di-tert-*N,N*-diethylphosphoramidite reagent.<sup>9</sup> In contrast, **55** was more efficiently prepared with diphenyl-*N,N*-diethylphosphoramidite (DDP).<sup>10</sup> Size-exclusion chromatography followed by radial chromatographic purification successfully separated the tetra-phosphorylate product from the tris-phosphorylated byproduct. (Evidence of the tris-phosphorylated cavitand as a separable by-product was obtained from MALDI MS spectra.)

Further optimization of the phosphorylation conditions gave improved results (see Table 2.1). From Table 2.1, it can be seen that increasing the ratio of cavitand **54**:DDP (entries 1,3,5) and extending the reaction time (entries 4-7) can increase the product yield tremendously, pushing the reaction to complete phosphorylation. It is believed that the first three OH- groups react very fast, while phosphorylation of the fourth hydroxyl group of cavitand **54** is the rate determining step. From entries 4-7, we can see that increasing the reaction time resulted in the formation of more tetra-phosphorylated product, and reduced the yield of tris-phosphorylated byproduct. Unfortunately, reaction times > 20 min. led to the



formation of another unidentified byproduct (as observed by TLC analysis). The optimized reaction conditions (entry 7) involved addition of 15 equivalents of DDP with a reaction time of 20 min, which gave **55** in 65% yield. Subsequent removal of the benzyl group by palladium (10% Pd/C) catalyzed hydrogenation (at 1 atm) afforded phosphate-footed 2-methyl cavitand **56** (in 86% yield, scheme 2.1). To increase the water-solubility of the phosphate footed cavitand at moderate pH, the ammonium salt **1** of cavitand **56** was prepared by dissolution in a pH 9 buffer consisting of 0.10 M ammonium carbonate, which was freeze-dried (ammonium carbonate was used as buffer due to its volatility). This procedure was repeated three times to ensure full conversion to the ammonium salt.

**Table 2.1** Reaction conditions and the yields of the phosphorylating reaction.

entry	Rxn time (min)	<b>54</b> :DDP:tetrazole (mole ratio)	Yield of <b>55</b>	Product ratio ( <b>55</b> : tris- byproduct) (mole ratio)
1	10	1:5:15	10%	-
2	5	1:10:30	11%	-
3	10	1:10:30	15%	-
4	5	1:15:45	18%	1.1:1
5	10	1:15:45	40%	1.9:1
6	15	1:15:45	57%	3.9:1
7	20	1:15:45	65%	Less than 1% of tris- phosphorated product

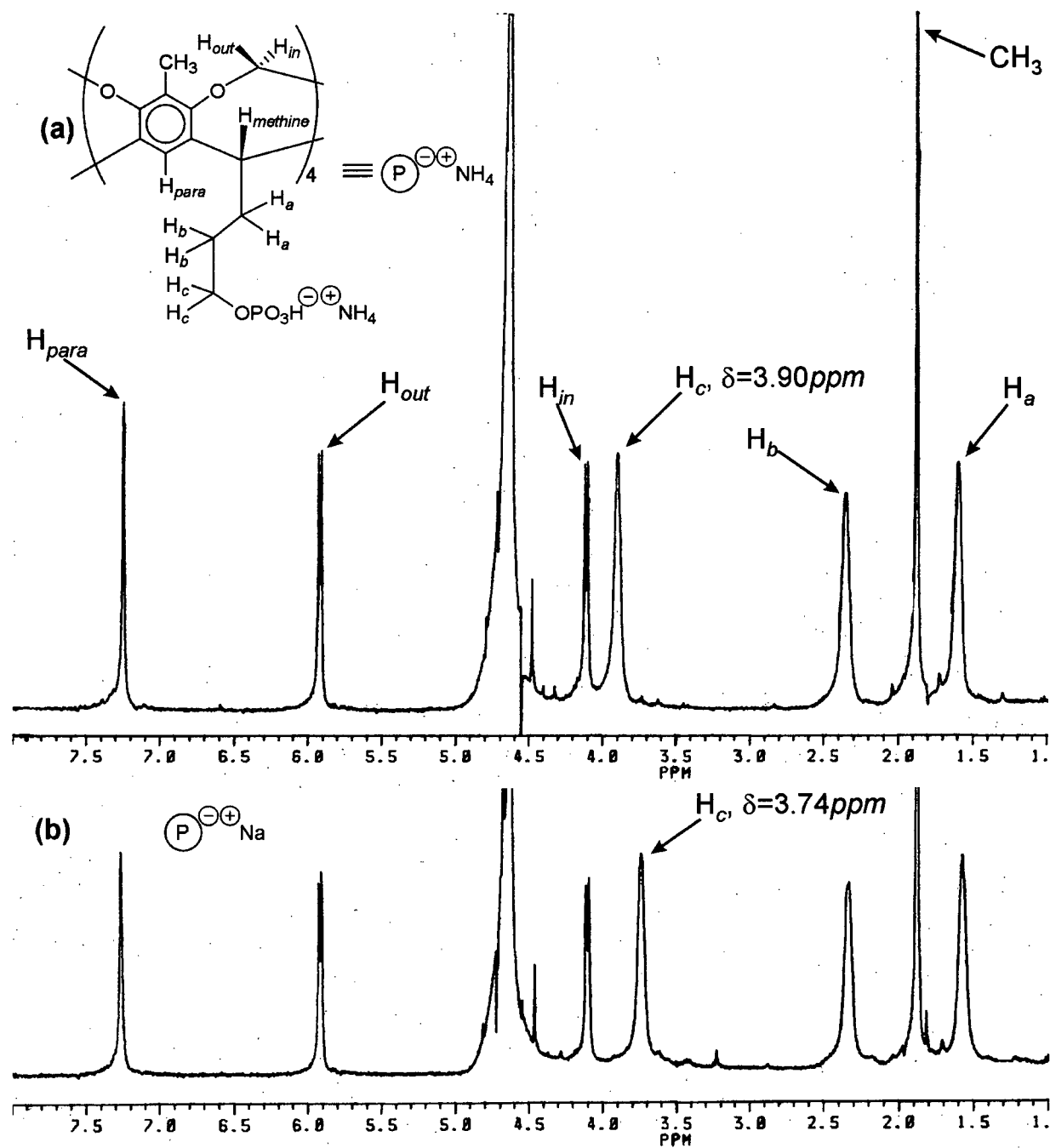
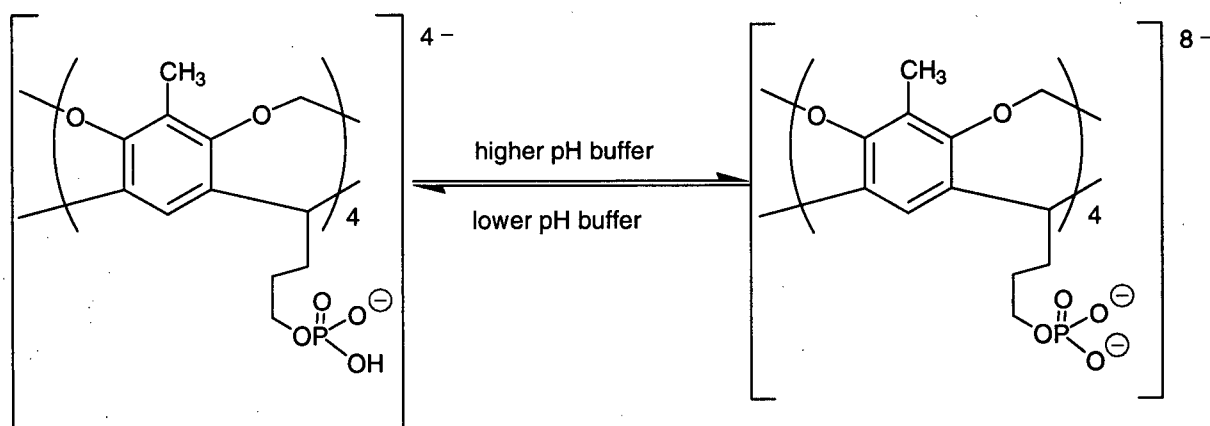


**Figure 2.1** 400 MHz  $^1\text{H}$  NMR spectra of the ammonium salt 1 (a) and its sodium salt analogue (b) in  $\text{D}_2\text{O}$  at ambient temperature. The symbols on the top-left corner of the spectra (a), (b) are just the symbolization of the specific salt, they don't present the true stoichiometry of the cation and anion in the salt.

Both sodium and ammonium salts of cavitand **56** were prepared to increase the water-solubility of the phosphate-footed cavitand at moderate pH.<sup>11</sup> The sodium salt of **56** was made by adding 8 equivalents of sodium hydroxide in methanol drop-wise to a methanol solution of **56**, then the salt was precipitated out by adding drops of THF in the solution and evaporating some of the solvent. The ammonium salt **1** was finally chosen as the host in the binding studies, since its synthesis and purification is much more straightforward. Interestingly, the <sup>1</sup>H NMR spectrum (Figure 2.1a) of the ammonium salt **1** shows a slight downfield chemical shift ( $\delta_{H_c}=3.90\text{ppm}$ ) for the  $H_c$  signal compared to the sodium salt counterpart of **56** ( $\delta_{H_c}=3.74\text{ppm}$ ). This phenomenon is also observed when dissolving compound **54** in different phosphate or borate buffer solutions of varied pH's. The  $H_c$  signal progressively shifts upfield with increasing basicity of the buffer solutions. This indicates that the protonation state of the four phosphate feet changes with pH and affects the chemical shift of the neighboring  $H_c$  (Scheme 2.3). The phosphate groups of the sodium salt are more fully deprotonated than those of the ammonium salt.



**Scheme 2.3** Schematic representation of different deprotonation states of the phosphate feet in the cavitand under varying conditions.

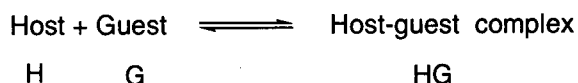
Microanalysis showed that only 3.5 protons were replaced by  $\text{NH}_3$  and 4  $\text{H}_2\text{O}$  molecules were bound to each cavitand molecule. The same results were obtained in a second run even after resubmitting the sample to a higher concentration of  $(\text{NH}_4)_2\text{CO}_3$  buffer followed by freeze-drying. Since there are four phosphate groups in each cavitand molecule which are spatially close to each other, complicated intra- and inter- molecular hydrogen-bonding interactions may exist amongst the phosphates,  $\text{H}_2\text{O}$  and ammonium ions. As more protons are removed from the phosphate feet, the acidity of the remaining protons decreases.

## 2.3. Binding Studies

### A. Theory and Procedure

Quantitative host-guest binding data is often obtained by measuring the association constants  $K_a$  of the complexation processes described by Equation 2.1. In most cases, a 1:1 stoichiometric complex forms between the host and the guest (Equation 2.1). Many experimental methods have been developed for determination of binding constants, utilizing NMR, fluorescence, and UV/vis spectroscopies, as well as calorimetry, liquid-liquid extraction and chromatography.<sup>12,13</sup> For systems involving interactions with aromatic rings, NMR spectroscopy has become the most useful method for the evaluation of binding constants ( $K_a$ ). This is typically done by titration experiments, recording complexation induced shifts (CIS) as a function of the host or guest concentrations.<sup>12,13</sup> The observed chemical shift changes are due to the different orientations of host and/or guest protons towards the shielding and deshielding regions of surrounding aromatic rings in the complex. Valuable structural information about the complexes in solution can also be obtained from the

NMR chemical shifts measurements of the complexed species; such information is difficult to extract from other methods.



**Equation 2.1**

$$K_a = \frac{[\text{HG}]}{[\text{H}] \cdot [\text{G}]}$$

**Equation 2.2**

([H], [G], [HG]= concentrations of the free host, free guest, and of the host-guest complex, respectively.)

Guest exchange could be fast or slow on the NMR time scale. In most binding systems, fast complexation-decomplexation rates (fast exchange) compared to the  $^1\text{H}$  NMR time scale are observed, where the observed chemical shifts are the weighted average between the bound and unbound species. In slow exchange, the chemical shifts of the bound and free species are both observed in the  $^1\text{H}$  NMR spectrum.

#### **i. Determination of Stoichiometry of the Complexes**

The stoichiometry of the binding between two species can be determined by applying the continuous variation method (Job's plot).<sup>12</sup> Basically, the method involves the preparation of a series of solutions that contain varied ratios of host and guest components. This is subject to the condition that the sum of the total host and guest concentration stays constant. If only a single stable complex formed in solution, the stoichiometry of the complex can be derived

from the maximum point of the conventional Job plot: For example, in a 1:1 binding system, the complex concentration [HG] will be the highest (maximum) in a solution where the total host concentration is equal to the total guest concentration ( $[H]_0 = [G]_0$ , guest mole fraction  $X_G = 0.50$ ). When  $[G]_0 < [H]_0$  (guest mole fraction is lower than 0.50) or  $[G]_0 > [H]_0$  (guest mole fraction is higher than 0.50), the [HG] will be lower due to the limitation of the guest concentration or the host concentration. Similarly, the maximum point achieved at  $X_G = 0.33$  ( $2[G] = [H]$ ) indicates formation of a 2:1 (H:G) binding stoichiometry. In a 3:1 (H:G) binding system, a maximum at  $X_G = 0.25$  will be achieved.

For each complex, ten solutions were typically prepared,  $^1\text{H}$  NMR spectra were recorded, and the H:G complex concentration [HG] for each solution is determined from Equation 2.3:

$$[\text{HG}] = [\text{G}]_0 \times \frac{\Delta}{\Delta_{\text{max}}}$$

### Equation 2.3

Where  $[G]_0$  is the initial guest concentration before binding,  $\Delta$  is the difference between the chemical shifts of free guest ( $\delta_G$ ) and the guest in the presence of the host ( $\delta_{\text{obs}}$ ), and  $\Delta_{\text{max}}$  is the difference between  $\delta_G$  and fully bound guest ( $\delta_{\text{HG}}$ ). (This equation is for the fast-exchange system.) From Equation 2.3, we can see that the [HG] is proportional to  $[G]_0 \times \Delta$  ( $\Delta_{\text{max}}$  is a constant for a particular bound guest). Hence, the Job's plot can be graphed as  $[G]_0 \cdot \Delta$  vs. guest mole fraction.

## ii. Determination of the Binding Constant

The binding constants were determined through the "mole ratio method".<sup>12</sup> These experiments involve preparing a series of solutions in which the concentration of either the host or guest is kept constant, while the other is varied. The chemical shift changes of the static component are recorded as a function of changes in concentration of the varied component. (In this thesis, the guest's chemical shift changes were monitored upon addition of the host.)

For a 1:1 binding system, in the fast exchange condition, the observed chemical shift difference of the guest has a hyperbolic dependence on the free (unbound) host concentration (Equation 2.4). Equation 2.4 is usually called the 1:1 binding isotherm

$$\Delta = \frac{\Delta_{\max} \cdot K_a \cdot [H]}{1 + K_a \cdot [H]}$$

**Equation 2.4**

The free host concentration,  $[H]$ , is related to the total host/guest concentrations ( $[H]_0$ ,  $[G]_0$ ) by Equation 2.5.

$$[H] = [H]_0 - [G]_0 \times \frac{\Delta}{\Delta_{\max}}$$

**Equation 2.5**

The 1:1 binding isotherm has three linear plotting forms as follows:

$$\frac{1}{\Delta} = \frac{1}{\Delta_{\max} \cdot K_a \cdot [H]} + \frac{1}{\Delta_{\max}}$$

**Equation 2.6**

Equation 2.6 is the double-reciprocal plotting form (also called Bensi-Hildebrand plot).

$$\frac{[H]}{\Delta} = \frac{[H]}{\Delta_{\max}} + \frac{1}{\Delta_{\max} \cdot K_a}$$

**Equation 2.7**

Equation 2.7 is the y-reciprocal plotting form.

$$\frac{\Delta}{[H]} = -K_a \cdot \Delta + \Delta_{\max} \cdot K_a$$

### Equation 2.8

Equation 2.8 is the x-reciprocal form (also known as the Scatchard plot).

The binding constant  $K_a$  and the maximum chemical shift change value  $\Delta_{\max}$  can be derived from Equation 2.4 or from one of its three linear form (Equation 2.6-2.8) by fitting the chemical shift data in one of these equations. To date, most people prefer to use the non-linear regression method (Equation 2.4) to estimate the binding constants, since it is superior to the linear transformations (Equation 2.6-2.7) when the condition  $[H]_0 \gg [G]_0$  is not valid (where the approximation  $[H] = [H]_0$  is not valid).<sup>12</sup> Also, linear transformations introduce error into the independent variable and transform the error in the data to a non-Gaussian distribution.<sup>12</sup> The changed data spacing in the linear transformations complicated the weight on certain measurement.<sup>12</sup> Recent research on the effect of experimental parameters on the reliability of the estimated binding constants further suggests nonlinear regression method give the most accurate and precise estimates for the binding constants.<sup>14</sup>

Due to the reasons mentioned above, Equation 2.4 combined with the mass balance on host (Equation 2.5) were used to derive the  $K_a$  and  $\Delta_{\max}$  in this thesis. The initial estimated  $K_a$  and  $\Delta_{\max}$ , which are used in the nonlinear regression procedure, are derived from the slope and intercept of double-reciprocal plot (Equation 2.6). The three linear equations are used to test the good fit of a particular experimental design to the 1:1 binding model (The linearities of the three linear plots are the diagnosis of 1:1 binding formation.). A thorough discussion of the mathematical basis of above equations and the curve fitting method used for extracting the  $K_a$  and  $\Delta_{\max}$  values can be found in various texts.<sup>12,13</sup>



### iii. Determination of Thermodynamic Data

Thermodynamic data such as enthalpy and entropy of binding systems can be obtained using variable temperature NMR data from a "van't Hoff plot". The enthalpy ( $\Delta H$ ) and entropy ( $\Delta S$ ) values are related to the binding constant  $K_a$  by Equation 2.9:

$$-R \cdot \ln(K_a) = \frac{1}{T} \cdot \Delta H^\circ - \Delta S^\circ$$

Equation 2.9

By measuring the binding constants over a range of temperatures, a plot of  $-R \cdot \ln(K_a)$  vs.  $(1/T)$  can be graphed, where the slope corresponds to  $\Delta H^\circ$  and the y-intercept correspond to  $\Delta S^\circ$ .

## B. Result and Discussion

### i. Solubility of Cavitand 1 in Aqueous Solutions

To perform successful  $^1\text{H}$  NMR experiments in water, both host and guest compounds must have reasonable water solubilities (at least in the millimolar range). Initial investigations into the water solubility of compound **56** suggested low solubility in neutral pH buffer solutions ( $< 2$  mM). The water solubility is sufficient only in buffers of  $\text{pH} > 8$ , probably due to elimination of the strong intramolecular hydrogen bond formed between the phosphate feet. However, in more basic solutions ( $\text{pH} > 10$ ), potential guests (i.e., EtOAc) undergo hydrolysis. To enhance the rate of dissolution at a more neutral pH, **56** was converted to its ammonium or

sodium salt, which was found to have good solubility in water ( $> 20$  mM). Ammonium salt **1** was finally chosen as the host molecule since it was easily synthesized and purified.

## ii. Aggregation Behavior of the Host **1**

For apolar complexation in water, one of the problems that needs to be addressed is the potential self-aggregation of host or guest molecules due to hydrophobic interactions, which leads to the formation of higher molecular weight aggregates. Diederich stated that “the hydrophobic interactions that act as driving forces for stoichiometric host-guest complexation can lead to the segregated association of host and/or guest molecules, and to the formation of mixed aggregated products with poorly defined orientation of host and guest similar to micellar systems”.<sup>15</sup> Therefore, the formation of stoichiometric complexes should be studied at concentrations where complexation equilibria are not perturbed by the aggregation equilibria.

The critical aggregation concentration (CAC) of the host molecule can be determined by  $^1\text{H}$  NMR spectroscopy.<sup>16</sup> At concentrations lower than the CAC value, the host is present in a molecular-dispersed form, and the chemical shifts are independent of the host concentration. At concentrations higher than CAC, the chemical shifts become dependent of the concentration. This is because the anisotropic regions of the aromatic rings influence the chemical shifts of the aggregating hosts. Also, strong line broadening of all signals can be observed above the CAC, due to the slow exchange between many aggregates.<sup>17</sup>

$^1\text{H}$  NMR spectra of **1** recorded in  $\text{D}_2\text{O}/(\text{NH}_4)_2\text{CO}_3$  buffer between 0.5~10 mM showed no line broadening and no significant changes in chemical shift ( $\Delta\delta \leq \pm 0.02$  ppm). This

indicated that the tested concentration range was well below the CAC and it was suitable to perform the binding experiments under 10 mM.

### **iii. Binding Studies**

#### **1. Guest Screening**

The inclusion of a particular guest in the cavity of host **1** can be easily probed through  $^1\text{H}$  NMR spectroscopy. Upon binding, the guest proton signals shift upfield due to the “aromatic ring current effect” provided by the aryl-lined host cavity. The observation of only one set of guest signals indicates the fast exchange between bound and unbound guests on the NMR time scale. Interestingly, no chemical shift changes of the host protons were observed.

Based on CPK models, cavitand **1** has a very rigid and enforced hydrophobic cavity, which is relatively small and can't be occupied by anything larger than a methyl group. Therefore, seventeen “small” molecules (see Table 2.2, 2.3) with different sizes, shapes and hydrophobicities were chosen as potential guests. The 1:1 complexes of each guest with **1** were analyzed in  $\text{D}_2\text{O}$  by  $^1\text{H}$  NMR. Binding constants ( $K_a$ 's) were quantified for the ten guests in Table 2.2 whose chemical shifts showed significant upfield shifts upon complexation. The other seven molecules (Table 2.3) showed very weak or no binding with **1**.

**Table 2.2** Successful guest molecules

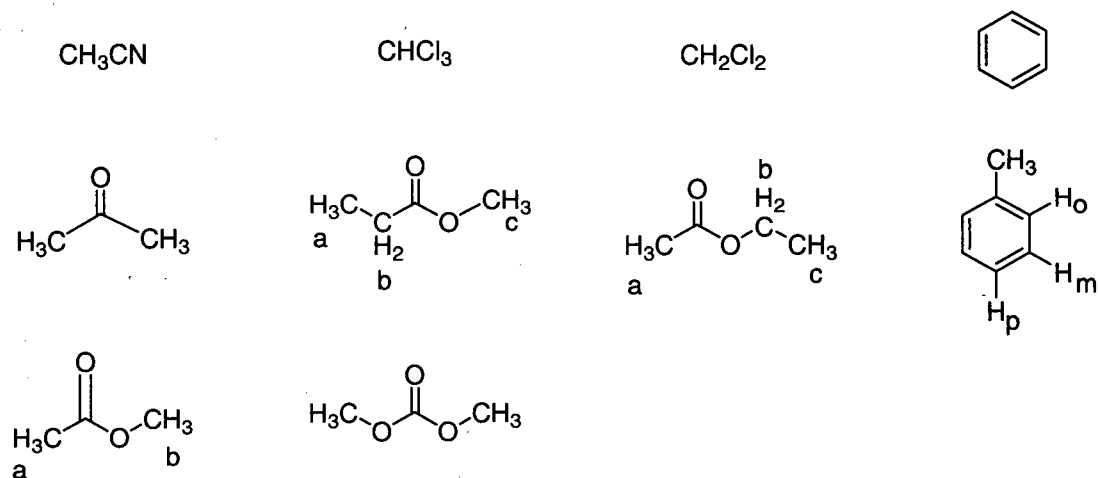
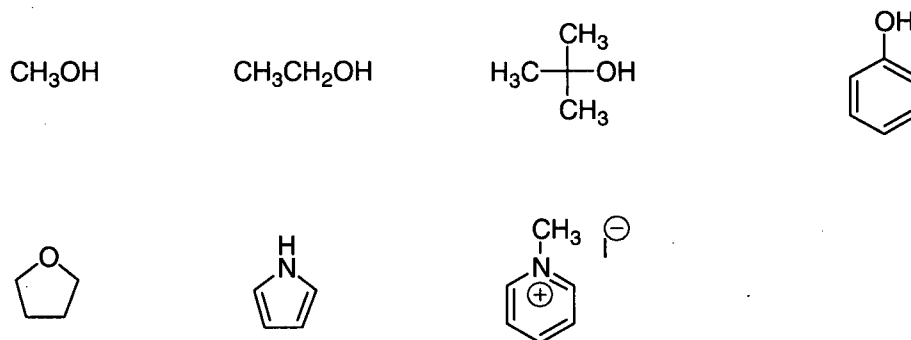


**Table 2.3** Unsuccessful guest molecules



#### a). Unsuccessful Guests

Methanol and methylpyridinium iodide showed very small upfield shifts of their proton signals ( $\Delta\delta \leq 0.02$ ), which indicated weak binding. To obtain meaningful binding constants, a sufficient portion of binding curve has to be covered in the titration experiments and  $\Delta\delta$  well outside of error must be observed. For the other guests in Table 2.3, no chemical shift changes

of the guest signals were observed. Poor binding may be either because the guests are not structurally complementary to the host's cavity, or because solvation of the guest is too strong, or both.

**b). Successful Guests that were not Included in Binding Studies**

$\text{CH}_2\text{Cl}_2$  and dimethyl carbonate showed multiple binding modes with host 1 in aqueous solution. The non-linear least-square plot (Equation 2.4) of these data was clearly inconsistent with a 1:1 binding mode (e.g.  $K_a < 0$ ), which indicates that higher order complexes are likely present. This results in a more complicated derivation of  $K_a$ . For example, suppose the system contains 1:1 (HG) and 1:2 ( $\text{H}_2\text{G}$ ) complexes, in the fast exchange condition, the observed chemical shift changes of the guest ( $\Delta$ ) has the relationship with the stepwise bind constants ( $K_{11}$  and  $K_{12}$ ) as shown in the Equation 2.10.

$$\Delta = \frac{\Delta_{11}K_{11}[\text{H}] + \Delta_{12}K_{11}K_{12}[\text{H}]^2}{1 + K_{11}[\text{H}] + K_{11}K_{12}[\text{H}]^2}$$

**Equation 2.10**

where  $\Delta_{11}$ ,  $\Delta_{12}$  are the chemical shift differences between the fully bound guest (in HG and  $\text{H}_2\text{G}$ , respectively) and the free guest.

The known experimental data ( $\Delta$  and  $[\text{H}]$ ) are not sufficient to extract all the parameters in the Equation 2.10. Also, examining the binding curve over an extensive range is essential to get reliable results, but this is impossible for these two binding systems due to the relatively weak binding.

## 2. Determination of Stoichiometry of the Complex 1·guest

The stoichiometries of complexes formed between 1 and methyl acetate, ethyl acetate, methyl propionate, and dimethyl carbonate were determined by the continuous variation method (Job's plot). The Job's plots are shown in Figure 2.2.

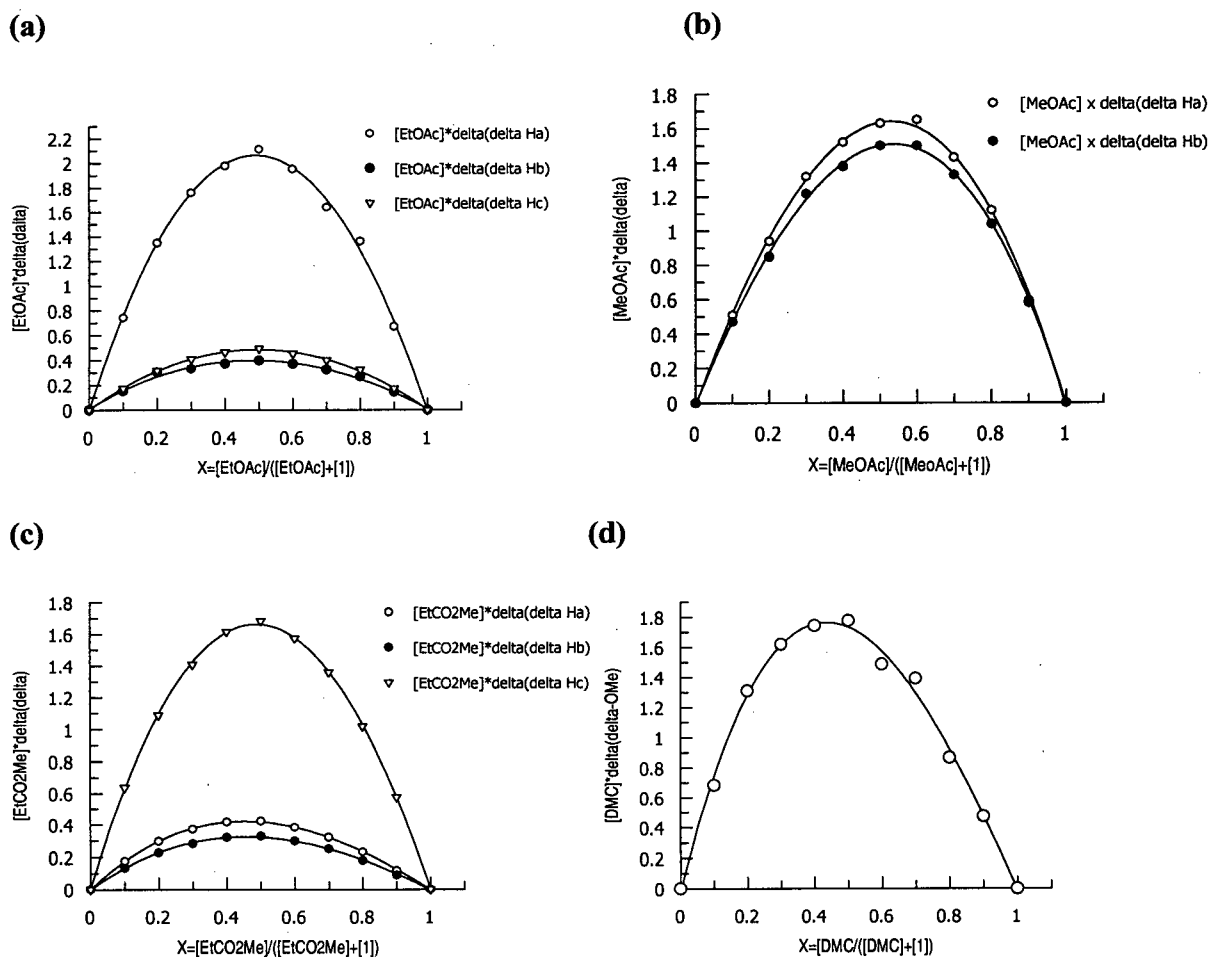


**Figure 2.2** Job's plots of (a) 1 with ethyl acetate binding system; (b) 1 with methyl acetate binding system; (c) 1 with methyl propionate binding system; (d) 1 with dimethyl carbonate binding system.<sup>a</sup>

<sup>a</sup> The  $^1\text{H}$  NMR data was extracted at ambient temperature and the curves were obtained by applying the polynomial curve-fitting procedure to the experimental data.

The Job's plot of ethyl acetate is very symmetrical, with maximum at  $X_{\text{guest}} = 0.50$ , indicating that ethyl acetate form a 1:1 complex with **1**. The same result was for **1**•methyl acetate ( $X_{\text{guest (max)}} = 0.52$ ) and **1**•methyl propionate ( $X_{\text{guest (max)}} = 0.50$ ). However, the Job's plot of dimethyl carbonate had a significantly asymmetrical appearance ( $X_{\text{guest (max)}} = 0.40$ ): the complex concentrations are much higher when  $X_{\text{guest}} < 0.5$  compared to the complex concentration in the solutions where  $X_{\text{guest}} > 0.5$ . This indicates that a single discrete complex is not formed. Probably, there exists a substantial amount of 2:1 (H:G) complex in equilibrium with the 1:1 complex. The existence of higher order equilibrium was also supported by using the "mole ratio method" to determine the binding constants ( $K_a$ 's) (see page 18).<sup>12</sup>

### 3. Determination of the Binding Constants $K_a$

As mentioned earlier in this chapter, no chemical shift changes for the host protons were observed upon binding. The upfield shifts of the guest's proton signals is due to the inclusion of guest into the hydrophobic cavity of the host **1**. For our system, fast exchange of the guest protons compared to the  $^1\text{H}$  NMR time scale leads to only one set of guest signals, which corresponds to the weighted average of the chemical shifts of free and bound guest. The binding constants of eight successful guests shown in Table 2.2 were determined by the "mole ratio"  $^1\text{H}$  NMR titration method.<sup>12</sup> Figure 2.3 exemplifies typical image of guest chemical shift change upon binding by  $^1\text{H}$  NMR spectroscopy. The guest chemical shift data was fit to the 1:1 binding mode (Equation 2.4) and tested by observing the curvature of the titration curve and the linearity of the three linear plots (Equation 2.6-2.8). Except dimethyl carbonate and  $\text{CH}_2\text{Cl}_2$ , most of the host-guest binding systems did fit a 1:1 binding mode very well.

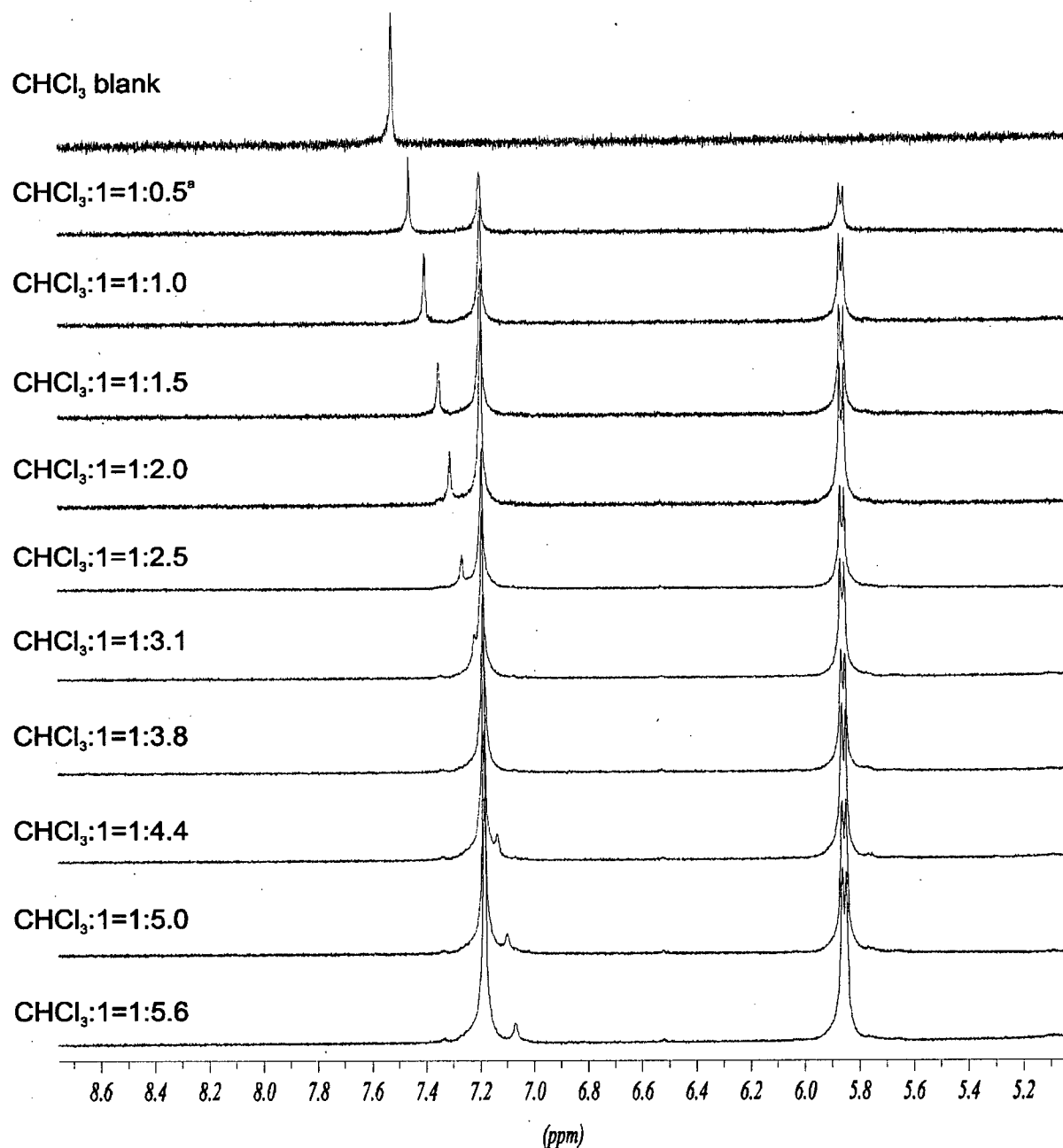


**Figure 2.3** Stack plot of  $^1\text{H}$  NMR (500 MHz) spectra of  $\text{CHCl}_3$  with increased amount of compound **1** in 50 mM  $(\text{NH}_4)_2\text{CO}_3$  buffered  $\text{D}_2\text{O}$  solutions.

<sup>a</sup> pD = 9.4.  $[\text{CHCl}_3] = 1.2$  mM. The ratio shown in the plot is the starting mole ratio of host **1** and guest  $\text{CHCl}_3$ .

As a representative,  $^1\text{H}$  NMR titration curve that of  $1 \cdot \text{CHCl}_3$  is shown in Figure 2.4 (related to Equation 2.4). The data points in the binding curve of Figure 2.4 were derived from  $^1\text{H}$  NMR spectra shown Figure 2.3. Figure 2.5a-c show the three linear transformations



(Equation 2.6-2.8) of the binding curve in Figure 2.4, in which the correlation coefficients  $R > 0.99$ .

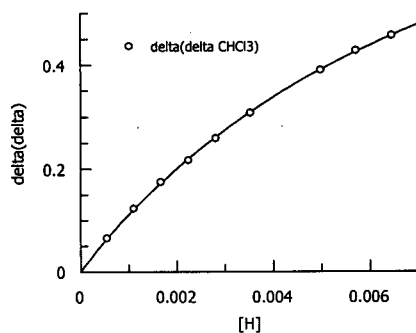


**Figure 2.4** Binding isotherm of  $1 \bullet \text{CHCl}_3$  binding system.

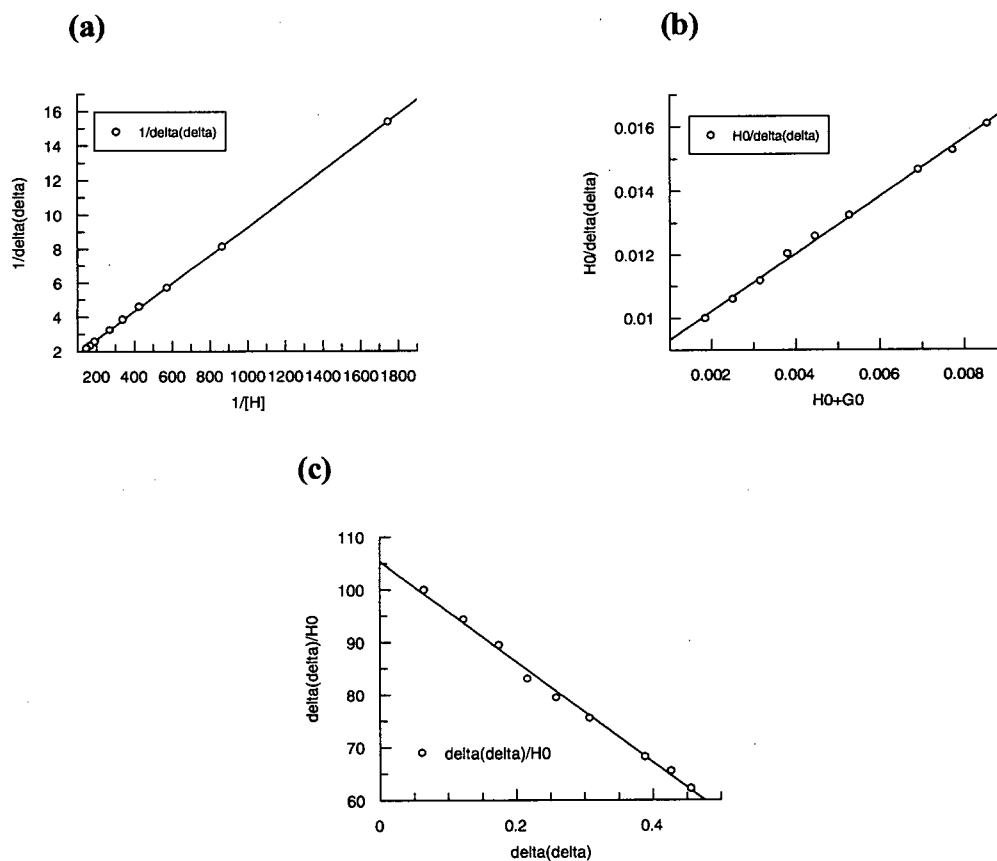


**Figure 2.5** Three linear forms of the binding isotherm shown in Figure 2.4. (a) double-reciprocal plot; (b) y-reciprocal plot; (c) x-reciprocal plot.

### a). Selection of the Optimal Concentration Range

In determining binding constants, it is generally accepted that over half of the saturation range of the binding curve should be covered to obtain a meaningful value and if possible, the test points should fall within 20%-80% of the binding saturation range.<sup>12</sup> Points either less than 20% or larger than 80% will cause significant error.<sup>12</sup> Person concluded that the ligand concentration should be extended to at least the value of  $0.1/K_a$  (when the ligand concentration is in excess).<sup>18</sup> This could be used as a guideline for choosing a starting point for a suitable concentration range. In practice, the end point of the concentration range is limited by host or guest solubility, the non-ideal behavior of the solution, and the sensitivity of the chosen instrumental method.<sup>12</sup>

Scatchard plots (Equation 2.8) were used to test the covered range of the binding curve in a particular experimental design, because the chemical shift range (from 0~100% binding) of the observed protons is visually apparent on the abscissa scale of the plot. For example, in the binding experiment with **1** and methyl propionate, the experiment was first designed as  $[G]_0 = 1$  mM,  $[H]_0$  varied from 0.1 to 5 mM. The resulting Scatchard plot is shown in Figure 2.6. We can see the chemical shift of  $H_c$  in the methyl propionate would shift upfield to about 3.2 ppm upon 100% binding. Only a small portion of binding saturation was covered (about 37%), most of the testing points fall into the region where the binding saturation fraction  $f_{HG} < 0.2$ ,<sup>19</sup> where the point of  $f_{HG} = 0.2$  corresponds to the  $[H] = 2$  mM. Therefore, this experimental design is not suitable for extracting a reliable  $K_a$ . The optimum host concentration range would be from 2 mM to at least 8 mM (which correspond to  $f_{HG} = 0.5$ ), and ideally up to 25 mM (which correspond to the  $f_{HG} = 0.8$ ).

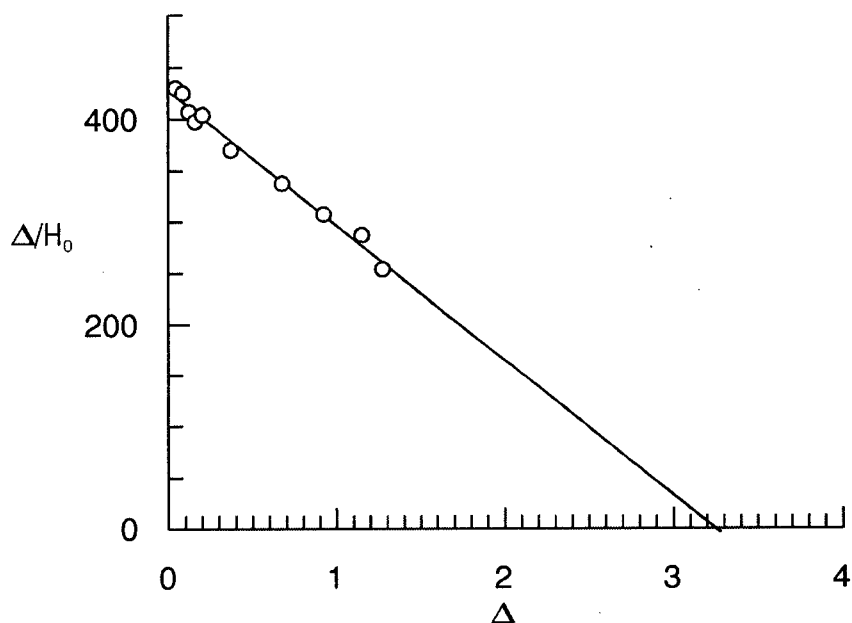


**Figure 2.6** Scatchard plot of 1-methyl propionate binding system ( $H_c$  was followed).

$[G] = 1\text{mM}$ ,  $[H]$  varied from 0.1~5 mM, chemical shift data was extracted from 400 MHz spectra.

In this thesis, a concentration of the host that is higher than 10 mM was not used, since the ideality of the solution may change in a higher concentration solution for such a high molecular weight molecule. Also, since the concentration of the host is subject to change, at higher  $[H]:[G]$  ratio ( $[H] \gg [G]$ ), the host peaks would be much bigger than the guest peaks, which makes the guest peaks disappear under the huge host peaks. It was found that the guest peaks were hard to detect due to the huge host peaks when the  $[H]:[G]$  ratio was higher than 10:1. Therefore, in addition to a maximum of 10mM host concentration, the host-guest ratio was not extended over 10:1.

### **b). Conformations of Complexation**

Having chosen the optimal concentration range, the titration experiment for each binding system was performed and the binding constants and the maximum chemical shift changes for

each guest were extracted (by fitting data in Equation 2.4). Table 2.4 shows the calculated complexation induced shifts (CIS) on 100% binding for different guests.

**Table 2.4** The calculated CIS on 100% binding of **1** with various guests

guest	$\Delta_{\max}^a$	b
(CH <sub>3</sub> ) <sub>2</sub> CO	2.25 ± 0.10	-CH <sub>3</sub>
CH <sub>3</sub> CN	3.00 ± 0.18	-CH <sub>3</sub>
Toluene	1.06 ± 0.05	-H <sub>p</sub>
	0.91 ± 0.14	-H <sub>m</sub>
	0.93 ± 0.08	-H <sub>o</sub>
	2.65 ± 0.23	-CH <sub>3</sub>
Benzene	0.58 ± 0.12	Aromatic-H
CHCl <sub>3</sub>	1.07 ± 0.02	-CH
CH <sub>3</sub> CH <sub>2</sub> C(O)OCH <sub>3</sub>	2.11 ± 0.11	-H <sub>a</sub>
	1.22 ± 0.04	-H <sub>b</sub>
	3.45 ± 0.05	-H <sub>c</sub>
CH <sub>3</sub> C(O)OCH <sub>2</sub> CH <sub>3</sub> <sup>c</sup>	3.52 ± 0.04	-H <sub>a</sub>
	0.74 ± 0.01	-H <sub>b</sub>
	0.93 ± 0.01	-H <sub>c</sub>
CH <sub>3</sub> C(O)OCH <sub>3</sub> <sup>d</sup>	2.19 ± 0.03	-H <sub>a</sub>
	2.01 ± 0.02	-H <sub>b</sub>

<sup>a</sup>. The error shown in the  $\Delta_{\max}$  is the standard error derived from non-linear curve fitting process. <sup>b</sup>. Protons that were used for the fitting procedure. The proton assignment is the same as those shown in Table 2.2. <sup>c</sup>.  $\Delta_{\max}$  value is the average from four runs of parallel experiments. <sup>d</sup>.  $\Delta_{\max}$  value is the average value from two runs of parallel experiments.

Careful analysis of the complexation-induced shift (CIS) data of gave us valuable information about the guest orientation in the bound state. Evidently the methyl protons experience the largest CIS compared to the other protons in the molecule for each guest

studied. Therefore it is very likely that the methyl groups protrude deeply into the cavity of the host. This is consistent with CPK molecular modeling, which indicated that the host cavity size is complementary to a methyl group. Acetyl methyl protons of acetone, methyl acetate and ethyl acetate experienced CIS values of different magnitudes, although they have similar steric demands. Since it is likely that the bound guest can bind in many orientations in the host cavity, the observed chemical shifts of the guest in the existence of the host are probably the weighted average arising from multiple binding orientations. If this is true, then the difference in the observed CIS data for similar protons in different guests is caused by the different ratio of the individual orientations of bound guest in different binding systems.

The existence of multiple binding orientations for the guest is evidenced by comparing the CIS for different protons in "unsymmetrical" guest molecules. The guest proton signals were found shifted upfield to different extents upon binding. For toluene, the protons experienced CISs in the following order:  $\text{CH}_3 > \text{H}_p > \text{H}_o > \text{H}_m$  (Figure 2.7a), which indicates there are two binding orientations for the guest toluene, namely: the  $\text{CH}_3$  site and the para-H site. Both sites are unselectively included into the host cavity. In methyl acetate, both methyl groups penetrate into the cavity (Figure 2.7d). A similar pattern was found in the cases of ethyl acetate and methyl propionate, in which both methyl and ethyl groups are competitively bound within the cavity of the host (Figure 2.7b,c). It is apparent that for the guests containing two or more potential binding modes, they form isomeric complexes with host **1** in aqueous solutions and the two binding modes are in equilibrium (Figure 2.8).

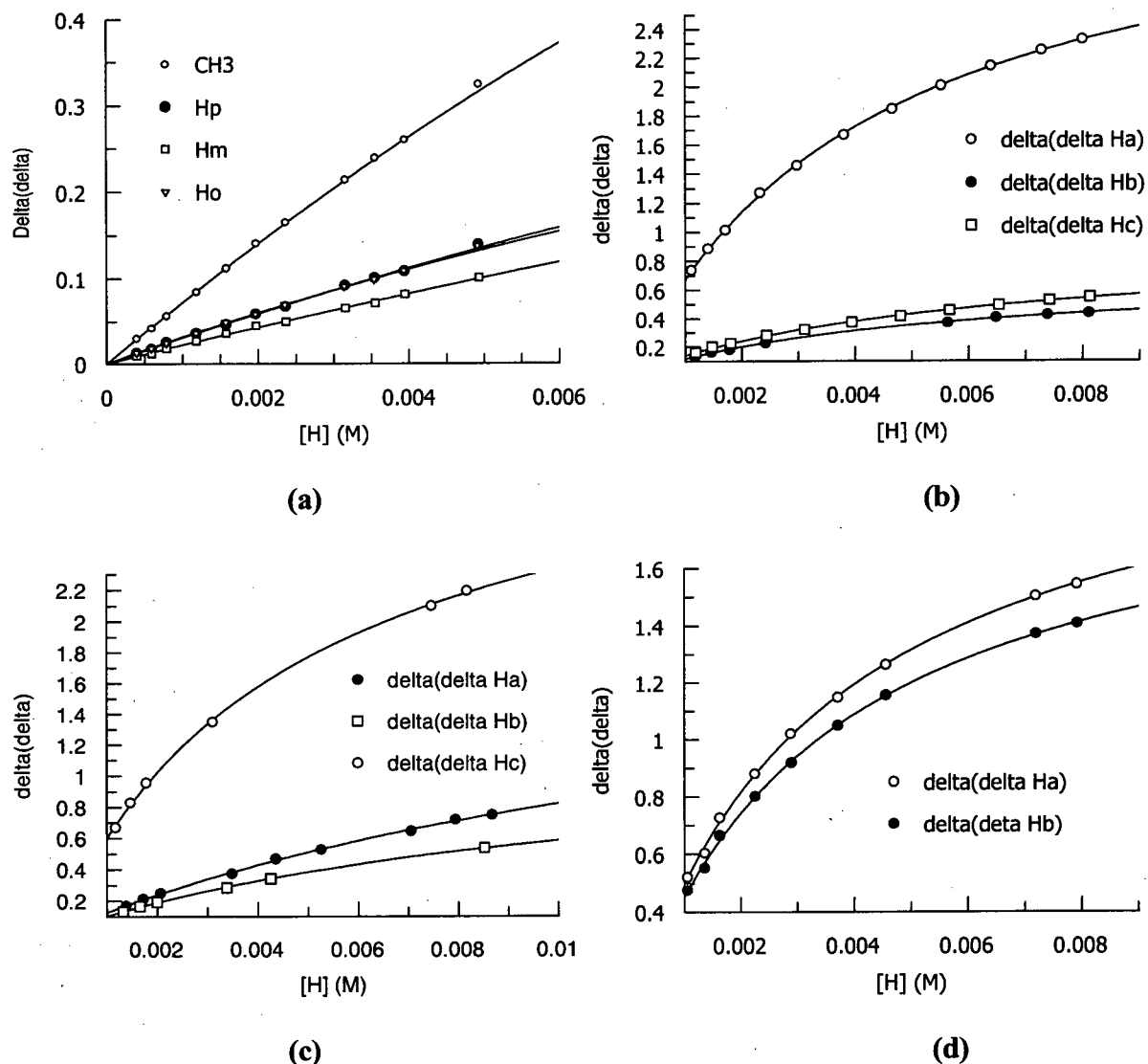


**Figure 2.7** Observed CIS as a function of host concentration for (a) 1•toluene, (b) 1•ethyl acetate, (c) 1•methyl propionate, (d) 1•methyl acetate binding systems.<sup>a</sup>  
a. Proton assignments are as shown in Table 2.2.

This is a very important observation, since the isomeric binding<sup>20</sup> (Figure 2.8) probably happens not only with the “unsymmetrical” guests, but also with the non-spherical symmetrical guests, such as acetone and benzene. If this is true, then the calculated CIS for the guest protons would be the weighted average of the CIS that results from each individual

isomeric complex (Equation 2.11) and the calculated binding constant would be the sum of the individual binding constants of each isomeric complexes (Equation 2.12).<sup>12,13</sup>

$$\Delta_{\max} = \frac{\Delta_{\text{HG}} K_{\text{HG}} + \Delta_{\text{GH}} K_{\text{GH}}}{K_{\text{HG}} + K_{\text{GH}}}$$

**Equation 2.11**

$$K_a = K_{\text{HG}} + K_{\text{GH}}$$

**Equation 2.12**

Where  $\Delta_{\text{HG}}$ ,  $\Delta_{\text{GH}}$  are the CIS of individual isomeric complex;  $K_{\text{HG}}$  and  $K_{\text{GH}}$  are the individual binding constants of the isomeric complexes.

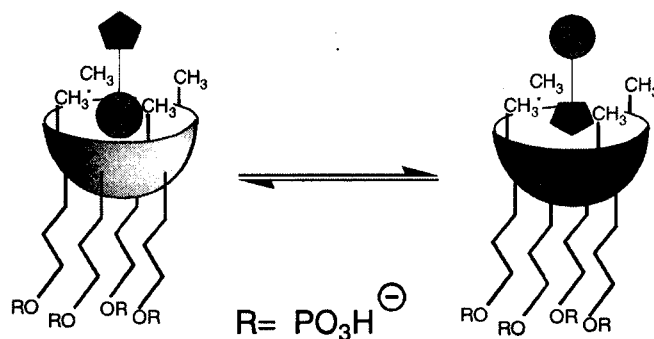


**Figure 2.8** Schematic presentation of dual modes inclusion of the guest.

### c). Stability of the Complexation

Table 2.5 shows all the calculated 1:1 binding constants ( $K_a$ 's) derived from  $^1\text{H}$  NMR titration experiments as well as binding free energies ( $\Delta G^\circ$ ).

**Table 2.5** The binding constants of **1**•guests and hydrophobicities of the guests at 298K.

Guest	$\log P_{oct}^a$	$K_a (M^{-1})^b$	$\Delta G^\theta$ (kcal/mole)	c
(CH <sub>3</sub> ) <sub>2</sub> CO	-0.24	19±1	-1.7±0.1	-CH <sub>3</sub>
CH <sub>3</sub> CN	-0.34	42±3	-2.2±0.1	-CH <sub>3</sub>
Toluene	2.69	30±3	-2.0±0.2	-CH <sub>3</sub>
Benzene <sup>d</sup>	2.13	55±16	-2.4±0.2	Aromatic-H
CHCl <sub>3</sub>	1.97	116±4	-2.8±0.2	-CH
CH <sub>3</sub> CH <sub>2</sub> C(O)OCH <sub>3</sub> <sup>e</sup>	0.68	210±6	-3.2±0.1	-OCH <sub>3</sub>
CH <sub>3</sub> C(O)OCH <sub>2</sub> CH <sub>3</sub> <sup>f</sup>	0.73	234±8	-3.2±0.1	-OCCH <sub>3</sub>
CH <sub>3</sub> C(O)OCH <sub>3</sub>	0.18	270±19	-3.3±0.1	-OCH <sub>3</sub>

<sup>a</sup>.  $\log P_{oct}$  = partition coefficient between octanol and water.<sup>23</sup> <sup>b</sup>. The titration experiments for each guest were repeated under optimized conditions at least once except for benzene. The errors shown were the standard deviations from non-linear curve-fit procedure or the standard deviations of averaged  $K_a$ 's from several repeating experiments under the same conditions. For toluene, benzene and chloroform, the concentrations were determined from the integration of the <sup>1</sup>H NMR signals, allowing 20% error. <sup>c</sup>. Protons that were used in the curve-fitting procedure. <sup>d</sup>. Measured under ambient temperature around 20°C, all the other  $K_a$ 's were measured under 298K. <sup>e</sup>. The titration experiment of EtOAc was repeated 4 times under optimized conditions. <sup>f</sup>. The titration experiment of MeOAc was repeated 2 times under optimized conditions.

*Data validity:* The binding constants shown in table 2.5 were calculated from the chemical shifts of those guest protons that had the largest CIS. For guests that have two potential binding orientations, other protons in the guests are also used to extract the  $K_a$ . The results are shown in Table 2.6.



**Table 2.6** Binding constants calculated from fitting of different proton data of the guests

Guest												
Methyl acetate			Ethyl acetate			Methyl propionate			Toluene			
Proton <sup>a</sup>	H <sub>a</sub>	H <sub>b</sub>	H <sub>a</sub>	H <sub>b</sub>	H <sub>c</sub>	H <sub>a</sub>	H <sub>b</sub>	H <sub>c</sub>	H <sub>m</sub>	H <sub>o</sub>	H <sub>p</sub>	CH <sub>3</sub>
K <sub>a</sub> <sup>b</sup>	270	270	234	179	170	64	92	210	26	36	32	30
	(21)	(19)	(8)	(14)	(6)	(5)	(4)	(6)	(4)	(4)	(2)	(3)

<sup>a</sup>. Proton labels are shown in Table 2.2 (pg. 54). <sup>b</sup>. Errors in  $K_a$  (in brackets) are derived from non-linear curve-fitting procedure.

We can see, from Table 2.6, that the binding constants calculated from fitting different CIS data of each type of protons agree for methyl acetate and toluene, but not for ethyl acetate and methyl propionate. Based on Connors' interpretation of isomeric binding, even in a dual mode binding function, only one binding constant should be derived from fitting of different proton's CIS, which is the sum of the individual 1:1 binding constants of the two binding modes.<sup>20</sup> Then, there must be some reason for the large deviation in magnitude of binding constants derived from different proton CIS data. Observing the CIS data shown in Figure 2.7 carefully, we would see that although there are two binding modes that exist in the complexes of **1**•ethyl acetate and **1**•methyl propionate, the inclusion of the two binding sites of the guests are not equal. Inclusion of the methyl group in the two guests is favored over inclusion of the CH<sub>3</sub> in the ethyl group. Also, from molecular modeling, the cavity size of the host **1** is limited and very rigid, which allows inclusion of only one methyl group inside the cavity. So, when inclusion of one site of the guest occurs, the other site of the guest is still exposed to the solvent phase. In a fast exchange system, the observed CIS is the weighted average of proton signals in different environments. In other words, not only the inclusion of a certain proton inside the cavity can induce the shift of this proton signal, some other factors, such as random collision of the guest with the host, can also cause the shifting of the proton signal. Stamm

called the shielding caused by random collision of the host and the guest as "additional unspecific shielding (AUS)".<sup>21</sup> He interpreted the problem of inconsistent  $K_a$ 's from different protons in the same binding system as the AUS effect. It is found that the size of the AUS is proportional to the host concentration and this AUS effect usually results in a markedly smaller  $K_a$  in the calculation.<sup>21</sup> In the case of ethyl acetate and methyl propionate, when the methyl site of the guest preferably sits in the cavity of the host, the ethyl site of the guest juts out from the cavity and experiences AUS, which leads to the error in  $K_a$ . And the magnitude of  $K_a$  extracted from the CIS data from different nuclei is consistent with the degrees of AUS on the individual protons. For example, in 1•methyl propionate complex system, the influence of AUS on the individual protons follow the order  $H_a > H_b > H_c$ , which results in  $K_a(H_a) < K_a(H_b) < K_a(H_c)$  as seen from Table 2.6.

So, due to the reasons above, only the protons with large CIS's were used in the calculation of thermodynamic parameters in order to minimize the error resulting from the AUS effect.

*Guest selectivity:* It is well known that host-guest complexation depends on the stereoelectronic complementary between the surfaces common to both host and guest.<sup>22</sup> Size and shape appear to be crucial to determine the binding strength of a guest to be included. Host 1 binds much stronger with the small aliphatic molecules than the bulky aromatic compounds. Investigation by CPK model shows that the cavity of host 1 can only include a methyl group deeply due to the limited dimensions of the host cavity. Aromatic compounds like benzene are probably too large to penetrate deeply into the cavity, which leads to a much weaker binding. The rationale for that is hydrophobic binding depends on desolvation of the

lipophilic guest molecules and the host hydrophobic cavity from water and release of the “structured” water molecules around the guest molecule and the host cavity into the bulky water phase. If the guest molecule can’t protrude deeply into the host cavity, then there must be a substantial area of the guest surface still exposed to the water phase, which leads to a small hydrophobic force. Also, less steric complementarity between the common surfaces of the host and guest also results in weaker non-covalent attractions.

Guest hydrophobicity also controls the binding strength. For a given guest molecule, the partition coefficient between octanol and water can be considered as a quantitative expression of its hydrophobicity (The more positive the value of  $\log P_{\text{oct}}$  is, the more hydrophobic the molecule is).<sup>23</sup> We noticed that for the bulky guests, no inclusion was observed for the more hydrophilic guests (e.g. THF, pyridine and phenol and t-butyl alcohol) or the guests with a charge (e.g. methyl-pyridinium ion), while the very hydrophobic guests like benzene and toluene can bind weakly with the host, despite their bulky size. For smaller linear or spherical guests, very hydrophilic molecules like methanol and ethanol don’t bind with the host **1**, probably because these molecules form strong interactions (i.e. hydrogen bonding) with water. Although sterically, they fit well into the cavity of the host, inclusion is not favored since the interactions between alcohols and water are weakened. Weak binding was observed for the hydrophilic guests like acetone and acetonitrile. Much stronger binding was observed for the hydrophobic guests like chloroform, and simple esters listed in Table 2.5. The binding strength followed the partition coefficient of these guests to some extent, but not strictly. Interactions other than the hydrophobic effect may play a role in binding.

Interestingly, host **1** binds the moderately polar esters selectively. Binding is favored by 0.5 kcal/mole compared to the binding of the more hydrophobic but less polar guest,

chloroform.. Hydrophobic interactions alone can't explain this selectivity, since the binding strength doesn't follow the hydrophobicity of the guests strictly. van der Waals attractive forces between the host and guest may contribute to binding stability. CPK models show that the overall sterics of chloroform versus esters might not be important, since only part of the guest can be included into the small host cavity. For chloroform, Cl is probably favored to be included into the cavity than H. For esters, both alkyl and acetyl methyl groups of esters can penetrate into the host cavity. Since host **1** contains a relatively electron rich cavity, there are possible attracting interactions between the  $\pi$ -rich rings of the host and the electron deficient groups on the guest. While, the methyl group in the  $\text{CH}_3\text{O}^-$  and  $\text{CH}_3\text{COO}^-$  is much electron deficient than the chlorine in the C-Cl. Upon binding, the favorable CH- $\pi$  interaction between the host aromatic system and the guest methyl group may be fairly strong, much stronger than the CCl- $\pi$  interaction. Strong CH- $\pi$  interactions may also account for favored binding Me- site over Et- site of the esters. Such strong CH- $\pi$  interactions between the host  $\pi$ -rich rings and the electron deficient guest have been reported in many other synthetic host binding systems.<sup>24</sup> Possible n- $\pi$  and  $\pi$ - $\pi$  interactions between the guest carbonyl group and the host aromatic rings may also strengthen binding.

#### **iv. Determination of Thermodynamic Data of Binding with Esters**

From binding studies of host **1** with various guest molecules mentioned above, we've seen that cavitand host **1** selectively binds small aliphatic esters over other guests. What is the nature of such a selective inclusion? To answer this, the thermodynamic parameters for these binding systems were determined by measuring the temperature dependence in the stabilities of complexation between host **1** and ester guests. The  $^1\text{H}$  NMR titration experiments were

performed at 4-5 different temperatures. Each binding constant  $K_a$  at each temperature was calculated and van't Hoff plots were graphed ( $\log K_a$  vs.  $1/T$ ). From these linear correlations, the enthalpies and entropies of the binding processes were obtained from the slope and the intercept of the van't Hoff plot, respectively.

Since  $K_a$  is a function of temperature, the quality of temperature control and measurement will decide the accuracy of  $K_a$  and finally influence the linearity of the van't Hoff plot. Hence, each temperature was measured and calibrated using ethylene glycol (0 °C ~ 143 °C) or methanol (-95 °C ~ 57 °C) standards (see Experimental). To ensure the temperature consistency during the whole titration process, each NMR tube was equilibrated in the NMR probe for 5-10 min before data acquisition. It was found that the lock signal of the solvent D<sub>2</sub>O drifted with temperature. Therefore, the time needed for each equilibration was easily monitored by observing the lock signal shift. Also, the consistent temperature inside the NMR probe depends on the sensitivity and stability of the temperature control system. The temperature may vary over an extended period of time. Due to this reason, the temperature was tracked during the whole titration process. Runs in which the temperature varied more than  $\pm 0.5$  °C from the first to last measurement gave larger errors for binding constant  $K_a$  and subsequently resulted in larger deviations from linear van't Hoff plots. Therefore these runs were not used in the van't Hoff plots.

Another factor that may influence the linearity of the van't Hoff plot is the temperature range in which the  $K_a$  was measured. van't Hoff plots were set up on the assumption that the enthalpy of the binding is constant with the temperature change. It is known that the enthalpy does change with the temperature by a factor of  $\Delta C_p$  (heat capacity) as can be seen from the equation:  $\Delta H = \Delta H^\circ + T \cdot \Delta C_p$  ( $\Delta H^\circ$  is the enthalpy under standard conditions.).<sup>25</sup> Thus, linear

van't Hoff plots are only valid when  $\Delta C_p$  is close to zero or the temperature is varied in a very narrow range. In several initial variable temperature experiments, binding constants of the investigated systems were found to be quite sensitive to temperature change, which indicated a large  $\Delta C_p$ . Hence, a comparatively narrow temperature range (20~25 K) was chosen to avoid non-linearity in van't Hoff plots.

Table 2.7-2.9 show the calculated binding constants of three **1**•guest systems at different temperatures.

**Table 2.7** Binding constants ( $K_a$ ) of complex **1**•methyl acetate at different temperatures

T (K)		285	292	298	304
$K_a^a$ ( $M^{-1}$ )	CH <sub>3</sub> CO	423±15	347±10	291±7	242±9
	CH <sub>3</sub> O	439±12	352±11	289±7	243±10
$K_a^b$ (average)		431±8	350±3	290±1	243±1

<sup>a</sup> Errors are derived from the non-linear curve-fit procedure. <sup>b</sup> Errors are the standard deviation of the average  $K_a$ .

**Table 2.8** The binding constants of complex **1**•ethyl acetate at different temperatures

T (K)	283	287	292	298	303
$K_a$ ( $M^{-1}$ ) <sup>a</sup> (CH <sub>3</sub> CO)	353±3	301±7	273±4	235±3	206±3

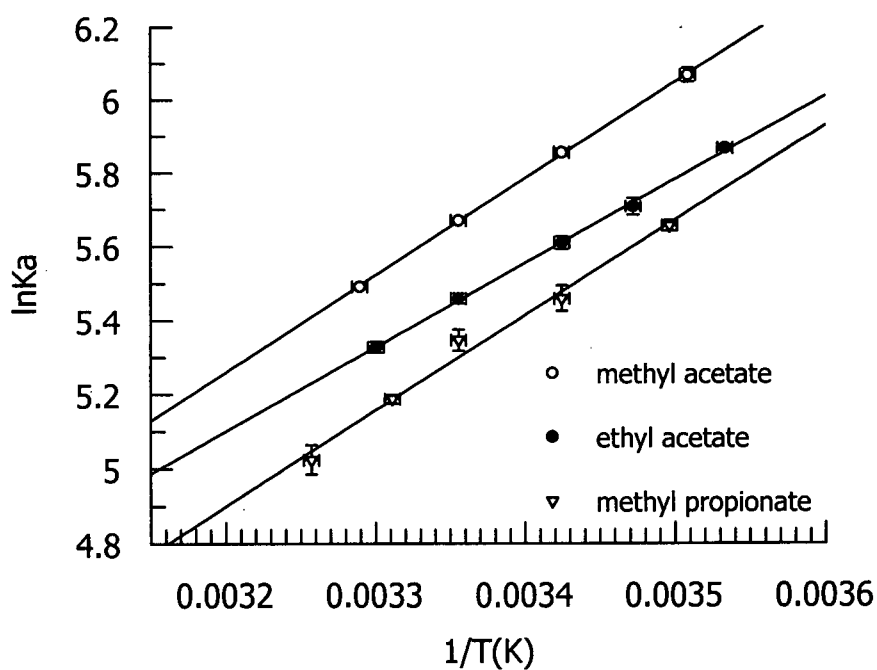
<sup>a</sup> Errors are derived from the non-linear curve-fit procedure.

**Table 2.9** The binding constants of complex **1**•methyl propionate at different temperatures

T (K)	286	292	298	302	307
$K_a$ (M <sup>-1</sup> ) <sup>a</sup>	286±4	235±8	210±6	179±2	152±6
(CH <sub>3</sub> O)					

<sup>a</sup> Errors are derived from the non-linear curve-fit procedure.

The van't Hoff plots of the three systems investigated are shown in Figure 2.9. The errors for each  $K_a$  was also shown in the plot. Temperatures were within  $\pm 0.5$ K around the true value. The extracted enthalpies, entropies and free energies for these systems are listed in Table 2.10. The thermodynamic data of EtOAc binding system shown in Table 2.10 are the average value derived from two parallel experiments.

**Figure 2.9** van't Hoff plots of investigated **1**-guest binding systems

• Correlation coefficient  $R > 0.99$  for all these plots.

**Table 2.10** Thermodynamic data (at 298K) for the investigated **1**-guest systems

guest	$\Delta G^\circ$	$\Delta H^{\circ a}$	$\Delta S^{\circ a}$	$T \cdot \Delta S^\circ$
	kcal/mol	kcal/mol	cal/mol $K$	kcal/mol
$\text{CH}_3\text{COOCH}_3$	-3.4	$-5.2 \pm 0.1$	$-6.2 \pm 0.2$	-1.8
$\text{CH}_3\text{COOCH}_2\text{CH}_3$	-3.2	$-4.2 \pm 0.2$	$-3.4 \pm 0.9$	-1.0
$\text{CH}_3\text{CH}_2\text{COOCH}_3$	-3.1	$-5.1 \pm 0.3$	$-6.6 \pm 1.1$	-2.1

<sup>a</sup> Errors are derived from the linear fit of the Van Hoff plot.

As can be seen from Table 2.10, the free energies of the three binding systems are similar and each of them is composed of a favorable enthalpy factor and an unfavorable entropy factor. This indicates that the complexations of host **1** with small esters are driven by the favorable attracting forces between the host and the guest upon binding. Judged from the nature of both binding sites in the host and guests, CH- $\pi$  interactions are probably the main driving forces for the formation of the complexes. The observed unfavorable entropy change of binding is consistent with the observations of many other binding systems formed between synthetic water-soluble hosts and aliphatic guests.<sup>26</sup> Upon binding, the internal rotational entropy of each guest is considerably reduced. Hydrophobic effects seemed to be a minor contributor to the binding abilities of these esters from the classical view that the hydrophobic effect is evidenced from a possible entropy change.

We may conclude that binding between host **1** and the tested guests are controlled by various favorable interactions between host and guests, but not by the hydrophobic effect. But we've seen (in section iii) that the hydrophobicity of the guests is relevant to the binding strength. If the hydrophobic effect plays a minor role in binding, similar studies in non-aqueous solvents should yield the same results, thereby proving that the binding is driven only



by interactions between the host and the guest. To address this question, the binding experiments of methyl acetate with the three analogues of host **1** (the hosts **54-56** in Scheme 2.1) in other organic solvents ( $\text{CDCl}_3$  and  $\text{CD}_3\text{OD}$ ) were performed. The protons of the two methyl groups of the guest MeOAc experienced only small upfield shifts (0.02-0.03 ppm) (Table 2.11) upon addition of the hosts, which indicates that methyl acetate is barely included in the host cavity in the organic solvents. These much weaker bindings in organic solutions, compared to those in aqueous solutions cannot be explained simply by differences in attractive host-guest interactions. Hence, the large differences in binding strengths must come from factors related to the nature of the different solvents.

**Table 2.11** Observed chemical shift change of methyl acetate protons in solutions with 5 times excess of various hosts at 298K in organic solvents

solvent		$\text{CD}_3\text{OD}$	$\text{CDCl}_3$	$\text{CD}_3\text{OD}$
Host		<b>54</b>	<b>55</b>	<b>56</b>
$\Delta_{\text{obs}}$ (ppm)	$\text{CH}_3\text{CO}$	0.03	0.03	0.03
	$\text{OCH}_3$	0.03	0.02	0.03

Diederich had similar observations on account of the solvent effect.<sup>27</sup> The complexation behavior of cyclophane type host **10** (shown in Chapter 1) with pyrene both in water and in other organic solvents was studied. The stability of the complex was found to be considerably reduced in organic solvents than in water (an extra 8.1 kcal/mol in free binding energy was found upon changing from water to carbon disulfide).  $^1\text{H}$  NMR studies showed that the pyrene complex adopts a very similar geometry in all solvents which indicates the host-guest interactions are very similar in aqueous and non-aqueous environment.<sup>27</sup> The study also showed that there is a linear relationship between the free energies of complexation and the

empirical solvent polarity parameters  $E_T(30)$ .<sup>27</sup> Binding is the strongest in solvents having low molecular polarizabilities and high cohesive interactions, such as water. Thermodynamic data also show that the binding is enthalpically driven and entropically unfavorable in water, and the much weaker binding in methanol mainly results from a less favorable enthalpic term.

As Diederich commented: “the host-guest binding in water is a comprehensive result of favorable and unfavorable interactions between host-guest (HG), host-solvent (SG), guest-solvent (SG) and solvent-solvent (SS).”<sup>27</sup>, as can be seen from Equation 2.13:

$$\Delta G^\circ = \Delta H^\circ - T \cdot \Delta S^\circ = (\Delta H^{\circ SH} + \Delta H^{\circ SG} + \Delta H^{\circ SS} + \Delta H^{\circ HG}) - T \cdot (\Delta S^{\circ S} + \Delta S^{\circ G} + \Delta S^{\circ H})$$

### Equation 2.13

Host-guest binding in water is a process in which the host and guest molecules lose their interactions with water molecules (positive  $\Delta H^{SH}$  and  $\Delta H^{SG}$ ) and develop up interactions with each other (negative  $\Delta H^{HG}$ , negative  $\Delta S^G$  and  $\Delta S^H$ ), at the same time, solvent (water) molecules are released to the bulk solvent phase (negative  $\Delta H^{SS}$  and positive  $\Delta S^S$ ).

Since the geometries of the complexes in water and methanol are very similar, the intermolecular host-guest enthalpic term,  $\Delta H^{HG}$ , should be similar.<sup>15</sup> In aqueous solutions, the interactions between solvent molecules and host and guest molecules are mainly induced dipole-induced dipole interactions, in other words, London dispersion forces. The dispersion forces between water molecules and the host or guest surface are weaker than the forces between the host and guest surfaces ( $(\Delta H^{SH} + \Delta H^{SG}) < \Delta H^{HG}$ ).<sup>15</sup> This is seen by comparing the polarizability  $\alpha$  of different groups since London dispersion interactions are proportional to the polarizability  $\alpha$ . For example, for water oxygen atoms  $\alpha = 0.84 \text{ \AA}^3$ , hydroxyl residues  $\alpha = 1.20 \text{ \AA}^3$ ,  $\text{CH}_2$   $\alpha = 1.77 \text{ \AA}^3$ ,  $\text{CH}_3$   $\alpha = 2.17 \text{ \AA}^3$ , aromatic CH group  $\alpha = 2.07 \text{ \AA}^3$ . Since methanol possesses a polarizable methyl group which interacts favorable with the host and the guest, the

resulting  $\Delta H^{SH}$  and  $\Delta H^{SG}$  becomes more positive. So, the differences in dispersion interactions between the non-binding and binding states in methanol are not as large as that in water,<sup>27</sup> which leads to a much weaker binding in methanol.

Although numerous van der Waals contacts in “tight” complexes generate a very favorable host-guest interaction term  $\Delta H^{HG}$ , the translational and rotational degrees of freedom of the guest upon binding are considerably reduced (the host entropy is not influenced very much because of its highly preorganized structure). As a result, the favorable entropy of desolvation  $\Delta S^S$  does not completely compensate for a large unfavorable entropy term  $\Delta S^G$  for host-guest association.<sup>15</sup>

In conclusion, hydrophobic effects can be reflected in not only a favorable entropy change but also a favorable enthalpy change in a binding process. This is contrary to the classical opinion that the hydrophobic binding is driven by the favorable entropy change upon releasing the structured water into the bulk water phase. It is really dependent on the nature of the host and the guest, as well as the pattern of how they bind each other.

## **v. Computer Assisted Molecular Modeling**

Hyperchem ChemPlus<sup>28</sup> package was used to simulate the binding of free host **1** and eight successful guests in a water box with MM+ force field. The optimized structures shown in Figure 2.13 refer most stable conformations of each complex (energy minimum, which are obtained by calculations starting from several different orientations of the guests in the host cavity). Some of the relevant distances are shown in Table 2.12. The distance between the upper rim methyl groups (**a** in Figure 2.11), and that between the bottom carbon atoms of the

aromatic rings (**b** in Figure 2.11), respectively, revealed that the cavity shape of the free host **1** in water is almost a perfect square (Top view), with one of the sides slightly longer than the other sides (Figure 2.10). This pseudo-square shape is in agreement with Cram's X-ray crystal structure of another cavitand containing a similar cavity.<sup>22</sup> In water, the host molecule must undergo a rapid  $C_{2v}$ - $C_{2v}$  interconversion to give an averaged structure with  $C_{4v}$  symmetry as evidenced from the  $^1\text{H}$  NMR spectrum. The data for free and complexed hosts show that the inclusion of the guests does not have large influence on the cavity shape of the host (Table 2.12) (except **l**). This reflects the high rigidity of the cavity. From Figure 2.12 (structures **b**, **c** and **f-m**) we can see that the guests orient themselves with the methyl groups protruding deeply into the cavity. Seen from the distance between the host and guest carbons (distance of  $C_G-C_t$  and  $C_G-C_b$  in Table 2.12), all the methyl groups of the aliphatic guests protrude deeply into the cavity (compared to the C-C van der Waal's distance 3.4Å) each to a similar extent. This indicates that the different CIS values observed in the  $^1\text{H}$  NMR titration experiment for methyl groups of different guests are the result of averaged values from two binding modes rather than the result of different orientations of the guests lying in the cavity. Inclusion of the aryl H's of the aromatic ring of toluene is not favored compared to inclusion of the methyl group since it substantially changes the cavity shape (structure **l** in Figure 2.12 compare to the top view of cavitand in Figure 2.10). Both surfaces of benzene and toluene are hardly covered by the cavity upon binding, which indicates low complementary between the surfaces of the host **1** cavity and the aromatic guests ( structures **e**, **m** and **i** in Figure 2.12). Since most of the surface area of these arenes are still exposed to water in the host-guest complex, binding is weak. The energy differences (Table 2.13) between the two binding modes of those "unsymmetrical" guests review the relative selectivity of binding one of the binding site in

these “unsymmetrical” guests. The results are consistent with those concluded from  $^1\text{H}$  NMR titration experiments for methyl acetate, methyl propionate and toluene but conflict for ethyl acetate binding system. This reflects that the calculation simulates the experiments well but not perfectly.

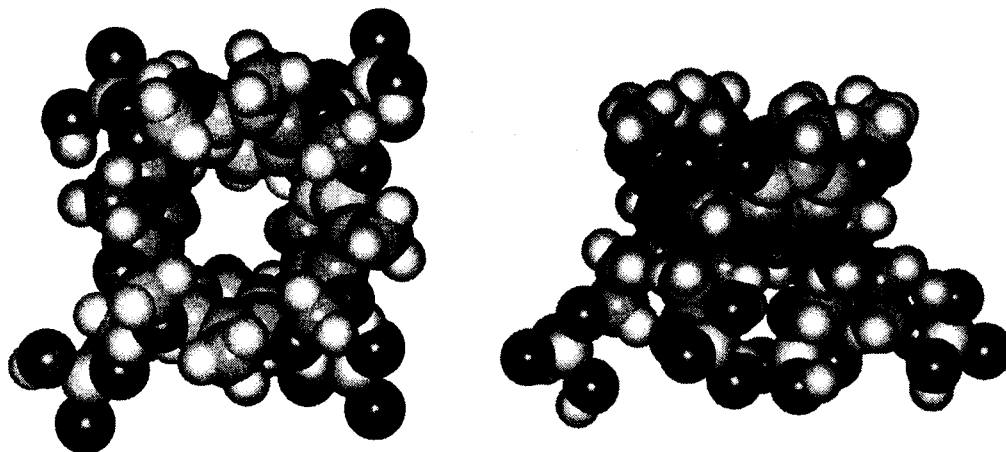


**Figure 2.10** Computed top (left) and side (right) view of cavitand 1

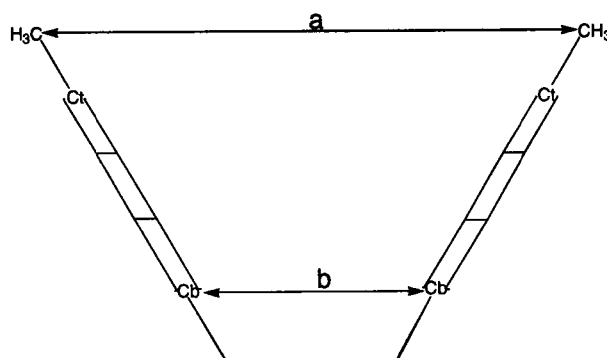


**Figure 2.11** Schematic presentation of cavity size of host 1 (side view)

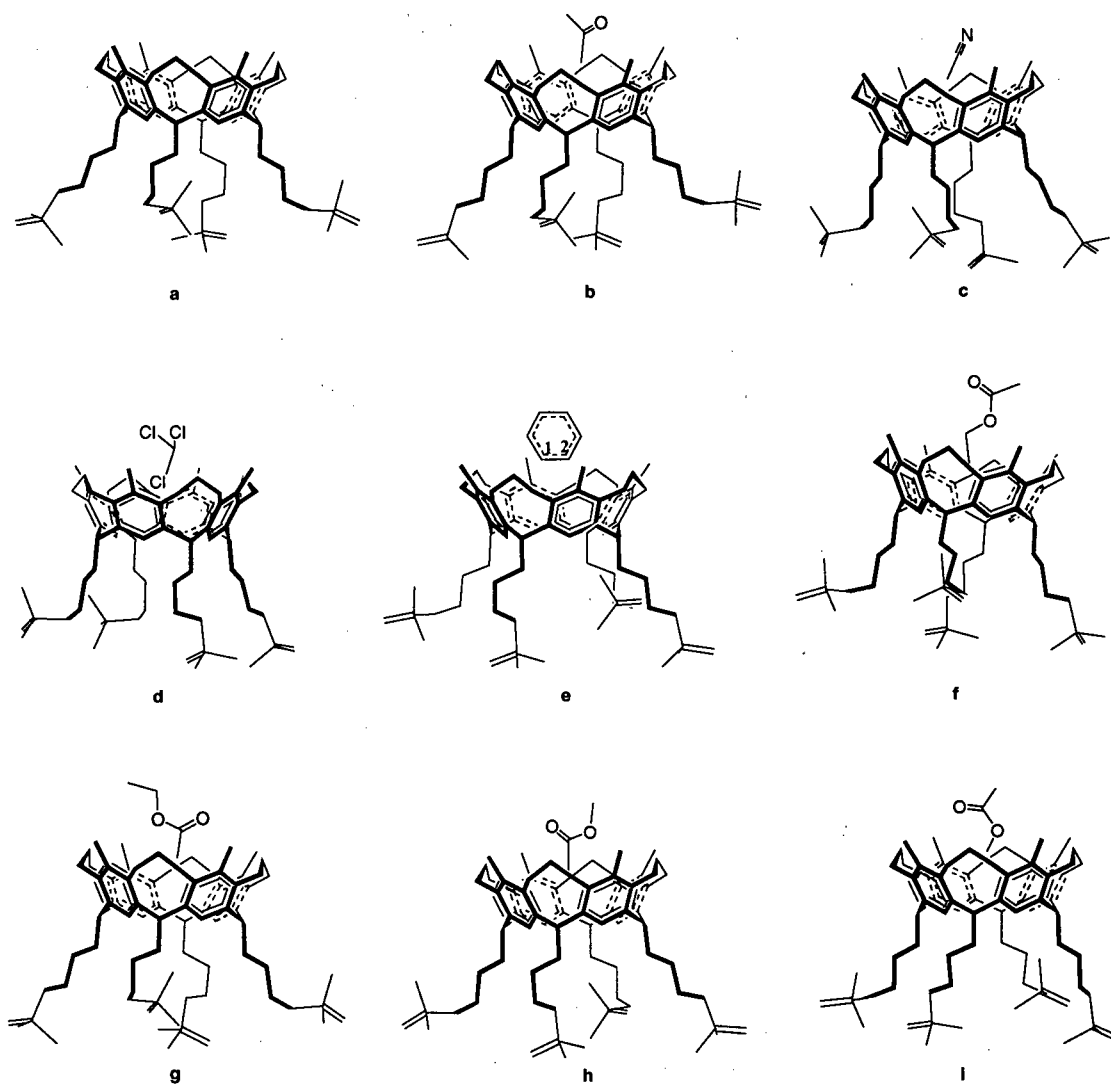


**Figure 2.12** Stable conformations of 1• guests obtained by MM+ optimization (to be continued)

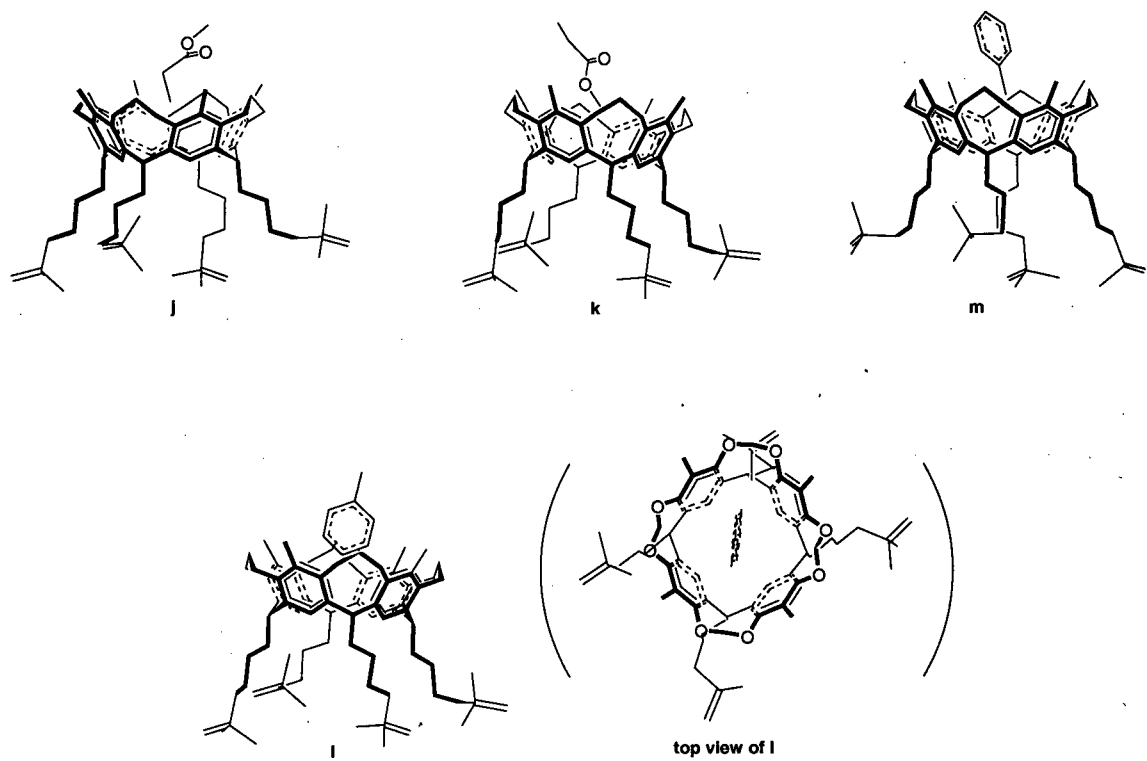


**Figure 2.13** Stable conformations of 1 • guests obtained by MM+ optimization

**Table 2.12** Relevant distances (in Å) for host 1 and its complexes with investigated guests obtained by MM+ optimization.

	1	Me <sub>2</sub> CO	MeCN	CHCl <sub>3</sub>	MeCO <sub>2</sub> Et		CH <sub>3</sub> CO <sub>2</sub> CH <sub>3</sub>		EtCO <sub>2</sub> CH <sub>3</sub>		CH <sub>3</sub> Ph		PhH	
					g	f	h	i	j	k	m	l	1	2
CH <sub>3</sub> -	9.77	9.78	9.71	9.81	9.72	9.74	9.76	9.78	9.79	9.78	9.86	9.74	9.94	
CH <sub>3</sub>	9.53	9.57	9.66	9.61	9.61	9.58	9.56	9.58	9.52	9.59	9.65	9.74	9.51	
C <sub>b</sub> -C <sub>b</sub>	5.10	5.09	5.09	5.09	5.12	5.13	5.12	5.08	5.09	5.09	5.10	5.09	5.04	
	5.17	5.15	5.14	5.14	5.14	5.16	5.17	5.15	5.17	5.14	5.11	5.09	5.17	
C <sub>G</sub> -CH <sub>3</sub> <sup>a</sup>		4.92	4.80	5.05	4.88	4.81	4.77	4.80	4.84	4.83	5.02	4.98	4.71	4.80
		4.80	4.94	4.38	4.84	4.89	5.11	4.95	4.97	4.88	4.67	4.79	4.30	5.69
		4.89	4.97	5.03	4.81	4.94	4.96	4.86	4.83	4.85	4.93	4.81	4.90	4.81
		4.83	4.80	5.42	4.95	5.00	4.79	4.89	4.93	4.98	5.08	5.00	5.65	4.26
C <sub>G</sub> -Ct		4.15	4.00	4.68	4.06	3.91	3.88	3.97	3.98	3.99	4.13	4.17	4.13	4.22
		4.02	4.11	4.10	4.02	3.99	4.22	4.13	4.10	4.03	3.82	3.96	3.72	5.04
		4.10	4.15	4.67	3.98	4.05	4.08	4.04	3.96	4.02	4.06	3.99	4.32	4.25
		4.04	3.98	5.01	4.13	4.10	3.90	4.07	4.06	4.14	4.23	4.19	5.00	3.71

<sup>a</sup> C<sub>G</sub> refers to the guest carbon which intrudes into the host cavity most deeply.

**Table 2.13** Calculated energy difference between two binding modes of “unsymmetrical” guest.

Guest	CH <sub>3</sub> COOEt		CH <sub>3</sub> COOCH <sub>3</sub>		EtCOOCH <sub>3</sub>		CH <sub>3</sub> Ph	
Conformation	f	g	h	i	j	k	l	m
E (kcal/mol) <sup>a</sup>	-660.4	-658.1	-690.8	-690.8	-689.2	-701.3	-694.3	-698.6
ΔE (kcal/mol)	2.3		0.0		2.1		4.3	

<sup>a</sup> E refers to the total energy relative to the same atoms that are not interacting.

## 2.4. Conclusion and Future

The synthesis and the binding properties of a water-soluble phosphate-footed cavitand 1 with four methyl groups on its upper rim was discussed. This cavitand is a good model for studying hydrophobic association in aqueous solutions, since it contains a pure hydrophobic and highly rigid cavity.



In aqueous solutions, host **1** selectively binds small neutral organic molecules and forms 1:1 stoichiometric complexes with most of the investigated guest molecules. The selectivity of the binding is controlled by the complementarity of the common surfaces between the host cavity and the guests as well as the hydrophobicity of the guests. For those guests containing two potential binding sites, it is believed more than one possible binding mode exists..

Thermodynamic parameters obtained by  $^1\text{H}$  NMR data indicated that various attractive intermolecular forces are the main driving forces of inclusions rather than the entropically favored desolvation of the guests. The enthalpically driven and entropically unfavorable character of the associations for host **1** with small neutral molecules supports Diederich's and many other scientists' work that the hydrophobic association formed from the tight complexation of small solutes in water is a process that is quite different from those established for the formation of looser aggregates in micelle and membrane systems.

The present work opens the door for the development of various water-soluble cavitands, designed for selective inclusion of particular guest molecules with different chemical/physical properties. The methyl groups on the upper rim of the host **1** can readily be converted to other functional groups, thereby increasing the selectivity of guest inclusion. Also it lays the groundwork for the formation of larger molecular assemblies in water.

## 2.5. Experimental

### A. Synthesis

#### i. General

All chemicals were reagent grade (Aldrich) except di-Benzyl-*N,N*-diethyl phosphoramidite (Toronto Research Chemicals) which was technical grade and used without further purification. THF was distilled under N<sub>2</sub> from sodium benzophenone ketyl. DMA (*N,N*-dimethyl acetamide) was dried over 4 Å molecular sieves.

Liquid secondary ionization mass spectra (LSIMS) were recorded on a Kratos Concept 2 HQ using various matrices as noted in the next section. Matrix-assisted laser desorption ionization (MALDI) mass spectra were recorded on a Bruker Reflex in reflectron mode using 2,5-dihydroxy benzoic acid (DHB) as the matrix. Melting points (uncorrected) were determined on a Fisher-Johns hot-stage melting point apparatus.

Microanalyses were performed by Mr. P. Borda of the UBC Microanalytical laboratory on a Carlo-Erba CHN elemental analyzer, model 1106 or a Fisons CHN-O elemental analyzer, model 1108.

<sup>1</sup>H NMR spectra were recorded on a Bruker WH-400 spectrometer at ambient temperature using residual H signals from deuterated solvents as a reference (CDCl<sub>3</sub>, 7.24; MeOD, 3.30; DMSO-*d*<sub>6</sub>, 2.49; D<sub>2</sub>O, 4.63 ppm)

<sup>31</sup>P NMR spectra were recorded on a Bruker AC-200 spectrometer referenced to external H<sub>3</sub>PO<sub>4</sub> (0.00 ppm).

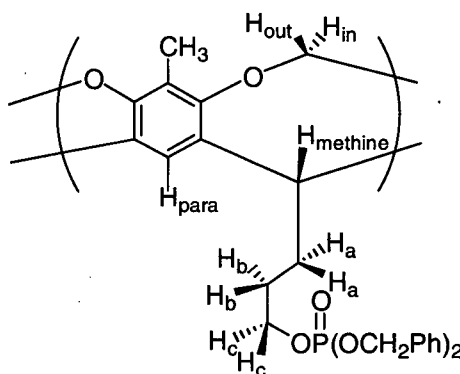
Silica gel (230-400 mesh, BDH) was used for column chromatography and silica gel glass backed analytical plates (0.2 mm, Aldrich) were used for t.l.c. with UV detection. Size

exclusion chromatography was performed using Sephadex LH-20. All products were dried overnight at RT and 0.1 Torr.

Radial Chromatography was performed on a Chromatotron (Model 7924T Harrison research) with self-made plates using silica gel (60 PF254 containing gypsum (EM science)).

## ii. Synthetic Procedures

### Benzyl Phosphorylated Methyl Cavitand **53**



**53**

1-H-Tetrazole (380 mg, 5.4 mmol) was added to a THF solution of hydroxyl-footed-2-methyl cavitand **52** (0.10 g, 0.12 mmol) and di-phenyl *N,N*-diethylphosphoramidite (0.54 mL, 1.82 mmol) and stirred for 20 min under  $N_2$  atmosphere. The reaction mixture was then cooled to  $-78^\circ C$  and  $H_2O_2$  (0.20 mL, 1.82 mmol) was added. After slowly warming to RT (over 30 min), the reaction mixture was washed with 10%  $Na_2S_2O_5$ , saturated  $NaHCO_3$  (aq.), saturated  $NaCl$  (aq.), and dried over  $MgSO_4$  and evaporated to dryness. The residue was purified by size-exclusion chromatography (EtOAc: MeOH:  $H_2O$  = 40:10:4) followed by radial chromatography (chromatotron)( $CHCl_3$ : MeOH = 100:2) to afford benzyl protected methyl phosphated **53** as a colorless oil (0.15 g, 65%).

**<sup>1</sup>H NMR** (CDCl<sub>3</sub>, 400MHz) δ 7.28 (s, 40H, CH<sub>2</sub>Ph), 6.90 (s, 4H, H<sub>para</sub>), 5.85 (d, *J* = 6.9 Hz, 4H, H<sub>out</sub>), 4.99 (d, *J* = 8.2 Hz, 16H, POCH<sub>2</sub>), 4.79 (t, *J* = 8.2 Hz, 4H, H<sub>methine</sub>), 4.23 (d, *J* = 6.9Hz, 4H, H<sub>in</sub>), 4.07 (m, 8H, H<sub>c</sub>), 2.25 (bm, 8H, H<sub>b</sub>), 1.95 (s, 12H, CH<sub>3</sub>), 1.63 (bm, 8H, H<sub>a</sub>) ppm

**<sup>31</sup>P NMR** (CDCl<sub>3</sub>, 81 MHz) δ 0.00 (s) ppm

**HRMS** (LSIMS<sup>+</sup>, 3-NBA) Calculated for (M + H)<sup>+</sup>: 1865.6251; Found 1865.6261

### Phosphated-Footed 2-Methyl Cavitand **54**

A catalytic amount of 10% palladium/carbon was added to a solution of pure benzyl phosphorylated cavitand **53** (140 mg, 0.075 mmol) in EtOAc: CH<sub>3</sub>OH (1:1, 30 mL) and stirred for 10 min under H<sub>2</sub> atmosphere. The reaction mixture was evaporated under vacuum to afford phosphate-footed-2-methyl cavitand **54** as a white solid (86.6 mg, 86%).

**<sup>1</sup>H NMR** (CD<sub>3</sub>OD, 500 MHz) δ 7.15 (s, 4H, H<sub>para</sub>), 5.83 (d, *J* = 7.1 Hz, 4H, H<sub>out</sub>), 4.76 (t, *J* = 7.6 Hz, 4H, H<sub>methine</sub>), 4.25 (d, *J* = 7.1 Hz, 4H, H<sub>in</sub>), 4.11 (bm, 8H, H<sub>c</sub>), 2.40 (bm, 8H, H<sub>b</sub>), 1.96 (s, 12H, CH<sub>3</sub>), 1.69 (bm, 8H, H<sub>a</sub>) ppm

**<sup>31</sup>P NMR** (CD<sub>3</sub>OD, 81 MHz) δ 1.77 (s, 4P) ppm

**HRMS** (LSIMS<sup>+</sup>, thioglycerol) Calculated for (M + H)<sup>+</sup>: 1145.2556; Found: 1145.2497

### Phosphate ammonium salt **1**

To a 15 mL centrifuge tube was added 20 mg of **54** and 10 ml of 0.1 M (NH<sub>4</sub>)<sub>2</sub>CO<sub>3</sub> buffer solution. The dissolved material was freeze dried. The procedure was repeated three times to assure full conversion of **54** to **1**.

**$^1\text{H}$  NMR** ( $\text{D}_2\text{O}$ , 400 MHz)  $\delta$  7.25 (s, 4H,  $\text{H}_{\text{para}}$ ), 5.92 (d,  $J = 7.2$  Hz, 4H,  $\text{H}_{\text{out}}$ ), 4.11 (d,  $J = 7.1$  Hz, 4H,  $\text{H}_{\text{in}}$ ), 3.90 (bm, 8H,  $\text{H}_{\text{c}}$ ), 2.35 (bm, 8H,  $\text{H}_{\text{b}}$ ), 1.88 (s, 12H,  $\text{CH}_3$ ), 1.60 (bm, 8H,  $\text{H}_{\text{a}}$ ) ppm

**$^{31}\text{P}$  NMR** ( $\text{D}_2\text{O}$ , 81 MHz)  $\delta$  3.41(s) ppm

**MS** (LSIMS<sup>+</sup>, thioglycerol +  $\text{H}_2\text{O}$ )  $m/z$  (rel intensity): 1145 ( $\text{M}-4\text{NH}_3 + \text{H}$ )<sup>+</sup>; 100)

**Anal.** Calcd for  $\text{C}_{48}\text{O}_{24}\text{H}_{60}\text{P}_4 \cdot 3.5\text{NH}_3 \cdot 4\text{H}_2\text{O}$ : C, 45.16; H, 6.20; N, 3.84. Found: C, 45.18; H, 6.13; N, 3.76.

## B. Binding Study

### i. General

All chemicals used as potential guests in the binding studies were HPLC grade or reagent grade (Fisher) and used without further purification except methyl pyridinium iodide, which was synthesized by a known literature procedure.<sup>29</sup>

$^1\text{H}$  NMR spectra were recorded on a Bruker AMX-500 spectrometer at 25°C, or on a Bruker WH-400 spectrometer at ambient temperature [(20±2)°C]. Chemical shifts ( $\delta$ ) were referenced to the residual proton signals of the solvents ( $\text{D}_2\text{O}$ , 4.63;  $\text{CD}_3\text{OD}$ , 3.30;  $\text{CDCl}_3$ , 7.24 ppm).

All of the aqueous binding experiments were performed in pD 9.4 ammonium carbonate- $\text{D}_2\text{O}$  buffer solution.

The pD's of the buffer solutions were determined using a Fisher Scientific Accumet® pH meter 915 calibrated with two purchased buffered standards (pH 4.0 and pH 10.0). pD value was then calculated as:  $\text{pD} = \text{pH} + 0.4$

## ii. Determination of Binding Stoichiometry

Stock solutions of host and guest were prepared (5 mM each) and separated into NMR tubes to give the following Guest:Host volume ratios (in  $\mu\text{L}$ ): 500:0, 450:50, 400:100, 350:150, 300:200, 250:250, 200:300, 150:350, 100:400, 50:450.  $^1\text{H}$  NMR spectra of all samples were obtained and the standard Job's plot was graphed to determine the binding stoichiometry.

The sample preparing information and guest proton chemical shift data are shown in Table 2.14-2.17, where X is the mole fraction of the guest in the sample solution ( $X = [\text{G}]_0/([\text{G}]_0 + [\text{H}]_0)$ ).

**Table 2.14**  $^1\text{H}$  NMR assignments of guest chemical shifts for Job's plot of methyl acetate at ambient room temperature.

	X									
	1	0.9	0.8	0.7	0.6	0.5	0.4	0.3	0.2	0.1
$[\text{G}]_0$ (mM)	5.0	4.5	4.0	3.5	3.0	2.5	2.0	1.5	1.0	0.5
$\delta_{\text{Ha}}$ (ppm)	1.97	1.84	1.69	1.56	1.42	1.32	1.21	1.09	1.03	1.95
$\Delta_{\text{Ha}}$ (ppm)	0	0.13	0.28	0.41	0.55	0.65	0.76	0.88	0.94	1.02
$[\text{G}]_0 \cdot \Delta_{\text{Ha}}$	0	0.58	1.1	1.4	1.6	1.6	1.5	1.3	0.94	0.51
$\delta_{\text{Hb}}$ (ppm)	3.57	3.44	3.31	3.19	3.07	2.97	2.88	2.76	2.72	2.64
$\Delta_{\text{Hb}}$ (ppm)	0	0.13	0.26	0.38	0.50	0.60	0.69	0.81	0.85	0.93
$[\text{G}]_0 \cdot \Delta_{\text{Hb}}$	0	0.59	1.0	1.3	1.5	1.5	1.4	1.2	0.85	0.47

**Table 2.15**  $^1\text{H}$  NMR assignment of guest signals for Job's plot of ethyl acetate at ambient room temperature.

	X									
	1	0.9	0.8	0.7	0.6	0.5	0.4	0.3	0.2	0.1
$[\text{G}]_0$ (mM)	5.0	4.5	4.0	3.5	3.0	2.5	2.0	1.5	1.0	0.5
$\delta_{\text{Ha}}$ (ppm)	1.97	1.83	1.64	1.51	1.33	1.13	0.99	0.81	0.63	0.49
$\Delta_{\text{Ha}}$ (ppm)	0	0.14	0.33	0.46	0.64	0.84	0.98	1.16	1.33	1.48
$[\text{G}]_0 \cdot \Delta_{\text{Ha}}$	0	0.63	1.3	1.6	1.9	2.1	2.0	1.7	1.3	0.74
$\delta_{\text{Hb}}$ (ppm)	4.03	4.01	3.97	3.95	3.92	3.88	3.85	3.82	3.74	3.74
$\Delta_{\text{Hb}}$ (ppm)	0	0.02	0.06	0.08	0.12	0.15	0.18	0.21	0.30	0.30
$[\text{G}]_0 \cdot \Delta_{\text{Hb}}$	0	0.10	0.24	0.29	0.34	0.38	0.36	0.32	0.30	0.15
$\delta_{\text{Hc}}$ (ppm)	1.14	1.11	1.07	1.03	1.00	0.95	0.92	0.87	0.83	0.80
$\Delta_{\text{Hc}}$ (ppm)	0	0.03	0.07	0.11	0.14	0.19	0.22	0.27	0.31	0.34
$[\text{G}]_0 \cdot \Delta_{\text{Hc}}$	0	0.14	0.29	0.37	0.43	0.47	0.45	0.40	0.31	0.17

**Table 2.16**  $^1\text{H}$  NMR assignment of guest signals for Job's plot of methyl propionate at ambient room temperature.

	X									
	1	0.9	0.8	0.7	0.6	0.5	0.4	0.3	0.2	0.1
$[\text{G}]_0$	5.0	4.5	4.0	3.5	3.0	2.5	2.0	1.5	1.0	0.5
$\delta_{\text{Ha}}$	0.98	0.95	0.92	0.89	0.85	0.81	0.77	0.73	0.68	0.63
$\Delta_{\text{Ha}}$	0	0.03	0.06	0.09	0.13	0.17	0.21	0.25	0.30	0.35
$[\text{G}]_0 \cdot \Delta_{\text{Ha}}$	0	0.12	0.23	0.32	0.38	0.42	0.42	0.37	0.30	0.17
$\delta_{\text{Hb}}$	2.29	2.27	2.24	2.22	2.19	2.16	2.13	2.10	2.06	2.02
$\Delta_{\text{Hb}}$	0	0.02	0.05	0.07	0.10	0.13	0.16	0.19	0.23	0.26
$[\text{G}]_0 \cdot \Delta_{\text{Hb}}$	0	0.09	0.18	0.25	0.30	0.33	0.32	0.28	0.23	0.13
$\delta_{\text{Hc}}$	3.58	3.45	3.33	3.19	3.06	2.91	2.77	2.64	2.49	2.31
$\Delta_{\text{Hc}}$	0	0.13	0.25	0.39	0.52	0.67	0.81	0.94	1.09	1.27
$[\text{G}]_0 \cdot \Delta_{\text{Hc}}$	0	0.58	1.0	1.4	1.6	1.7	1.6	1.4	1.1	0.64

**Table 2.17**  $^1\text{H}$  NMR assignment of guest signals for Job's plot of dimethyl carbonate

	X									
	1	0.9	0.8	0.7	0.6	0.5	0.4	0.3	0.2	0.1
$[\text{G}]_0$	5.0	4.5	4.0	3.5	3.0	2.5	2.0	1.5	1.0	0.5
$\delta_{\text{CH}_3\text{O}}$	3.63	3.53	3.42	3.23	2.14	2.92	2.76	2.55	2.32	2.26
$\Delta_{\text{CH}_3\text{O}}$	0	0.10	0.22	0.40	0.49	0.71	0.87	1.08	1.31	1.37
$[\text{G}]_0 \Delta_{\text{CH}_3\text{O}}$	0	0.45	0.87	1.4	1.5	1.8	1.7	1.6	1.3	0.68

### iii. General Procedure for Determination of Binding Constants

Stock solutions of host **1** were prepared as follows: Host **1** (36.4 mg, 28.5  $\mu\text{mol}$ ) was weighed into a 3.0 mL volumetric flask and the remaining volume was filled with ammonium carbonate- $\text{D}_2\text{O}$  buffer (50 mM). 100 mM stock solutions of each guest were prepared in a similar fashion in  $\text{D}_2\text{O}$ . For the very hydrophobic guests such as chloroform, dichloromethane, benzene, and toluene, the saturated solutions were prepared and the concentration of the solutions were determined through NMR integrations against a standard solution of EtOH in  $\text{D}_2\text{O}$  (100.5 mM).

An equal volume of the stock solution of a guest (10  $\mu\text{L}$ ) were added to 12 NMR tubes. The host stock solution was then added to each NMR tube in increasing increments as follows (in  $\mu\text{L}$ ): 0, 80, 100, 120, 160, 200, 250, 300, 350, 400, 450, 490. This provided a range of host:guest ratios from 0 to 5 equivalents. The solutions in each NMR tube were then diluted to 500  $\mu\text{L}$  with  $\text{D}_2\text{O}$  buffer. The NMR tubes were then capped and wrapped with parafilm. Diagnostic guest peak shifts were followed by NMR and the titration curves ( $[\text{H}]$  against  $\Delta$ ) were fit to the 1:1 binding model using the nonlinear least-squares curve-fitting program GraFit<sup>TM</sup>.<sup>30</sup> The errors reported with the binding constant values are derived from this



procedure. For those very hydrophobic guests (benzene, toluene and chloroform), the saturated solutions of a particular guest in D<sub>2</sub>O under room temperature were prepared as the stock solutions. Both host and guest stock solutions were then adjusted to proper volumes to perform binding experiments.

The chemical shifts of the guest protons from the titration experiments are shown in the following tables where **R** is the mole ratio of host:guest; [H]<sub>0</sub>, [G]<sub>0</sub> are the initial host/guest concentrations, respectively; V<sub>H</sub>, V<sub>G</sub> are the volumes of host or guest stock solutions for preparing a specific sample solution with host:guest ratio equal to **R**;  $\delta$  is the observed chemical shift for a specific guest proton;  $\Delta$  is the chemical shift difference between guest proton chemical shifts with presence and absence of host.

**Table 2.18** Guest signal assignment for acetone binding in pD 9.4 carbonate buffer at 298K.

	<b>R</b>									
	0	0.8:1	1.0:1	1.1:1	1.9:1	2.9:1	3.3:1	3.8:1	4.3:1	4.7:1
[H] <sub>0</sub> (mM)	0	1.52	1.90	2.28	3.80	5.71	6.66	7.61	8.56	9.32
[G] <sub>0</sub> (mM)	2.00	2.00	2.00	2.00	2.00	2.00	2.00	2.00	2.00	2.00
$\delta_{\text{CH}_3}$ (ppm)	2.06	2.00	1.98	1.97	1.91	1.85	1.81	1.78	1.75	1.72
$\Delta_{\text{CH}_3}$ (ppm)	0	0.06	0.08	0.09	0.15	0.22	0.25	0.28	0.31	0.33

**Table 2.19** <sup>1</sup>H NMR assignment of guest signal for CH<sub>3</sub>CN binding in pD 9.4 carbonate buffer at 298K.

	<b>R</b>								
	0	1.0:1	1.5:1	1.9:1	2.9:1	3.3:1	3.8:1	4.3:1	4.7:1
[H] <sub>0</sub> (mM)	0	1.90	3.04	3.80	5.71	6.66	7.61	8.56	9.32
[G] <sub>0</sub> (mM)	2.00	2.00	2.00	2.00	2.00	2.00	2.00	2.00	2.00
$\delta_{\text{CH}_3}$ (ppm)	1.90	1.69	1.58	1.51	1.36	1.27	1.20	1.14	1.10
$\Delta_{\text{CH}_3}$ (ppm)	0	0.21	0.32	0.38	0.55	0.63	0.70	0.76	0.81

**Table 2.20**  $^1\text{H}$  NMR assignment of guest signal for benzene binding in pD 9.4 carbonate buffer at 298K.<sup>a</sup>

	R							
	0	0.5:1	0.7:1	0.9:1	1.1:1	2.3:1	2.8:1	3.4:1
$V_{\text{H}}$ ( $\mu\text{l}$ )	0	40	60	80	100	200	250	300
$[\text{H}]_0$ (mM)	0	0.76	1.14	1.52	1.90	3.80	4.76	5.71
$V_{\text{G}}$ ( $\mu\text{l}$ )	200	200	200	200	200	200	200	200
$[\text{G}]_0$ (mM)	1.69	1.69	1.69	1.69	1.69	1.69	1.69	1.69
$\delta_{\text{CH}}$ (ppm)	7.31	7.29	7.28	7.21	7.26	7.22	7.20	7.18
$\Delta_{\text{CH}}$ (ppm)	0	0.02	0.03	0.04	0.05	0.09	0.11	0.14

<sup>a</sup> 4.2 mM stock solution of benzene was used.

**Table 2.21**  $^1\text{H}$  NMR assignment of guest signals for toluene binding in pD 9.4 carbonate buffer at 298K.

	R											
	0	0.6:1	0.9:1	1.2:1	1.8:1	2.5:1	3.1:1	3.7:1	4.9:1	5.5:1	6.1:1	7.7:1
$V_{\text{H}}$ ( $\mu\text{l}$ )	0	20	30	40	60	80	100	120	160	180	200	250
$[\text{H}]_0$ (mM)	0	0.38	0.57	0.76	1.14	1.52	1.90	2.28	3.04	3.42	3.80	4.76
$V_{\text{G}}$ ( $\mu\text{l}$ )	250	250	250	250	250	250	250	250	250	250	250	250
$[\text{G}]_0$ (mM)	0.62	0.62	0.62	0.62	0.62	0.62	0.62	0.62	0.62	0.62	0.62	0.62
$\delta_{\text{CH}_3}$ (ppm)	2.19	2.16	2.15	2.14	2.11	2.08	2.05	2.03	1.98	1.95	1.93	1.87
$\Delta_{\text{CH}_3}$ (ppm)	0	0.03	0.04	0.06	0.08	0.11	0.14	0.16	0.21	0.24	0.26	0.32
$\delta_{\text{H}_o}$ (ppm)	7.13	7.12	7.11	7.10	7.09	7.08	7.07	7.06	7.04	7.03	7.02	6.99
$\Delta_{\text{H}_o}$ (ppm)	0	0.01	0.02	0.03	0.04	0.05	0.06	0.07	0.09	0.10	0.11	0.14
$\delta_{\text{H}_m}$ (ppm)	7.19	7.18	7.18	7.17	7.16	7.15	7.14	7.14	7.12	7.12	7.11	7.09
$\Delta_{\text{H}_m}$ (ppm)	0	0.01	0.01	0.02	0.03	0.04	0.05	0.05	0.07	0.07	0.08	0.10
$\delta_{\text{H}_p}$ (ppm)	7.08	7.07	7.07	7.06	7.05	7.04	7.03	7.02	6.99	6.98	6.97	6.94
$\Delta_{\text{H}_p}$ (ppm)	0	0.01	0.02	0.03	0.04	0.05	0.06	0.07	0.09	0.10	0.11	0.14

**Table 2.22**  $^1\text{H}$  NMR assignment of guest signal for chloroform binding in pD 9.4 carbonate buffer at 298K.<sup>a, b</sup>

	R										
	0	0.5:1	1.1:1	1.6:1	2.2:1	2.7:1	3.4:1	4.1:1	4.8:1	5.4:1	6.1:1
$V_{\text{H}}$ ( $\mu\text{l}$ )	0	40	80	120	160	200	250	300	350	400	450
$[\text{H}]_0$ (mM)	0	0.65	1.30	1.96	2.61	3.26	4.08	4.89	5.71	6.52	7.34
$V_{\text{G}}$ ( $\mu\text{l}$ )	50	50	50	50	50	50	50	50	50	50	50
$[\text{G}]_0$ (mM)	1.20	1.20	1.20	1.20	1.20	1.20	1.20	1.20	1.20	1.20	1.20
$\delta_{\text{CH}}$ (ppm)	7.53	7.46	7.40	7.35	7.31	7.27	7.22	N/A	7.14	7.10	7.07
$\Delta_{\text{CH}}$ (ppm)	0	0.07	0.12	0.17	0.22	0.26	0.31	N/A	0.39	0.43	0.46

<sup>a</sup>. 12.0 mM stock solution of guest was used; <sup>b</sup>. 8.15 mM stock solution of host was used. The host concentration of the stock solution is determined from  $^1\text{H}$  NMR integration;

**Table 2.23**  $^1\text{H}$  NMR chemical shift of guest protons for methyl acetate binding in pD 9.4 carbonate buffer at 298K.

	R									
	0	0.8:1	1.0:1	1.1:1	1.5:1	1.9:1	2.4:1	2.9:1	4.3:1	4.7:1
$[\text{H}]_0$ (mM)	0	1.52	1.90	2.28	3.04	3.80	4.76	5.71	8.56	9.32
$[\text{G}]_0$ (mM)	2.00	2.00	2.00	2.00	2.00	2.00	2.00	2.00	2.00	2.00
$\delta_{\text{Ha}}$ (ppm)	1.93	1.41	1.33	1.20	1.05	0.91	0.78	0.67	0.43	0.39
$\Delta_{\text{Ha}}$ (ppm)	0	0.52	0.60	0.73	0.88	1.02	1.15	1.26	1.50	1.55
$\delta_{\text{Hb}}$ (ppm)	3.52	3.05	2.97	2.86	2.72	2.61	2.47	2.37	2.15	2.11
$\Delta_{\text{Hb}}$ (ppm)	0	0.48	0.55	0.67	0.80	0.92	1.05	1.16	1.37	1.41

**Table 2.24**  $^1\text{H}$  NMR assignment of guest protons for ethyl acetate binding in pD 9.4 carbonate buffer at 298K.

	R											
	0	0.8:1	1.0:1	1.1:1	1.5:1	1.9:1	2.4:1	2.9:1	3.3:1	3.8:1	4.3:1	4.7:1
$[\text{H}]_0$ (mM)	0	1.52	1.90	2.28	3.04	3.80	4.76	5.71	6.66	7.61	8.56	9.32
$[\text{G}]_0$ (mM)	2.00	2.00	2.00	2.00	2.00	2.00	2.00	2.00	2.00	2.00	2.00	2.00
$\delta_{\text{Ha}}$ (ppm)	1.92	1.25	1.12	0.99	0.74	0.55	0.35	0.16	0.02	-0.11	-0.21	-0.29
$\Delta_{\text{Ha}}$ (ppm)	0	0.67	0.81	0.94	1.18	1.37	1.57	1.76	1.90	2.03	2.14	2.21
$\delta_{\text{Hb}}$ (ppm)	3.99	3.86	3.83	3.81	3.77	N/A	N/A	N/A	3.63	3.59	3.56	3.55
$\Delta_{\text{Hb}}$ (ppm)	0	0.12	0.15	0.17	0.22	N/A	N/A	N/A	0.36	0.40	0.42	0.44
$\delta_{\text{Hc}}$ (ppm)	1.09	0.94	0.90	0.87	0.82	0.77	0.72	0.67	0.63	0.59	0.56	0.54
$\Delta_{\text{Hc}}$ (ppm)	0	0.15	0.19	0.22	0.27	0.32	0.37	0.42	0.46	0.50	0.53	0.55

**Table 2.25**  $^1\text{H}$  NMR assignment of the guest protons for the methyl propionate binding in pD 9.4 carbonate buffer at 298K.

	R									
	0	0.8:1	1.0:1	1.1:1	1.9:1	2.4:1	2.9:1	3.8:1	4.3:1	4.7:1
[H] <sub>0</sub> (mM)	0	1.52	1.90	2.28	3.80	4.76	5.71	7.61	8.56	9.32
[G] <sub>0</sub> (mM)	2.00	2.00	2.00	2.00	2.00	2.00	2.00	2.00	2.00	2.00
δ <sub>Ha</sub> (ppm)	0.94	0.77	0.73	0.69	0.56	0.47	0.41	0.29	0.22	0.19
Δ <sub>Ha</sub> (ppm)	0	0.17	0.21	0.25	0.37	0.47	0.53	0.64	0.72	0.75
δ <sub>Hb</sub> (ppm)	2.24	2.11	2.08	2.05	1.96	1.90	N/A	N/A	N/A	1.71
Δ <sub>Hb</sub> (ppm)	0	0.13	0.17	0.19	0.28	0.34	N/A	N/A	N/A	0.54
δ <sub>Hc</sub> (ppm)	3.54	2.87	2.71	2.58	2.19	N/A	N/A	N/A	1.44	1.34
Δ <sub>Hc</sub> (ppm)	0	0.67	0.83	0.96	1.35	N/A	N/A	N/A	2.10	2.19

#### iv. Variable temperature (VT) $^1\text{H}$ NMR experiments

VT  $^1\text{H}$  NMR spectra were recorded on a Bruker AMX-500 spectrometer. The entire titration experiments for a certain guest were run at 4 to 5 different temperatures. The NMR tubes were equilibrated for at least 5 min in the spectrometer prior to data acquisition. The probe temperature was calibrated against either a methanol or an ethylene glycol thermometer (see page 97 for the preparation of the thermometers). The binding constants for each temperature points were calculated using a non-linear least square procedure and binding enthalpies and entropies were obtained from the slope and intercept of the van't Hoff plot ( $1/T$  against  $\ln K_a$ ). Errors of the calculated enthalpies and entropies were obtained from the linear fit of the Equation 2.9.

**Table 2.26**  $^1\text{H}$  NMR assignment of guest protons for methyl acetate VT experiments

		R									
		0	0.8:1	1.0:1	1.1:1	1.5:1	1.9:1	2.4:1	2.9:1	4.3:1	4.7:1
304 K	$[\text{H}]_0$ (mM)	0	1.52	1.90	2.28	3.04	3.80	4.76	5.71	8.56	9.32
	$[\text{G}]_0$ (mM)	2.00	2.00	2.00	2.00	2.00	2.00	2.00	2.00	2.00	2.00
	$\delta_{\text{Ha}}$ (ppm)	1.93	N/A	1.39	1.28	1.14	0.99	0.87	0.77	0.52	0.48
	$\Delta_{\text{Ha}}$ (ppm)	0	N/A	0.54	0.65	0.79	0.94	1.06	1.16	1.41	1.45
	$\delta_{\text{Hb}}$ (ppm)	3.52	3.11	3.03	2.93	2.79	2.67	2.56	2.45	N/A	2.20
	$\Delta_{\text{Hb}}$ (ppm)	0	0.42	0.49	0.59	0.73	0.85	0.96	1.07	N/A	1.32
298 K	$\delta_{\text{Ha}}$ (ppm)	1.93	1.41	1.33	1.20	1.05	0.91	0.78	0.67	0.43	0.38
	$\Delta_{\text{Ha}}$ (ppm)	0	0.52	0.60	0.73	0.88	1.02	1.15	1.26	1.50	1.55
	$\delta_{\text{Hb}}$ (ppm)	3.52	3.05	2.97	2.86	2.72	2.61	2.47	2.37	2.15	2.11
	$\Delta_{\text{Hb}}$ (ppm)	0	0.48	0.55	0.67	0.80	0.92	1.05	1.16	1.37	1.41
292 K	$\delta_{\text{Ha}}$ (ppm)	1.93	1.34	1.27	1.14	0.97	0.83	0.68	0.57	0.34	0.30
	$\Delta_{\text{Ha}}$ (ppm)	0	0.59	0.66	0.79	0.96	1.10	1.25	1.36	1.59	1.63
	$\delta_{\text{Hb}}$ (ppm)	3.52	2.98	2.91	2.80	2.64	2.51	2.38	N/A	2.07	2.03
	$\Delta_{\text{Hb}}$ (ppm)	0	0.54	0.61	0.73	0.88	1.01	1.14	N/A	1.45	1.49
286 K	$\delta_{\text{Ha}}$ (ppm)	1.93	1.28	1.19	1.04	0.89	0.76	0.60	1.49	0.25	0.22
	$\Delta_{\text{Ha}}$ (ppm)	0	0.65	0.74	0.89	1.04	1.17	1.33	1.44	1.68	1.71
	$\delta_{\text{Hb}}$ (ppm)	3.52	2.92	2.84	2.71	2.55	2.41	N/A	2.18	1.98	1.95
	$\Delta_{\text{Hb}}$ (ppm)	0	0.60	0.69	0.82	0.97	1.11	N/A	1.34	1.54	1.57

**Table 2.27**  $^1\text{H}$  NMR assignment of guest protons for of ethyl acetate VT experiments

		R											
		0	0.8:1	1.0:1	1.1:1	1.5:1	1.9:1	2.4:1	2.9:1	3.3:1	3.8:1	4.3:1	4.7:1
[H] <sub>0</sub> (mM)		0	1.52	1.90	2.28	3.04	3.80	4.76	5.71	6.66	7.61	8.56	9.32
[G] <sub>0</sub> (mM)		2.00	2.00	2.00	2.00	2.00	2.00	2.00	2.00	2.00	2.00	2.00	2.00
303 K	δ <sub>Ha</sub> (ppm)	1.92	1.25	1.11	0.99	0.74	0.55	0.35	0.16	0.02	-0.11	-0.21	-0.29
	Δ <sub>Ha</sub> (ppm)	0	0.67	0.81	0.93	1.18	1.37	1.57	1.76	1.90	2.03	2.14	2.21
298 K	δ <sub>Ha</sub> (ppm)	1.92	1.18	1.03	0.91	0.65	0.46	0.25	0.07	-0.08	-0.22	-0.33	-0.40
	Δ <sub>Ha</sub> (ppm)	0	0.74	0.89	1.01	1.27	1.46	1.67	1.85	2.00	2.14	2.25	2.32
292 K	δ <sub>Ha</sub> (ppm)	1.92	1.09	0.94	0.79	0.52	0.32	0.10	-0.09	-0.25	-0.38	-0.50	N/A
	Δ <sub>Ha</sub> (ppm)	0	0.83	0.98	1.13	1.40	1.60	1.82	2.01	2.17	2.30	2.42	N/A
288 K	δ <sub>Ha</sub> (ppm)	1.92	1.04	0.88	0.75	0.45	0.26	-0.01	-0.16	-0.33	-0.43	-0.55	-0.64
	Δ <sub>Ha</sub> (ppm)	0	0.88	1.04	1.17	1.47	1.66	1.93	2.08	2.25	2.35	2.47	2.55
283 K	δ <sub>Ha</sub> (ppm)	1.92	0.96	0.79	0.63	0.35	0.12	-0.12	-0.30	-0.46	-0.59	-0.67	-0.74
	Δ <sub>Ha</sub> (ppm)	0	0.95	1.13	1.29	1.57	1.80	2.03	2.22	2.38	2.50	2.59	2.66

**Table 2.28**  $^1\text{H}$  NMR assignment of guest protons for methyl propionate VT experiments<sup>a,b</sup>

		R										
		0	0.8:1	1.0:1	1.1:1	1.9:1	2.4:1	2.9:1	3.8:1	4.3:1	4.7:1	
	[H] <sub>0</sub>	0	1.52	1.90	2.28	3.80	4.76	5.71	7.61	8.56	9.32	
307K	δ <sub>Ha</sub> (ppm)	3.49	2.93	2.80	2.69	2.34	2.12	2.00	1.72	1.58	1.51	
	Δ <sub>Ha</sub> (ppm)	0	0.56	0.69	0.81	1.16	1.37	1.49	1.77	1.91	1.98	
302 K	δ <sub>Ha</sub> (ppm)	3.49	2.86	2.72	2.60	N/A	2.00	1.83	N/A	N/A	1.37	
	Δ <sub>Ha</sub> (ppm)	0	0.63	0.77	0.89	N/A	1.49	1.66	N/A	N/A	2.12	
298 K	δ <sub>Ha</sub> (ppm)	3.54	2.87	2.71	2.58	2.19	N/A	N/A	N/A	1.44	1.34	
	Δ <sub>Ha</sub> (ppm)	0	0.67	0.83	0.96	1.35	N/A	N/A	N/A	2.10	2.19	
292K	δ <sub>Ha</sub> (ppm)	3.47	2.72	2.55	2.42	2.00	1.82	1.62	1.33	1.20	1.10	
	Δ <sub>Ha</sub> (ppm)	0	0.74	0.92	1.04	1.47	1.65	1.85	2.14	2.27	2.36	
286K	δ <sub>Ha</sub> (ppm)	3.51	2.67	2.50	2.35	N/A	1.67	N/A	1.26	1.13	1.08	
	Δ <sub>Ha</sub> (ppm)	0	0.84	1.00	1.15	N/A	1.83	N/A	2.25	2.38	2.43	

<sup>a</sup>. Guest concentration was calculated from the  $^1\text{H}$  NMR integration data due to the partial decomposition of methyl propionate in buffer solution. For runs at 298K and 292K, [G]<sub>0</sub>=1.79 mM. For runs at 307K, 302K, and 286K (after one week), [G]<sub>0</sub>=1.63 mM; <sup>b</sup>. HDO peaks were not calibrated at different temperature.

## 1. Calibration of the Temperature

*Preparing the thermometers:*<sup>31</sup> (a) 500~750  $\mu\text{l}$  of pure methanol (HPLC grade, Fisher) or ethylene glycol (reagent grade, Aldrich) were added to a 5 mm NMR tube, respectively. The tube was then connected to a vacuum line, and the other side of the tube was inserted into a liquid nitrogen bath to freeze the methanol/ethylene glycol inside. The air in the tube was pumped away and the tap to the vacuum line was closed. The methanol/ethylene glycol was allowed to melt. The cooling and evacuation were repeated several times to remove the dissolved oxygen. Finally, the tube was sealed with a gas-oxygen flame. (b) 500  $\mu\text{L}$  of a  $\text{D}_2\text{O}$  pD 9.4 ammonium carbonate buffer was added to a 5 mm NMR tube and a capillary sealed with pure ethylene glycol was put into the bottom of the NMR tube. The NMR tube was then capped and wrapped with parafilm.

Two methods were used to calibrate the temperature:

*Calibration from a temperature calibration chart.* The methanol or ethylene glycol thermometer was placed in the spectrometer and the spectrometer was set at a specific temperature ( $T$ ). After the temperature was equilibrated, a spectrum was acquired and the chemical shift difference ( $\Delta\delta$ ) between the OH peak and the CH peak were recorded. These  $\Delta\delta$  values were graphed against  $T$  ( $T$  was read directly from the temperature measurement device attach on the NMR instrument). On the same plot, the standard curve of  $\Delta\delta$  against  $T$  was also drawn (Figure 2.13).<sup>32</sup> The actual temperature was then extrapolated from this calibration chart. For example: if the temperature shown on the temperature measuring device is 340K, from the calibration chart we can see that the point corresponds to 340 K on the measured curve gives  $\Delta\delta = 1.05$  ppm. Consequently, the point on the standard curve which corresponds to 1.05 ppm gives the actual temperature of 360 K.

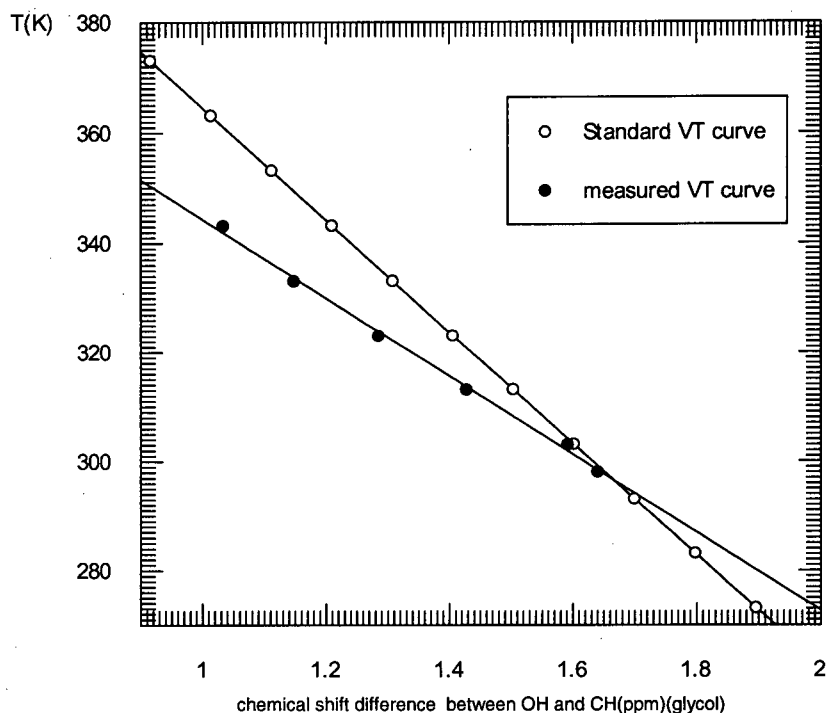


**Figure 2.14** VT calibration curves for Bruker AMX 500 spectrometer. (ethylene glycol as a thermo-standard)

*Determined from calibration equations.* During the  $^1\text{H}$  NMR titration experiment at a certain temperature, the sample tube was displaced by the thermometer and the chemical shift difference ( $\Delta\delta$ ) between the CH and OH proton resonances was recorded. The temperature was calculated using the following two equations:<sup>32b</sup>

$$T (\text{K}) \text{ Methanol} = 409.0 - 36.53 \Delta\delta - 21.85 (\Delta\delta)^2$$

$$T (\text{K}) \text{ Ethylene glycol} = 466.5 - 102.0 \Delta\delta$$

The above temperature measurement was repeated at the beginning, the middle and the end of each titration experiment. This method was finally chosen as a better method to calibrate the temperature in VT experiments for van't Hoff plot, since the air current and the



liquid N<sub>2</sub> level used in the temperature control procedure may vary each time when one does the VT experiments.

## 2. Calibration of the Chemical Shift of the D<sub>2</sub>O Solvent Residue Peak

The chemical shift of the D<sub>2</sub>O solvent residue peak (HOD) is temperature dependent.<sup>33</sup> The calibration curve of the residual HOD chemical shifts against temperature were graphed by referencing the EtOAc acetyl proton chemical shift ( $\delta = 1.92$  ppm). The calibration curve was shown in Figure 2.14 (The temperatures used in the Figure 2.14 were calibrated using the method shown on page 98).

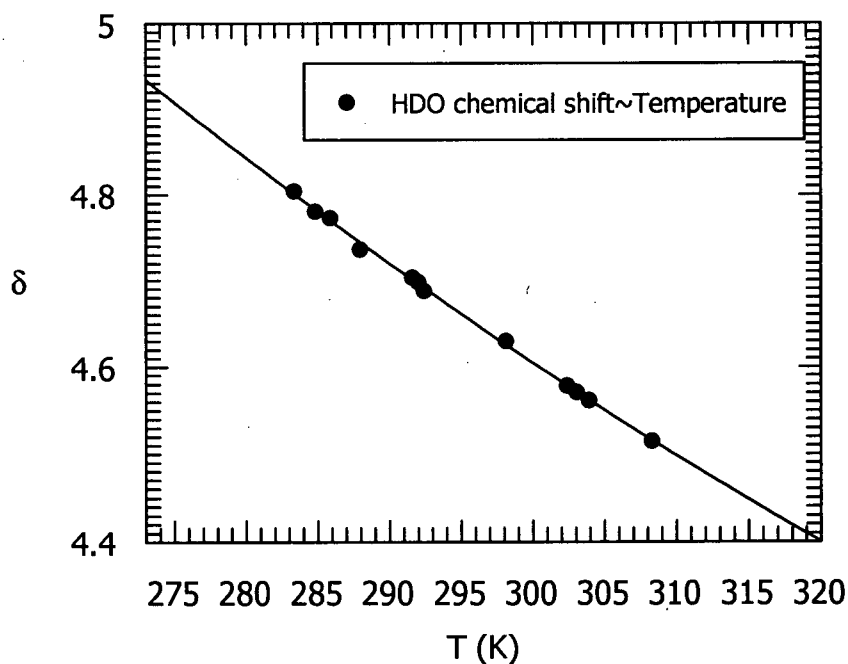


**Figure 2.15** D<sub>2</sub>O residue peak chemical shift as a function of temperature

## v. Molecular Mechanics Calculations

The calculations were performed with the Hyperchem/Chemplus package.<sup>28</sup> First, the conformation minimum was found for the host and the guests through a conformational search using an MM+ force field. Then, the atomic charges of the host and guests molecules were calculated by the semi-empirical AM1 method. Next, the free host or guest was put into a box containing 200 water molecules, and a minimum was calculated for each host/guest. Finally, each complex was inserted into a box containing around 300 water molecules and minima were calculated. The calculations were performed with the MM+ force field, using the standard parameters of the package. The minimization was performed by the conjugate gradient method (Polak-Ribiere) and was carried out until the RMS (Root-mean-square) gradient reached a value of 0.1 kcal Å<sup>-1</sup>mol<sup>-1</sup>.

## 2.6. References and Notes

1. Cram, D. J. *Angew. Chem. Int. Ed. Engl.* **1986**, *25*, 1039.
2. Moran, J. R.; Karbach, S.; Cram, D. J. *J. Am. Chem. Soc.* **1982**, *104*, 5826.
3. (a) Tucker, J. A.; Knobler, C. B.; Trueblood, K. N.; Cram, D. J. *J. Am. Chem. Soc.* **1989**, *111*, 3688; (b) Rudkevich, D. M.; Hilmersson, G.; Rebek, J. *J. Am. Chem. Soc.* **1997**, *119*, 9911.
4. (a) Yoon, J.; Cram, D. J. *Chem. Commun.* **1997**, 497. (b) Piatnitski, E. L.; Flowers II, R. A.; Deshayes, K. *Chem, Eur, J.* **2000**, *6*, 999.
5. Mezo, A. R.; Sherman, J. C. *J. Org. Chem.* **1998**, *63*, 6824.
6. Gibb, B. C.; Chapman, R. G.; Sherman, J. C. *J. Org. Chem.* **1996**, *61*, 1505.
7. Perich, J. W.; Johns, R. B. *Tetrahedron Letters* **1987**, *28*, 101.

8. (a) Nifant'ev, E. E.; Grachev, M. K. *Russ. Chem. Rev. (Engl. Trans.)* **1994**, *63*, 575. (b) Beaucage, S. L.; Lyer, R. P. *Tetrahedron* **1992**, *48*, 2223.
9. Nurminen, E. J.; Mattinen, J. L.; Lönnberg, H. *J. Chem. Soc., Perkin Trans. 2*, **1988**, 1621.
10. Perich, J. W.; Johns, R. B. *Tetrahedron Letters* **1987**, *28*, 101.
11. LaBrenz, S. R.; Bekele, H.; Kelly, J. W. *Tetrahedron* **1998**, *54*, 8671.
12. Connors, K. A. *Binding Constants* A Wiley-interscience publication, John Wiley & Sons, **1987** and the references there in.
13. Schneider, H.-J.; Hacket, F.; Rüdiger, V. *Chem. Rev.* **1998**, *98*, 1755.
14. (a) Bowser, M. T.; Chen, D. D. Y. *J. Phys. Chem. A* **1998**, *102*, 8063. (b) Bowser, M. T.; Chen, D. D. Y. *J. Phys. Chem. A* **1999**, *103*, 197.
15. Diederich, F. *Cyclophane* London: Royal Society of chemistry, **1991**.
16. Diederich, F.; Dick, K.; *J. Am. Chem. Soc.* **1984**, *106*, 8024.
17. Fraser, J. R.; Borecka, B.; Trotter, J.; Sherman, J. C. *J. Org. Chem.* **1995**, *60*, 1207.
18. Person, W. B. *J. Am. Chem. Soc.* **1965**, *87*, 167.
19.  $f_{HG}$  is the binding saturation fraction. It denotes the mole ratio of the complexed substrate HG formed in the solution compare to the total amount of the substrate (G). In a 1:1 binding system, under fast exchange condition, 
$$f_{HG} = \frac{[HG]}{[G]_0} = \frac{\Delta_{obs}}{\Delta_{max}}$$
20. (a) Connors, K. A. *Chem. Rev.* **1997**, *97*, 1325. (b) Liu, L.; Guo, Q.-X. *J. Phys. Chem. B* **1999**, *103*, 3461.
21. Stamm, H.; Lamberty, W.; Stafe, *J. Am. Chem. Soc.* **1980**, *102*, 1529.
22. Cram, D. J.; Karch, S.; Kim, H.-E.; Knobler, C. B.; Marerick, E. F.; Ericson, J. L.; Helgeson, R. C. *J. Am. Chem. Soc.* **1988**, *110*, 2229.
23. (a) Dalcanele, E.; Costantini, G.; Soncini, P. *J. Inclusion Phenom. Mol. Recognit. Chem.* **1992**, *13*, 87. (b) Leo, A.; Hunch, C.; Elkins, D. *Chem. Rev.* **1971**, *71*, 525.
24. (a) Fujimoto, T.; Yanagihara, R.; Asakawa, Y. Aoyama, Y. *Bull. Chem. Soc. Jpn.* **1995**, *68*, 2113. (b) Piatnitski, E. L.; Flowers II, R. A.; Deshayes, K. *Chem, Eur, J.* **2000**, *6*, 999. (c) Kobayashi, K.; Asakawa, Y.; Kikuchi, Y.; Toi, H.; Aoyama, Y. *J. Am. Chem. Soc.* **1993**, *115*, 2648.

25. Stauffer, D. A.; Barrans, R. E. Jr.; Dougherty, D. A. *J. Org. Chem.* **1990**, *55*, 2762.
26. Rekharsky, M. V.; Inoue, Y. *Chem. Rev.* **1998**, *98*, 1875.
27. (a) Smithrud, D. B.; Diederich, F. *J. Am. Chem. Soc.*, **1990**, *112*, 339. (b) Diederich, F. *Angew. Chem. Int. Ed. Engl.* **1988**, *27*, 362.
28. (a) Hyperchem® 5.01 , **1996**, Hypercube, Inc. (b) The calculation is based on the methods that were used for calixarene host-guest complexes: Arena, G.; Casnati, A.; Contino, A.; Lombardo, G. G.; Sciotto, D.; Ungaro, R. *Chem. Eur. J.* **1999**, *5*, 738.
29. Bergmann, E. D.; Crane, F. E. Jr.; Fuoss, R. M. *J. Am. Chem. Soc.* **1952**, *74*, 5979.
30. R.J. Leatherbarrow, *GraFit® Version 3.0*, **1990**, Erithacus Software ltd., Staies, UK.
31. Sandström, J. *Dynamic NMR Spectroscopy* London; New York: Academic Press. Inc. **1982**.
32. The NMR temperature measurement references are from the website:  
[http://bmrl.med.uiuc.edu:8080/~dmorris/nmrt\\_ref.html](http://bmrl.med.uiuc.edu:8080/~dmorris/nmrt_ref.html). Also see reference: Ammann, C.; Meier, P.; Merbach, A. E. *J. Magn. Reson.*, **1982**, *46*, 319-312.
33. Gottlieb, H. E.; Kotlyar, V.; Nudelman, A. *J. Org. Chem.* **1997**, *62*, 7512.